

**Microstructural, Electrical and Mechanical Properties
of MgB₂/Mg Metal Matrix Composites**

By

Mehmet EĞİLMEZ

**A Dissertation Submitted to the
Graduate School in Partial Fulfillment of the
Requirements for the Degree of**

MASTER OF SCIENCE

**Department: Material Science and Engineering
Major: Material Science Program**

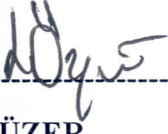
**Izmir Institute of Technology
Izmir, Turkey**

May, 2004

**İZMİR YÜKSEK TEKNOLOJİ ENSTİTÜSÜ
REKTÖRLÜĞÜ
Kütüphane ve Dokümantasyon Daire Bşk.**

We approve the thesis of **Mehmet EĞİLMEZ**

Date of Signature

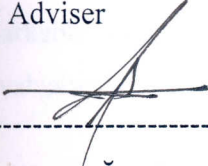


June 25, 2004

Lütfi ÖZYÜZER

Assist. Professor of Physics

Thesis Adviser




August 3, 2004

Metin TANOĞLU

Assoc. Professor of Mechanical Engineering

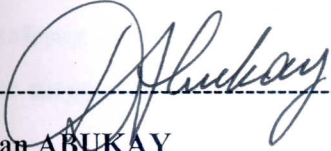
Thesis Co-Adviser



August 5, 2004

Salih OKUR

Assist. Professor of Physics



July 23, 2004

Doğan ABUKAY

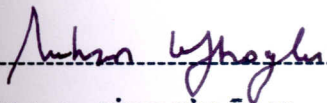
Professor of Physics



August 9, 2004

Kemal KOCABAŞ

Professor of Physics



August 5, 2004

Muhsin ÇİFTÇİOĞLU

Head of Interdisciplinary Material Science and
Engineering Program

İZMİR YÜKSEK TEKNOLOJİ ENSTİTÜSÜ
REKTÖRLÜĞÜ
Kütüphane ve Dokümantasyon Daire Bşk.

ACKNOWLEDGEMENT

I would like to thank my thesis advisor Asst. Professor Lutfi Özyüzer for his guidance, continuous support and encouragement throughout the preparation of this thesis. I would like to express my gratitude to Assoc. Professor Metin Tanođlu for his remarkable comments on my research. I am also grateful to Asst Professor Salih Okur for his valuable suggestions.

I am greatly indebted to the staff of Center for Material Research of İzmir Institute of Technology for their contribution. During this graduate study, I acknowledge the financial support from TUBITAK TBAG 2031 and TBAG 2215. I wish to extend my thanks to İzmir Institute of Technology for providing Research Assistantship during my thesis.

I would like to express my gratefulness to Professor Yıldırhan Öner and Assoc. Professor Orhan Kamer for their contribution to this thesis with providing the opportunity for magnetization measurements at İstanbul Technical University.

I am also thankful to my colleagues, Oktay Göktaş, Cihan Kurter, Savaş Ulucan and Tarik Özalp for their helpful discussion.

Finally, special thanks to my family for their support and motivation.

ABSTRACT

The recent discovery of superconducting MgB_2 (2001) has risen a great interest because of its relatively high T_c (39 K). Furthermore, simple crystal structure, large coherence lengths, high critical current densities (J_c) and critical fields (B_{c2}), promise that MgB_2 will be a good material for large-scale applications based on production of superconducting wires. However, MgB_2 is not a stand-alone material to produce wires because of its brittle nature. The potential of MgB_2/Mg composites for producing superconducting wires, is investigated. MgB_2/Mg composites were prepared using metal matrix composite fabrication technique, which is an alternative to conventional wire fabrication methods such as powder in tube. MgB_2 and Mg powders were mixed at different weight fractions and uniaxially pressed in a cylindrical die under the pressure of 0.5 GPa and 1GPa for two hours at different temperatures in the air. X-Ray Diffraction (XRD), Scanning Electron Microscopy (SEM) and Electron Dispersive X-Ray Spectroscopy (EDX) techniques were used for phase identification and microstructural studies. D.C resistivity measurements were carried on the pellet segments of the MgB_2/Mg composites in the temperature range 20-300 K. Magnetization measurements were done on the composites using a vibrating sample magnetometer to characterize the magnetic properties of the samples. The effects of pressing temperature on the mechanical properties of MgB_2/Mg composites were also investigated. For this purpose, compressive mechanical testing were performed to measure elastic modulus and strength at failure values of the composites. It was found that the relative weight fractions of Mg and the pressing temperature have some considerable effect on the electrical, magnetic, microstructural and the mechanical properties of the composites.

ÖZ

2001 yılında keşfedilen MgB_2 39 K gibi göreceli olarak yüksek bir geçiş sıcaklığına sahip olması nedeniyle oldukça fazla ilgi çekmiştir. Bununla birlikte, basit kristal yapıya sahip olması, geniş koherens uzunluğuna sahip olması, yüksek kritik akım (J_c) değerleri ve kritik alan (B_{c2}) değerlerine sahip olması bu malzemeyi üstüniletken tel üretimi için oldukça umut verici bir malzeme olarak düşünülmesini sağlamıştır. Fakat MgB_2 tek başına üstüniletken tel üretimi için uygun bir malzeme değildir. Bu çalışmada MgB_2/Mg kompozitlerin, üstüniletken tel gibi uygulamalarda kullanılabilirliği araştırılmıştır. Tüp içinde toz yöntemi gibi geleneksel tel üretimi metodlarına bir alternatif olan metal matris kompozit üretimi tekniği kullanılarak MgB_2/Mg kompozitler hazırlanmıştır. Üstüniletken kompozitler, MgB_2 ve Mg tozları çeşitli kütle oranlarında karıştırılarak 1 GPa ve 0.5 GPa basınçlar altında çelik bir kalıpta değişik sıcaklıklarda hava ortamında 2 saat ısıtılma tabi tutularak üretilmiştir. Üretilen MgB_2 /Mg kompozitlerin mikroyapıları ve faz tanımlamaları XRD, SEM ve EDX teknikleri kullanılarak karakterize edilmiştir. Üstüniletken kompozitlerin elektriksel ve manyetik özellikleri sıcaklığa bağlı özdirenç ve manyetizasyon ölçümleri yapılarak belirlenmiştir. Sıcaklığın kompozitlerin mekanik özellikleri üzerindeki etkisi incelenmiştir bu amaçla kompozitlerin zor – zorlanma davranışı incelenerek kırılma zor değerleri belirlenmiştir. Örnek hazırlama sıcaklığının, basıncın ve Mg katkısının kompozitlerin mikroyapısal, elektriksel, manyetik ve mekanik özellikleri üzerinde önemli miktarda etkisinin olduğu belirlenmiştir.

TABLE OF CONTENTS

LIST OF FIGURES	viii
LIST OF TABLES.....	x
CHAPTER 1.....	1
INTRODUCTION.....	1
1.1 A Brief History of Superconductivity.....	1
1.2 Basic Properties of Superconductors	3
1.3 Applications of Superconducting Devices.....	5
1.4 Possible Applications of MgB ₂	7
1.5 Objectives of the Thesis.....	7
CHAPTER 2.....	9
BASIC PROPERTIES OF MgB ₂ SUPERCONDUCTOR.....	9
2.1 The Crystal Structure	9
2.2 Physics of MgB ₂	10
2.2.1 Isotope Effect and Phonons.....	10
2.2.2 Two-gap Superconductor.....	11
2.2.3 Normal State Properties.....	12
2.2.4 Superconducting Properties.....	14
2.3 Preparation of Bulk Samples From MgB ₂	17
2.3.1 Synthesis of MgB ₂	17
2.3.2 Powder In Tube Method.....	18
2.3.3 Metal Matrix Composite Method.....	20
CHAPTER 3.....	22
EXPERIMENTAL METHODS.....	22
3.1 Material.....	22
3.2 Experimental.....	23
3.3 Measurements.....	25
3.3.1 Determination of Transition Temperature	25
3.3.2 Mechanical Tests.....	28

CHAPTER 4	30
RESULTS AND DISCUSSIONS	30
4.1 Density and XRD Results.....	30
4.2 SEM and EDX Results.....	39
4.3 Resistivity and Magnetization Results.....	43
4.4 Mechanical Properties.....	62
CHAPTER 5	68
CONCLUSIONS	68
APPENDIX	73
REFERENCES	75

LIST OF FIGURES

Figure 2.1 The crystal structure of MgB ₂ , consisting of Mg and B atoms.....	9
Figure 2.2 Temperature dependence of resistivity of MgB ₂	13
Figure 2.3 Hall coefficient in MgB ₂	14
Figure 2.4 Powder In Tube Method.....	19
Figure 2.5 SEM images of Fe clad tapes.....	20
Figure 3.1 XRD peaks of commercial MgB ₂	22
Figure 3.2 XRD peaks of commercial Mg.....	23
Figure 3.3 Experimental set up for sample preparation.....	24
Figure 3.4 Four point probe resistivity measurement.....	26
Figure 3.5 The CRYO Pump System.....	27
Figure 3.6 A Typical Stress-Strain curve obtained from MgB ₂ /Mg composites.....	28
Figure 3.7 Determination of Fracture Strength and Elastic Modulus values from Stress-Strain curves.....	29
Figure 4.1 The powder XRD pattern of MgB ₂ /Mg composites prepared at 400°C, 0.5 GPa.....	34
Figure 4.2 The powder XRD pattern of MgB ₂ /Mg composites prepared at 500°C, 0.5 GPa.....	35
Figure 4.3 The powder XRD pattern of MgB ₂ /Mg composites prepared at 550°C, 0.5 GPa.....	36
Figure 4.4 The powder XRD pattern of MgB ₂ /Mg composites prepared at 400°C, 1 GPa.....	37
Figure 4.5 The powder XRD pattern of MgB ₂ /Mg composites prepared at 500°C, 1 GPa.....	38
Figure 4.6 SEM fracture surface images for samples prepared at 400 and 550°C, 0.5 GPa.....	40
Figure 4.7 SEM fracture surface images for samples prepared at 0.5 GPa and 1GPa, 500°C.....	41
Figure 4.8 EDX analyses results samples prepared at different temperatures.....	42

Figure 4.9 Determination of T_c from Resistivity versus Temperature curves.....	43
Figure 4.10 Magnetization versus Temperature curve.....	45
Figure 4.11 Derivative of the data given in Figure 4.3.2.....	46
Figure 4.12 Temperature dependence of normalized resistivity of MgB_2/Mg composites prepared at 400°C and 0.5 GPa.....	47
Figure 4.13 Temperature dependence of normalized resistivity of MgB_2/Mg composites prepared at 500°C and 0.5 GPa.....	48
Figure 4.14 Temperature dependence of normalized resistivity of MgB_2/Mg composites prepared at 550°C and 0.5 GPa.....	49
Figure 4.15 Temperature dependence of normalized resistivity of MgB_2/Mg composites prepared at 400°C and 1 GPa.....	50
Figure 4.16 Temperature dependence of normalized resistivity of MgB_2/Mg composites prepared at 500°C and 1 GPa.....	51
Figure 4.17 Magnetization versus Temperature plot of samples prepared at 400°C and 0.5 GPa.....	56
Figure 4.18 Magnetization versus Temperature plot of samples prepared at 500° C and 0.5 GPa.....	57
Figure 4.19 Magnetization versus Temperature plot of samples prepared at 550° C and 0.5 GPa.....	58
Figure 4.20 Magnetization versus Temperature plot of samples prepared at 400°C and 1 GPa.....	59
Figure 4.21 Magnetization versus Temperature plot of samples prepared at 500° C and 1 GPa.....	60
Figure 4.22 Stress strain behavior of unsubstituted and 20% Mg samples prepared at 400°C and 0.5 GPa.....	62
Figure 4.23 Stress strain behavior of unsubstituted and 20% Mg samples prepared at 500° C and 0.5 GPa.....	63
Figure 4.24 Fracture strength values of samples prepared at 400°C and 0.5 GPa.....	64
Figure 4.25 Fracture strength values of samples prepared at 500°C and 0.5 GPa.....	65

LIST OF TABLES

Table 2.1 The recent status of critical current density (J_c) of MgB_2	15
Table 2.2 Effects of additives on J_c of MgB_2 at 20 K	16
Table 4.1 Density of the samples prepared at 0.5 GPa.....	31
Table 4.2 Density of the samples prepared at 1GPa.....	31
Table 4.3 The T_c , ΔT and T_c^{Onset} values of MgB_2/Mg composites prepared at 400°C and 0.5 GPa.....	47
Table 4.4 The T_c , ΔT and T_c^{Onset} values of MgB_2/Mg composites prepared at 500°C and 0.5GPa.....	48
Table 4.5 The T_c , ΔT and T_c^{Onset} values of MgB_2/Mg composites prepared at 550°C and 0.5 GPa.....	49
Table 4.6 The T_c , ΔT and T_c^{Onset} values of MgB_2/Mg composites prepared at 400°C and 1GPa.....	50
Table 4.7 The T_c , ΔT and T_c^{Onset} values of MgB_2/Mg composites prepared at 500°C and 1 GPa.....	51
Table 4.8 The resistivity values of samples prepared at 500°C and 0.5 GPa.....	54
Table 4.9 The resistivity values of samples for different preparing conditions.....	54
Table 4.10 ΔT and T_c^{Onset} values of samples prepared at 400°C and 0.5 GPa.....	56
Table 4.11 ΔT and T_c^{Onset} values of samples prepared at 500°C and 0.5 GPa.....	57
Table 4.12 ΔT and T_c^{Onset} values of samples prepared at 550°C and 0.5 GPa.....	58
Table 4.13 ΔT and T_c^{Onset} values of samples prepared at 400°C and 1 GPa.....	59
Table 4.14 ΔT and T_c^{Onset} values of samples prepared at 500°C and 1GPa.....	60
Table 4.15 Fracture strength and Elastic modulus values for MgB_2/Mg composites.....	66
Table A-1 T_c values of some selected superconductors.....	73
Table A-2 Basic properties of Mg.....	74

CHAPTER 1

INTRODUCTION

After Kammerlingh Onnes discovered superconductivity in pure mercury (4.2 K), the science society became aware of the great potential of lossless current transport for applications in magnet and energy technology. Great effort had been spent by many scientists in finding of theoretical background of this new phenomenon on the search for new superconducting materials with high transition temperatures. As a result of this endeavor on this subject many superconducting materials has been found to be superconducting and the critical temperature recently has increased to a value of 133 K in $\text{HgBa}_2\text{Ca}_2\text{Cu}_3\text{O}_8$. Moreover, in the last 50 years, it was shown that the applications of superconductivity are not limited with magnet and energy technology, the technology based on superconductor electronics brought new devices into use that have unique properties. Although there are a number of superconducting materials, which have transition temperature above 77 K, the boiling point of liquid nitrogen, some structural and superconducting properties of these materials plagued the widespread commercialization of these materials. Therefore, 99% of the superconductivity applications are based on superconductors, which have a transition temperature of less than 20 K. Recent discovery of MgB_2 (39 K) aroused interest of researchers on this subject and studies have been carried on for last 30 months from the discovery of this compound revealed that this material is a promising material to replace with current available superconductors such as Nb_3Sn (18 K) in industry.

1.1 A Brief History of Superconductivity

The most remarkable properties of the superconductivity are zero resistance and perfect diamagnetism. Below a certain critical temperature (T_c), the electrical resistance of a superconducting material vanishes. The discovery of the superconductivity is closely related with the development of helium liquefaction techniques in the laboratory of Heike Kammerlingh Onnes at the University of Leiden. Onnes managed to liquefy Helium in 1908 so very low temperatures down to 4 K became available for further explorations. One

of the first question addressed was the electrical resistivity of pure metals at very low temperatures. The effect of purity on the residual resistivity of the metals was Onnes's research topic at that time. Mercury was selected for further research because this metal could be easily purified by repeated distillation. In 1911 Kammerlingh Onnes found that the electrical resistivity of Mercury suddenly undergoes to an immeasurably small value at a temperature of nearly 4.2 K [1]. During the following decades superconductivity was observed in large number of metals, alloys and compounds. The second important discovery in superconductivity is perfect diamagnetism. This effect was discovered by W. Meissner and R. Ochenfeld in 1933. They found that a magnetic field is expelled from the interior of a superconductor as soon as the superconducting state is reached [2].

In appendix, Table A1 lists the development of transition temperatures and their year of discovery. Superconductivity at 35 K in the (La,Ba)CuO₄ system by Bednorz and Muller [3] in 1986 was a breakdown point, if the increase of the transition temperatures T_c before and after this discovery is considered. In 1987 it was found that Yttrium Barium Copper Oxide (YBa₂Cu₃O₇) becomes superconducting at a critical temperature of 93 K, which is above the boiling temperature of liquid nitrogen (77K). The discovery was particularly important because liquid nitrogen is an inexpensive cryogen that is readily liquefied. At present, the critical temperature is above 130 K in HgBaCaCuO. These superconductors are called high temperature superconductors (HTS).

The highest transition temperature of metals and compounds was 23.2 K in Nb₃Ge [4, 5] until the discovery of MgB₂ with a transition temperature (T_c) of 39 K in 2001 [6]. For compounds the transition temperature of Nb₃Ge remained highest critical temperature for more than 25 years, underlying the difficulty of achieving higher transition temperatures in intermetallic compounds, therefore the discovery of MgB₂ stimulated a great interest in this superconducting system. Many studies have been done last 30 months and origin of the superconductivity of MgB₂ and potential of this superconducting material was successfully explained.

1.2 Fundamental Properties of Superconductors

As mentioned before, not only resistance drop but also the perfect diamagnetism is one of basic property of superconductors. Meissner and Ochenfeld found that whether a superconductor is cooled in a magnetic field or not the net magnetic field inside a superconductor below the transition temperature of superconductor is zero ($B=0$).

The superconductivity below the critical temperature has been observed to disappear in the presence of a applied magnetic field exceeding a critical value denoted by B_c . This critical field depends on the temperature and is a characteristic of the material. The critical field is maximum, $B_c(0)$, when $T=0$ K. Meissner effect states that in the superconducting state, the applied magnetic field lines are expelled from sample. The external field, in fact does penetrate the sample from the surface into the bulk, however the magnitude of this penetrating field decreases as exponentially from the surface. If the field at the surface of the superconductor is B_0 , then at a distance x from the surface, the field is given by an exponential decay, Equation 1.1, where λ is a characteristic length called the penetration depth

$$B(x)=B_0 \exp (-x/\lambda) \quad 1.1$$

Superconductors are classified into two types, namely type I and type II based on their diamagnetic properties. In type I superconductors, as the applied magnetic field increases, so does the opposing magnetization M until the field reaches the critical field, B_c , where the superconductivity vanishes. A type I superconductor below critical field (B_c) is in the Meissner state, where it expels all magnetic flux from the inside of the sample. Above the critical field (B_c), it is in the normal state, where the magnetic flux penetrates the sample and the conductivity of the sample is finite. Generally pure elements are type I superconductors and the values of the critical field (B_c) are always too low for type I superconductors to have any useful applications. In the case of type II superconductors, the transition does not occur directly from the Meissner state to the normal state but goes through an intermediate phase in which the applied field is able to pierce through certain local regimes of the sample. As the magnetic field increases, firstly the specimen behaves as perfect diamagnet exhibiting the Meissner effect and rejecting all the magnetic flux lines. When the applied field increases a critical field namely B_{c1} ,

the lower critical field, the magnetic flux lines are no longer totally expelled from the sample. The overall magnetization M in the sample opposes the field, but its magnitude does not cancel the field everywhere. As the field increases, M becomes smaller and more flux lines penetrate into the specimen until at B_{c2} , the upper critical field, all field lines goes into the sample and superconductivity vanishes. The state between B_{c1} and B_{c2} is called as the mixed state (vortex state) since there exist both superconducting state and normal state together. Magnetic flux lines called vortices in this mixed region have fine conductivity and a quantized amount of flux through them. Each normal state region is a vortex of flux lines. In this mixed region, the magnetic flux through the superconducting matrix is zero, therefore there should be currents circulating around the walls of vortices.

Another important characteristic feature of the superconducting state is that, superconductivity vanishes when the current density through the sample exceeds a critical value, critical current density (J_c). This is not an astonishing situation because the current through the superconductor will it self generate a magnetic field and at sufficiently high current densities, the magnetic field at the surface of the specimen will exceed the critical field and superconductivity disappears. However, this direct relation between critical field (B_c) and critical current density (J_c) is only true for type II superconductors. J_c depends on a complicated way on the interaction between the current and the flux vortices.

Although superconductivity was discovered in 1911, the understanding of superconductivity did not changed until 1957 when Bardeen, Cooper and Schriffer formulated the theory in terms of quantum mechanics (BCS) [7]. This theory states that below the transition temperature (T_c), two oppositely spinning and traveling electrons can attract each other indirectly through the deformation of the crystal lattice of positive metal ions. This indirect interaction at sufficiently low temperatures is able to overcome the coulomb repulsion between the electrons and therefore it binds two electrons each other. These binded two electrons are called Cooper pairs. The net spin of the cooper pair is zero and their net linear momentum is zero. There is a further significance to the pairing of electron spins in the cooper pair. As a particle, the cooper pair has no net spin and hence the cooper pairs do not obey the Fermi-Dirac Statistics. They can therefore all condense to the lowest energy state and possess one single wave function, which can describe the whole of cooper pairs. All the paired electrons are described collectively by a single wave

function Ψ , which extends over the whole sample. A crystal defect, which is the one of reasons of resistivity in normal metals at low temperatures, can not simply scatter a single cooper pair, because all the pairs behaves as a single body like a huge molecule. Scattering one pair involves scattering all pairs, which is not possible.

Superconductivity is said to be macroscopic manifestation of quantum mechanics. The BCS theory has had good success with low temperature superconductors. The BCS theory predicts the maximum transition temperature as 30 K, however there are many superconductors with a transition temperature higher than 30 K. Newly discovered MgB_2 has also a transition temperature higher than 30 K but recent publications show that BCS theory can explain the mechanism of superconductivity in MgB_2 . On the other hand, there seems to be some doubts about applicability to high temperature superconductors. There are number of theories that try to explain the mechanism of pairing in high temperature superconductor materials. The theories of high temperature superconductors are not scope of this study.

1.3 Applications of Superconducting Devices

Superconductors are absolutely unique in many of their properties. A wide variety of superconducting devices have been proposed and developed, a few of them are in commercial use. The discovery of High Temperature Superconductors (HTS) has extended the practical range of some of these applications and enable the development of new ones. However, the basic problem, cooling the device remained very much the same. Therefore, a limited use area is a reality for superconductors. To have a very widespread application area, it is obvious that a room temperature or a transition temperature close to room temperature is essential.

Superconducting devices tend to operate in one of the three general regimes. There are those based on the zero resistance of the superconducting state, those based on transition between the superconducting state and normal state and those based on Josephson Junctions. In terms of zero resistance, the main application is absolutely superconducting magnet. To produce high magnetic fields, there is not any alternative to superconducting wires. This involves winding of kilometer length wires into large solenoids. Superconducting magnets are recently used primarily in medical and scientific

instrumentation namely MRI (magnetic resonance imaging) and particle accelerators. Other bulk applications of superconductors that focus on the low frequency magnetic properties include magnetic levitation MAGLEVS, magnetic bearings and magnetic shielding.

Most of the other applications are based on the superconducting thin film technology rather than wires, since the total currents needed are not so large. Superconductors exhibit extremely small resistance at Radio Frequency (RF) and microwave frequencies and resonance cavities, lossless transmission structures, and microwave filters are among the applications that are being developed. Another application relies on the transition between the superconducting and the normal state. In an ideal superconductor, the resistive transition at T_c is very sharp, that prepares the basis for a variety of thermally based detectors and switches. That means, a superconductor held at T_c can be a very sensitive Bolometer or thermal detector for heat radiation. A superconductor held at transition temperature can be switched from zero resistance to quite a large resistance with only a small exposure to thermal or optical energy.

Furthermore, Josephson junctions have provided the basis for the widest range of superconducting devices. Superconducting Quantum Interference Device (SQUID) magnetometers are the most sensitive detectors of low frequency magnetic fields, available in many technology, with sensitivity down to the femtotesla range. This makes SQUID arrays useful in localizing sources of magnetic fields in the brain, for instance. At microwave frequencies, Josephson junctions have been used as detectors and sources of radiation based on the a.c. Josephson relation

In the paragraphs above, we have given some information about the current applications of superconductors. One of the recent question addressed in the superconductor society nowadays is where is the place of newly discovered MgB_2 in this application area.

1.4 Possible Applications of MgB_2

MgB_2 has significance on the superconductivity field for a number of reasons. The first is that the transition temperature at 39 K is the highest superconducting transition temperature among intermetallic compounds (the second highest is 23 K in Nb_3Ge [4,5] and $YPd_5B_3C_{0.3}$ [8]). A transition temperature of 39 K is seems to be not very high

compared to the high temperature superconductors. However, 99.9% of the current superconductor technology is based on two low temperature superconductors NbTi ($T_c=9$ K) and Nb₃Sn ($T_c=18$ K). MgB₂ superconductor with a transition temperature of 39 K seems to be a promising material to replace the technology based on current available superconductors. Recent studies on isotope effects show that MgB₂ is a phonon mediated BCS superconductor. Therefore many important properties of the MgB₂ including the mechanism of superconductivity is not so complicated among the superconductors which have a transition temperature higher than 30 K. In the engineering point of view, the investing money on a well understood material is more wise. Furthermore, MgB₂ has many properties that make it attractive for superconducting thin film applications especially its isotropy compared to High Temperature Superconductors, such as lower material complexity, fewer interface problems and longer coherence lengths [9, 10]. Many basic superconducting properties that will be discussed more comprehensively in Chapter 2 reveals that MgB₂ is a good candidate both for large scale applications (based on wires) and small scale applications (based on thin films).

1.5 Objectives of the Thesis

The recent discovery of MgB₂ (2001) has endured a great interest because of its high T_c (39 K). Furthermore, simple crystal structure, large coherence lengths, high critical current densities (J_c) and critical fields (B_{c2}), and transparency of grain boundaries to current promise that MgB₂ will be a good material for both large-scale applications and electronic device applications. Since the worldwide 99% of the superconductor market depends on large-scale applications based on production of wires and tapes, MgB₂ suggests a higher operating temperature (20 K) than the current technology in use by Nb based superconductors at 4.2 K. Therefore, production of wires from MgB₂ has great significance in terms of science and industry. However, MgB₂ is not a stand alone material to produce wires because of its brittle nature. In this study, we have produced MgB₂/Mg Metal Matrix Composites (MMC) to investigate the potential of wire production from these composites. MgB₂/Mg composites were produced by MMC method using hot pressing technique to improve the mechanical properties of MgB₂. Mg is chosen as the metal matrix because of its low melting point (653°C) and its inertness to

MgB₂ at very high temperatures. To demonstrate the superconducting properties of produced composites, DC resistivity and magnetization measurements were carried on pellet segments in the temperature range of 20-300 K. Microstructural characterization was done by Scanning electron microscopy (SEM) coupled with electron dispersive X Ray spectroscopy (EDX) and X Ray diffractometer (XRD) for phase identification. To investigate the mechanical properties of the composites, standard mechanical tests carried on composite samples.

CHAPTER 2

BASIC PROPERTIES OF SUPERCONDUCTING MgB_2

2.1 The Crystal Structure

It is not surprising that 39 K superconductivity in MgB_2 aroused a great interest on this subject within the physics society. There exist many superconductors, which have higher critical temperatures. What is so important in MgB_2 ? One important reason is simplicity of MgB_2 . It has a hexagonal AlB_2 -type crystal structure, where the Boron atoms form graphite like sheets separated by hexagonal layers of Mg atoms, Figure 2.1, [11]. The lattice constants are $a= 3.086 \text{ \AA}$ and $c= 3.524 \text{ \AA}$.

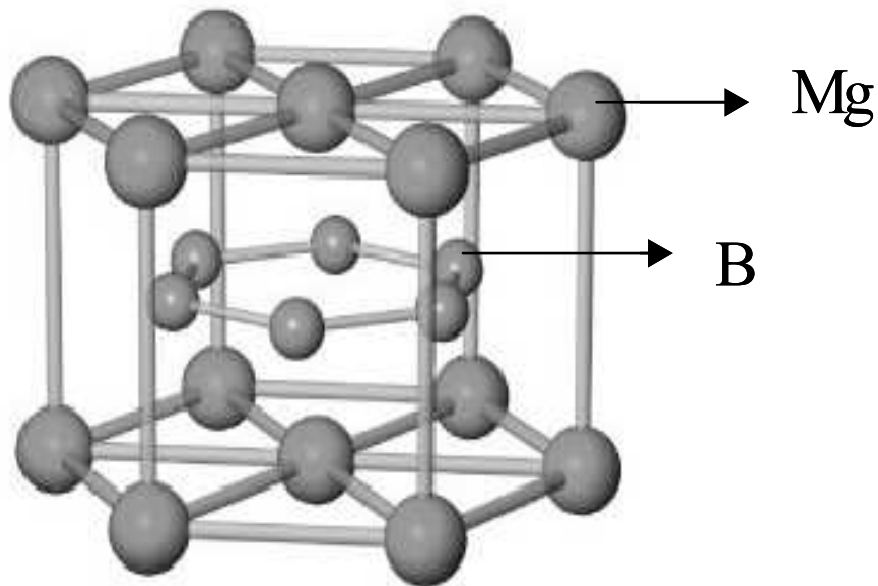


Figure 2.1 The crystal structure of MgB_2 , consisting Mg and B atoms [12].

2.2 PHYSICS OF SUPERCONDUCTING MgB₂

2.2.1 Isotope Effect and Phonons

Isotope effect has great significance since it indicates the role of phonons for superconductivity. This is due to the fact that superconducting transition temperature T_c depends obviously on the isotopic mass. The isotope effect can be formulated in this formula given in Equation 2.1, for a single component system where M is the atomic mass.

$$\alpha = -d\ln T_c / d\ln M \approx (-\Delta T_c / T_c) / (M / \Delta M) \quad 2.1$$

For a multi component system the isotope effect can be defined as the sum of the isotope effect coefficient for all components.

$$\alpha_t = \sum \alpha_i = \sum -d\ln T_c / d\ln M \quad 2.2$$

The isotope effect in MgB₂ is first measured by Budko [13] and his co-workers. They reported an increase in T_c by substituting ¹⁰B for ¹¹B and they find the isotope effect coefficient $\alpha=0.28$ for B. This was the first clue about the phonon-mediated superconductivity in MgB₂. The isotope effect both B and Mg was measured by Hinks et al. [14]. They found the isotope effect coefficient $\alpha=0.30$ harmonious with the result of Budko and $\alpha=0.02$ for Mg. This results reported by Hinks revealed that phonons involve a role in the superconductivity mechanism of MgB₂ were mainly phonons from B. Mg atoms contribute to the pairing mechanism a little. Both Mg and B are light elements and both have stable isotopes. This makes MgB₂ special among all superconductors. Thus it is one of the High T_c materials that isotope effect can be measured correctly. The total measured isotope effect coefficient $\alpha_t=0.32$ is less than the value $\alpha=0.5$ predicted for the BCS type phonon mediated superconductors. This decrease in the isotope effect coefficient can be explained by strong coulomb repulsion [15] and large anharmonicity of B atom vibrations [16]. Furthermore, as often in the case for BCS superconductors the T_c decreases with pressure in MgB₂ up to highest pressure studied. This behavior can be

understood as the lattice stiffness increase with pressure, the electron–phonon interaction decreases [17].

2.2.2 Two gap superconductor

As mentioned, MgB₂ is an attractive material with its relatively high transition temperature and possible applications. Moreover from the point of fundamental physics its very interesting because it is the clearest example of a two gap superconductors ever studied. The superconducting energy gap of MgB₂ has been determined from different spectroscopic probes (tunneling, point contact, photoemission, far-infrared optics) as well as from the temperature dependence of specific heat, microwave surface resistance and penetration depth at low temperatures [9, 18]. It was found that the Fermi surface consists of two tubular networks arising from three-dimensional π bonding and antibonding bands, and two nearly cylindrical sheets from the two-dimensional σ bands. Usually, these actually four bands are considered as two effective bands. The superconductivity arises from strong electron-phonon coupling in the 2D σ bands. The main source of the superconductivity behavior of the π electrons is their interband coupling to σ electrons. As a result there are two distinct energy gaps. The 2D band shows a large gap, $\Delta_\sigma \sim 7\text{-}8$ meV, whereas the 3D band has a small gap $\Delta_\pi \sim 2\text{-}3$ meV, both closing at the same critical temperature $T_c = 39$ K [19, 20, 21].

Addition to the experimental indication of the two band superconductivity, in MgB₂ the postulation of two-gap superconductivity was proved from the band calculations [19, 20]. The calculations reported by several authors gave similar results and it is summarized below [22].

(i) Mg is substantially ionized, and MgB₂ can be well described as the ionic form Mg²⁺(B₂)²⁻.

(ii) The band near the Fermi level mainly derive from the distinct sets of boron orbitals: $sp^2(\sigma)$ states and $p_z(\pi)$ states. The σ bands are 2D in character and form cylindrical Fermi surfaces, whereas the π bands have more of a 3D character owing to a substantial c-axis transfer integral and form 3D tubular networks of Fermi surfaces.

(iii) The σ bands (2D FS) interact strongly with the E_{2g} phonon mode and are predicted to have a large 2D superconducting gap. However, the π bands have weaker electron-phonon interaction and their superconducting gap is about 3 times smaller in magnitude.

2.2.3 Normal State Properties

The basic physical properties of MgB_2 were studied initially using polycrystalline samples. The reported values for the resistivity are different from group to group (from 100 m Ω .cm to 0.3 $\mu\Omega$.cm) [23]. Soon after, several groups began to measure single crystals produced by using high-pressure furnaces or single crystalline films using a two-step method [24]. This resulted in making experimental data more consistent. The resistivity value of MgB_2 at room temperature is approximately 5-6 $\mu\Omega$.cm. Figure 2.2, which can be compared to $\rho(300\text{ K})$ of nearly 2 $\mu\Omega$.cm for Cu, $\sim 15\ \mu\Omega$.cm for Nb, $\sim 80\ \mu\Omega$.cm for Nb_3Sn and 150 $\mu\Omega$.cm for $YBa_2Cu_3O_x$. The low temperature resistivity value of MgB_2 is between 0.3 $\mu\Omega$.cm and 3 $\mu\Omega$.cm [23,25]. Simple explanation attributes this large variation to the amount of the impurity scattering, stoichiometry variations and to porosity [23, 26].

As I mentioned, there are four bands near Fermi level, two hole like σ bands forming 2D cylindrical Fermi surfaces, hole and electron like 3D π bands in the band structure of MgB_2 . Due to the multi band structure of MgB_2 , the hall coefficient show strong anisotropy as seen in Figure 2.3 [27]. In $H \parallel c$, the hole like carriers dominate the behavior of R_H , and give positive values of R_H . When magnetic field (H) applied parallel to the ab plane, the σ bands became less important, and electron like carriers dominate the R_H . Due to the fact that MgB_2 is a superconductor which has multiband structure, the absolute value of the R_H is not the direct measure of the carrier density. The carrier densities are estimate to be $n \sim 3.4 \cdot 10^{22}\text{ cm}^{-3}$ and $p \sim 2.6 \cdot 10^{22}\text{ cm}^{-3}$ at 40 K in single crystalline samples [28]. The absolute values of R_H are about one order larger than R_H in polycrystalline samples [29] and in thin films [30]. This difference can be explained by the compensation between the positive and negative components due to the randomly oriented grains. In Figure 2.3 both R_H values show substantial temperature dependence. This situation can be explained by different T dependence of scattering rate for different bands.

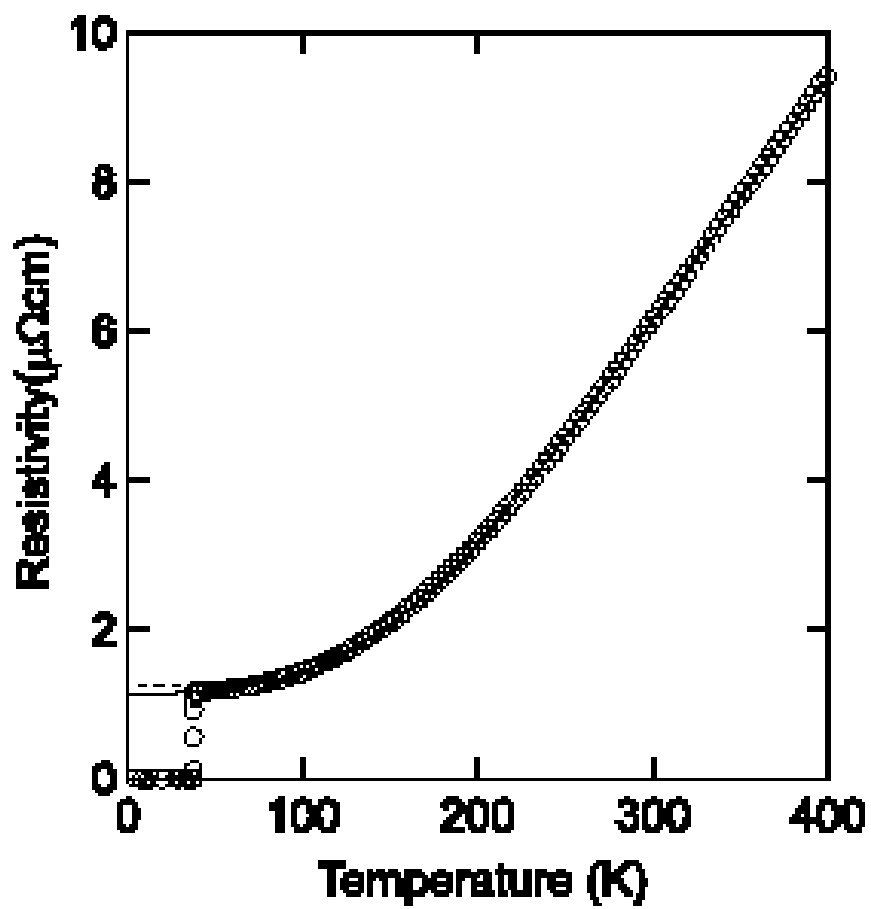


Figure 2.2 Temperature dependence of resistivity of MgB_2 [27].

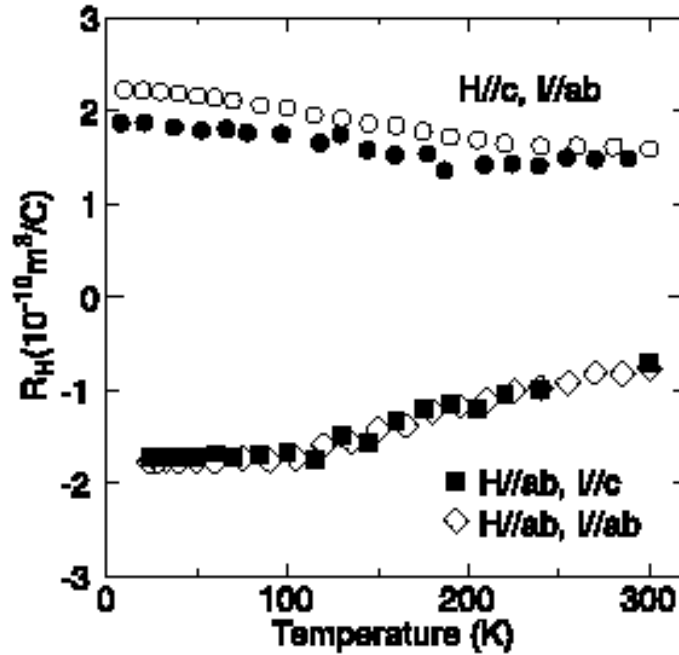


Figure 2.3 Hall coefficient in MgB_2 [27].

2.2.4 Superconducting Properties of MgB_2

Many comprehensive studies have been done on the superconducting properties of MgB_2 since the time of discovery (2001). Since the critical temperature of MgB_2 is well above 30 K, it seems as a potential industrial superconductor which can operate at 20 K. Operating above 20 K is very advantageous than the current available technology operating at boiling point of liquid helium (4.2 K). On the point of engineering view besides operate at relatively high temperature, a superconducting device should operate in a sufficiently high magnetic field. The current status of the critical current densities of MgB_2 superconductor in different magnetic fields for wire, tape, bulk and thin film samples are summarized in Table 2.1

Table 2.1 The recent status of critical current density (J_c) of MgB_2

4.2 K					
Type	Sheath material / Substrate	J_c at 8 T (A/cm ²)	J_c at 6 T (A/cm ²)	J_c at 2 T (A/cm ²)	Reference
WIRE	Ta, Cu			2.10^4	31
	Cu		10^4	6.10^4	32
	SS		2.10^4	10^5	33
	Fe		2.10^4	10^5	34
FILM	Al_2O_3	5.10^4	10^5	2.10^6	35
	$SrTiO_3$	$1.6.10^5$	$2.7.10^5$	8.10^5	36
	YSZ	10^5	2.10^5	2.10^5	37
BULK	-	10^2	$6. 10^2$	10^4	38
	-		10^2	5.10^4	39
20 K					
	Sheath material / Substrate	J_c at 4 T (A/cm)	J_c at 2T (A/cm)	J_c at 0 T (A/cm)	Reference
WIRE	Fe	2.10^3	5.10^4	5.10^5	40
	Ta			2.10^5	31
	SS		10^5		41
FILM	Al_2O_3		4.10^4	2.10^6	42
	$SrTiO_3$		1.710^5	2.10^6	36
	Al_2O_3			7.10^6	43
BULK		5.10^3	3.10^4	7.10^5	44
		10^3	7.10^3	8.10^4	45

As mentioned in the introduction part, recently there are two superconductors that can be the rivals of the MgB_2 superconductor, NbTi and Nb_3Sn . Their critical current density values at zero field, 8 Tesla are 10^7 A/cm², 8.10^4 A/cm² and 10^7 A/cm², 10^5 A/cm² respectively at 4.2 K. From Table 2.1 for wires and bulk samples of MgB_2 critical current density values are less than the values of superconductors in use at 4.2 K. Many groups have studied the chemistry and stoichiometry variation of MgB_2 . The field and temperature dependence of the critical current density (J_c), after introducing various additive elements or substitutions on the Mg or on the B site have been studied in bulk MgB_2 samples with the elements, Li, Na, Ca, Ag, Cu, Al, Zn, Zr, Ti, Mn, Fe, Co and C. However only Al has so far been found to really substitute for Mg yielding a solid solution with gradually decreasing transition temperature (T_c). Although all of the additives decrease the transition temperature, of among all additives mentioned above Ti, Zr_2O and SiC provides an improvement on the critical current density values in zero field

and especially in magnetic field. Zhao et al. [45] reported an increase of J_c after doping with Ti and Zr, which was interpreted as being due to nanosize defects at grain boundaries of MgB_2 [45]. As a type II superconductor in MgB_2 creating more pinning centers in the superconductor improves the J_c of the MgB_2 . In the Ti addition case, Ti does not occupy an atomic site in the MgB_2 , the TiB_2 phase grows at the grain boundaries of MgB_2 in nano size and behaves as pinning centers. Thus increases the critical current density. List of the additives, which has a positive improvement on the superconducting properties of MgB_2 are summarized in Table 2.2.

Table 2.2 Effects of additives on J_c of MgB_2 at 20 K.

20 K					
Type	Additive	J_c at 4 T (A/cm ²)	J_c at 2 T (A/cm ²)	J_c at 0 T (A/cm ²)	Reference
BULK		$2 \cdot 10^3$	$3 \cdot 10^4$	$5 \cdot 10^5$	31
	Ti	10^4	10^5	10^6	45
	Y_2O_3	$5 \cdot 10^3$	$8 \cdot 10^4$	$3.5 \cdot 10^5$	46
	SiC	$3 \cdot 10^4$	$2 \cdot 10^5$	$6 \cdot 10^5$	46

Moreover, effects of unreacted Mg on the normal state and superconducting properties of MgB_2 were studied by Jung et al. [47]. It was found that unreacted Mg improves the critical field and critical current density of the MgB_2 . Also, studies on the substitutional chemistry of MgB_2 indicated the inertness of Mg to MgB_2 even if at high temperatures. Therefore, Mg has been chosen as substitution in this study.

Addition to critical current density, critical fields (upper critical field, H_{c2} and irreversibility field, H_{irr}) of the superconductors are important parameters on the application point of view. The upper critical field of MgB_2 is anisotropic because of its layered structure. Recent measurements of H_{c2} on single crystals indicates that the H_{c2} parallel to the c axis is low about 3 to 4 Tesla at $T=0$ K. The H_{c2} value for H parallel to the ab plane is about 15-20 Tesla at $T=0$ K. The resultant anisotropy is (the ratio of the value parallel to ab plane to c plane) is ~ 4 [9]. The calculated values of the GL coherence length of the MgB_2 is $\xi_{ab} = 5-8$ nm and $\xi_c = 2-3$ nm. The mean free path (l_{ab}) of MgB_2 single

crystals is as large as 50-100 nm [48], which reveals that MgB_2 is in the clean limit ($l_{ab}/\xi_{ab} \gg 1$). On the other hand, in terms of applications the value of irreversibility field is important than upper critical fields of superconductors. Because the applications are limited by the irreversibility field. The value of irreversibility field for MgB_2 is about 8-12 Tesla for single crystals. The upper critical field and the irreversibility field strengths of MgB_2 are unfavorable for applications compared with Nb based superconductors. However the artificial introduction of impurities or defects may lead to reduction in ξ , and therefore an increase in H_{c2} by the Ginzburg-Landau-Abrikosov-Gorkov (GLAG) impurity effect. For instance for Fe clad wires an upper critical field of 28 T was reported by Flukiger et al [46]. Existence of anisotropic nature is also observed in the lower critical field (H_{c1}) of MgB_2 . The H_{c1} value parallel to c axis is 27.2 mT at $T=0$ K. The H_{c1} value parallel to ab axis is 38.4 mT at $T=0$ K [49]. From the polycrystalline data for H_{c1} , the magnetic penetration depth can be roughly estimated as $\lambda(0) \sim 170$ nm using $H_{c1} = \phi_0 \ln \kappa / (2\pi\lambda^2)$.

2.3 PREPARATION OF BULK SAMPLES FROM MgB_2

2.3.1 Synthesis of MgB_2

MgB_2 is an intermetallic compound, which was known since early 1950's. MgB_2 is obtained from the solid-state reaction between Mg and B atoms. The stoichiometry mixture of Mg and B ($\text{Mg} + 2\text{B}$) is annealed at 900°C for 2 hours in argon atmosphere in sealed tube. Due to the fact that Mg is a highly volatile element a sealed media is necessary. For applications the quality of the obtained powder is important. Hinks et al. studied the effects of stoichiometry variation on the sintering MgB_2 [50]. In this study Hinks studied the excess Mg and deficient Mg as in Mg_xB_2 , $0.5 \leq x \leq 1.3$ formula. Even if $x=0.5$ and $x=1.3$ the grow of MgB_2 phase is observed. A similar study was carried on by Ribeiro et al. and formation of MgB_4 phase in the Mg deficient samples was reported [51]. Both Hinks and Ribeiro observed the highest transition temperature in stoichiometric samples (Mg_xB_2 , $x=1$). Furthermore a decreasing residual resistivity ratio (RRR) is observed for Mg deficient samples. Consistently, an increasing RRR is observed

in samples, which has excess Mg. Different from Hinks, Ribeiro studied the effects of boron purity on the sample quality and the RRR of the samples. A higher RRR and lower resistivity $0.4 \mu \Omega\text{cm}$ was observed in the samples that have highest boron purity.

MgB_2 has very low fracture toughness. Therefore it is difficult to obtain dense MgB_2 bulk samples. The theoretical density of MgB_2 is 2.62g/cm^3 . There are several methods to obtain dense MgB_2 bulk samples. High density MgB_2 samples were prepared using hot isostatic pressing technique. In this study, the densities between $2.3\text{-}2.62 \text{ g/cm}^3$ were obtained which were very close to theoretical density of MgB_2 [52]. Since MgB_2 is not a stand-alone material for producing bulk samples, it needed to use some methods to produce bulk samples like wires. The widespread method for producing wires from brittle powders is Powder In Tube Method (PIT). Besides PIT method there is an alternate method for producing tapes, wires and bulk samples from brittle powders called Metal Matrix Composite Method (MMC). Specific information about these two methods will be given in the following sections.

2.3.2 Powder In Tube Method (PIT)

A very practical way of producing MgB_2 tapes and wires of industrial lengths, namely Powder In Tube method (PIT). The PIT process is very advantageous because of low material costs and relatively simple deformation techniques. Furthermore it is the only way of producing multi filamentary wires and tapes. As known from the Nb_3Sn and Bi-2223 wires multi filamentary wires withstand larger uniaxial and bending strains than single filaments and they exhibit a higher thermal stability due to the smaller cross section of the individual filaments. This method has been widely used for both traditional and HTS superconductors. In this method brittle superconducting powder is filled into a ductile metal tube and than swaged into small diameters for various applications. The schematic representation of PIT method used with Fe metal sheet is seen in Figure 2.4.

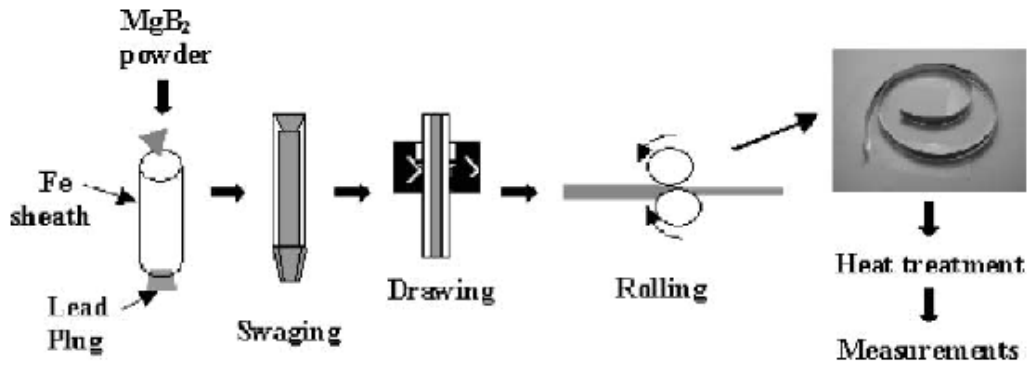


Figure 2.4 Powder In Tube Method.

Recently, many research groups produced wires and tapes successfully with PIT method either with or without an application of a heat treatment [53, 54, 55, 56]. Maintaining critical temperature (T_c) and critical current density (J_c) while improving mechanical properties of the superconductor during the mechanical deformation or following annealing process in PIT is essential. On the other hand, a possible reaction between metal and superconducting phase may relegate the superconducting properties of the wire. For this reason, substitutional chemistry of the superconducting material is important. Accordingly, the PIT method has been used to produce MgB_2 /metal composite wires with various metal sheaths such as stainless steel SS [56], Cu [54], Ag [54], Cu-Ni [56], and Fe [57, 58]. Iron was determined to be the best sheath material for MgB_2 wires providing high critical current density of $1.42 \times 10^5 \text{ A cm}^{-2}$ (4.2 K, 4T) and inertness to MgB_2 even with annealing at 900°C [58]. In Figure 2.5 SEM macrographs of cross section of monofilamentary Fe clad MgB_2 tape is seen. The transverse and longitudinal cross section of a deformed Fe/ MgB_2 are quite uniform and shown in Figure 2.5(a) and 2.5(b). The densification during the heat treatment can be clearly seen by comparing the SEM picture of a polished crossed section of MgB_2 core after deformation Figure 2.5(c) with one of the same core after annealing at 950°C for 30 minutes figure 2.5(d). The fill factor of the tape is very important for carrying high critical currents. In PIT heat treatment improves fill factor by densification. However, heat treatment may lead to a oxidation in the superconducting core. In the Fe clad tapes mentioned above XRD results showed that a increase in the amount of MgO. Fortunately in MgB_2 this amount of MgO behaves as pinning centers and improves the critical current density of

the tape [58]. The examples of PIT given above are tapes and wires prepared by exsitu preparation technique. On the other hand this technique can be used with insitu preparation technique. By this way Mg powder and B powder are filled into a metal sheath and annealing is followed. Using insitu preparation technique new pinning centers can be introduced except intrinsic pinning centers as MgO, by doping with different elements like Ti [45].

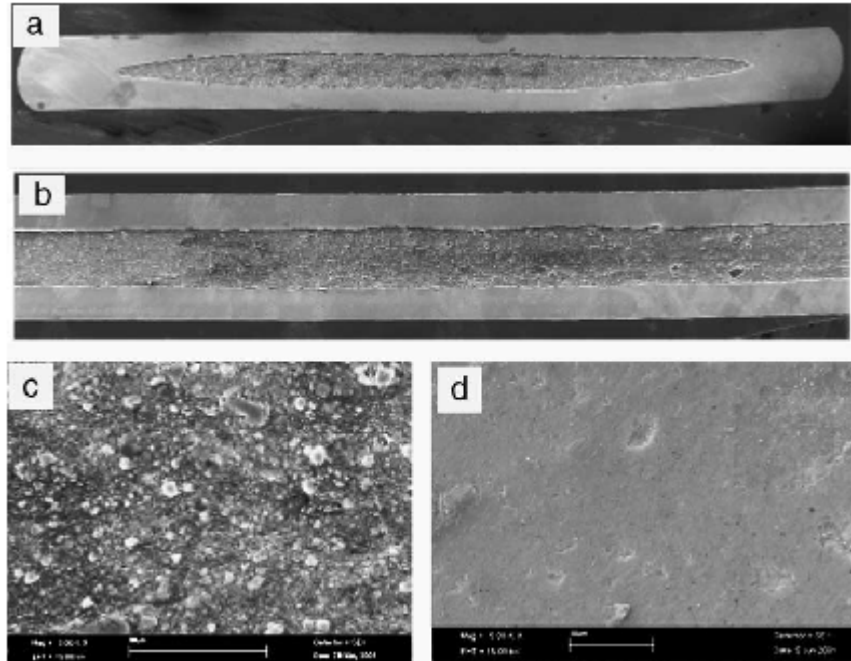


Figure 2.5 SEM Images of Fe clad tapes a) Transverse b) Longitudinal c) After Deformation d) After Annealing.

2.3.2 Metal Matrix Composite Method (MMC)

An alternative approach to PIT is metal matrix composite fabrication method where a ceramic perform (consisting of packed powders, whiskers or fibers) is infiltrated usually under pressure to overcome capillary forces, by a metallic melt which is subsequently solidified. Metal matrix composites (MMC) in general consists of at least two components; i.e. one obviously is the metal matrix, and the second component is in general an intermetallic compound in the particulate form. Metal matrix improves

ductility and the fracture toughness of the resulting composite while the particulate constituent increases the hardness and Elastic modulus. MMC method is new method for superconductors. Most common ways of obtaining MMC are liquid infiltration and hot pressing. Dunand and Giunchi et al. obtained MgB_2 metal matrix composites with liquid infiltration method with Mg metal phase [59, 60]. Dunand used both traditional infiltration method (commercial MgB_2 and liquid Mg) and reactive infiltration method (B powders and liquid Mg) following a heat treatment. In this study MgB_2/Mg composites produced liquid infiltration of Mg into MgB_2 were observed to have a density about 2.07 g/cm^3 and a transition temperature of 38 K. However MgB_2/Mg composites produced by liquid infiltration of Mg into B powders were observed to be very brittle after heat treatment and have critical temperature below 37 K [59]. As mentioned above MMC method is new method for superconductors and there are a few studies about this method only used with liquid infiltration. There is no study about MgB_2 MMC s produced by hot pressing technique.

For producing MMCs some physical properties of the metal matrix phase should be taken into account (such as melting point of the metal, electrical conductance) to obtain composites, which has sufficient characteristics.

In this study MgB_2/Mg composites were produced by MMC method using hot pressing technique. Mg is chosen as the metal matrix because of its low melting point (653°C) and its inertness to MgB_2 at very high temperatures. Some basic properties of Mg is given in Appendix, Table A2. To investigate the possibility of producing superconducting wires from MgB_2 , pellets of MgB_2/Mg composites were fabricated at various temperatures and pressures. The specific information about the experimental routine will be given in the chapter 3. In practice superconductors are not generally used in the form of pellets but fabrication of pellets provides cost effective and easy method to test several properties such as electrical resistance measurements, critical current measurements and mechanical tests.

CHAPTER 3

EXPERIMENTAL METHODS

3.1 Material

In this study, commercially available MgB_2 powders obtained from Alfa Aesar (31-44 micron average particle size, 98.5% purity) and Mg obtained from Alfa Aesar (31-44 micron average particle size, 99.9999% purity) was used. The X-Ray Diffraction Patterns of used MgB_2 , and Mg powders were given in Figure 3.1 and Figure 3.2. The MgB_2 powder has a purity of 98.5% and the residual 1.5% is MgO.

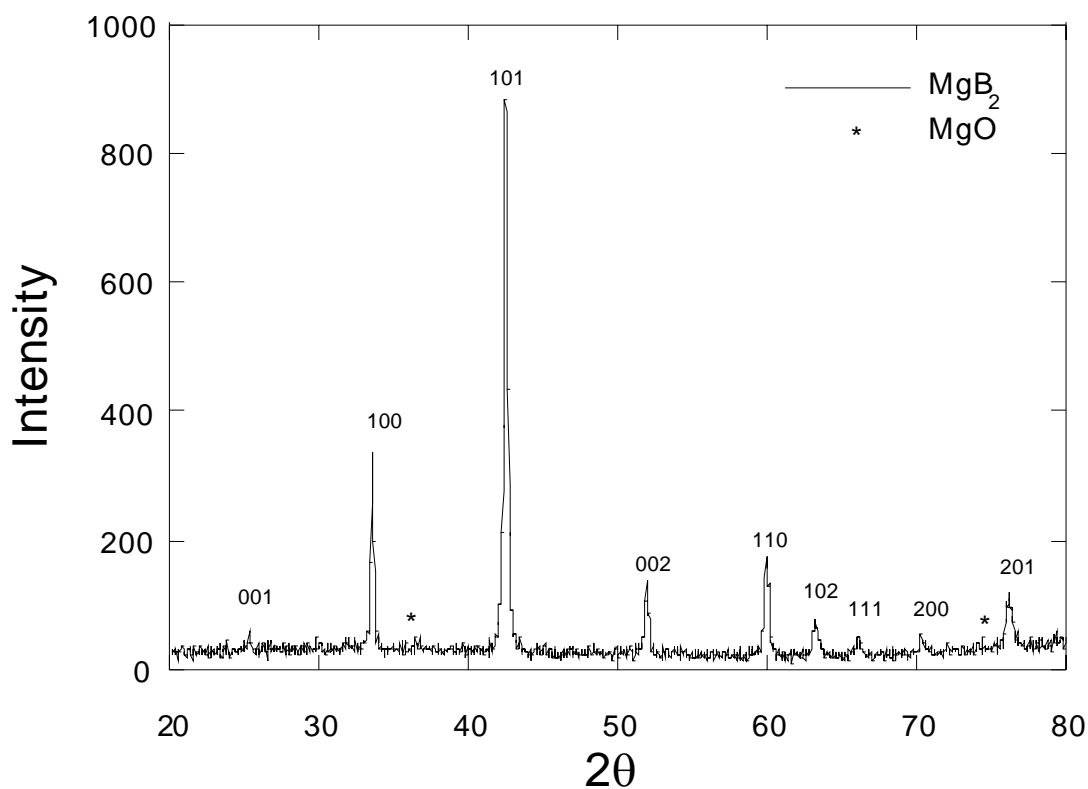


Figure 3.1 XRD peaks of commercial MgB_2 .

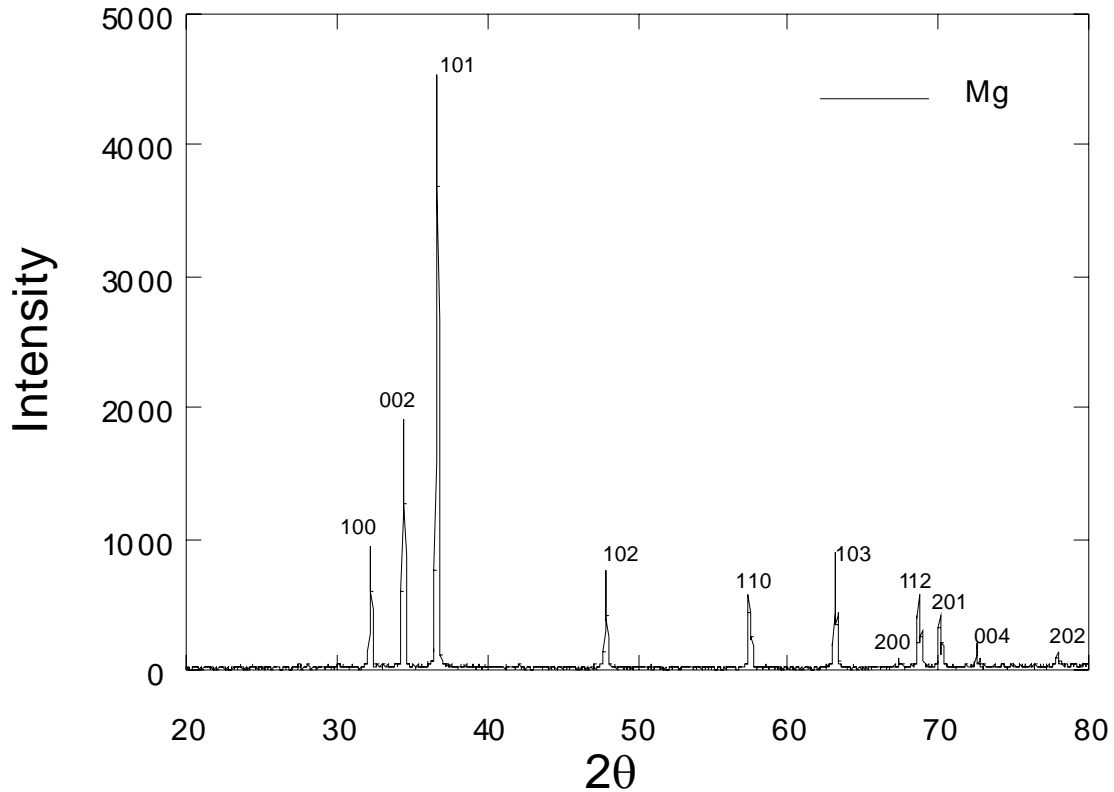


Figure 3.2 XRD peaks of commercial Mg.

3.2 Experimental

Commercial MgB_2 powder (Alfa Aesar) and Mg powders (325 mesh 99.99% purity) were used for the fabrication of MgB_2/Mg composites. The weight ratio of Mg to MgB_2 was 0, 5%, 10%, 15% and 20% for different set of samples; MgB_2 and Mg powders were mixed homogenously and uniaxially pressed under pressure of 0.5 GPa and 1 GPa in a metallic dye. The dye was heated to 400, 500 and 550°C and kept at these temperatures for 2 hours in air as shown in Figure 3.3 the temperature was controlled with a variac and a thermocouple connected to Omega temperature controller. Based on previous studies oxidation of MgB_2 in air begins at 400°C however oxidation is not expected to be very strong under 700°C [61]. Therefore selected temperatures for producing MgB_2/Mg composites are convenient to prevent the oxidation of MgB_2 to MgO in huge amounts. Melting point of Mg is 654 °C hence no preponderant oxidation reaction is expected for Mg at selected temperatures especially for 400 and 500 °C. For electrical and microstructural characterization, fabricated pellets were about 0.9 mm in height and

15.6 mm diameter. I prepared pellets 7 mm in height and 10 mm in diameter for the mechanical testing. Three set of samples with the given weight ratios at different temperatures namely 400, 500 and 550 °C were prepared under 0.5 GPa pressure. Two sets of samples were prepared at 400 and 500 °C under 1 GPa. For mechanical tests two sets of samples prepared at 0.5 GPa pressure, 400 and 500 °C. To have more reliable results three pellets were produced for every weight ratio and temperature for mechanical tests. Totally 30 pellets fabricated for mechanical tests and totally 25 pellets were produced for further research. Figure 3.3 summarizes the fabrication process of MgB₂/Mg composites.

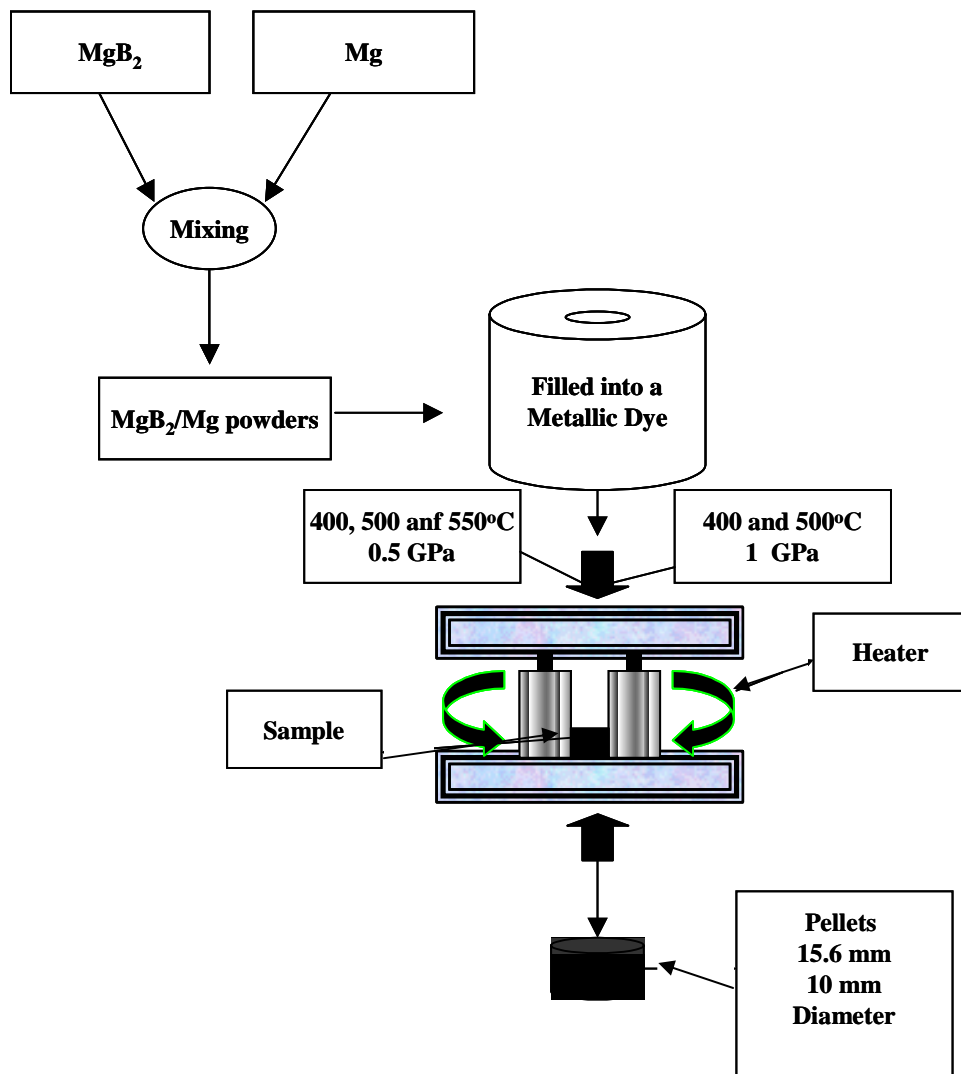


Figure 3.3 Experimental set up for sample preparation.

3.3 MEASUREMENTS

In this study, we have used both resistivity measurements and magnetization measurements for determining T_c of MgB_2/Mg composites. The traditional four-probe method was used for determining the T_c . The pellets in diameters 10 and 15.6mm were cut into $10 \times 1.5 \times 0.9 \text{mm}^3$ for resistivity measurements. Addition to temperature dependence of resistivity of samples DC magnetization measurements were carried on samples cooled at 18 mT magnetic strength using a vibrating sample magnetometer. Since this study examines the potential of MgB_2/Mg composites for applications the mechanical properties of fabricated composites are very important. For this purpose, the compressive mechanical testing were performed to measure elastic modulus and strength at failure values of the composites. XRD, SEM and EDX techniques were used for phase identification and microstructural studies.

3.3.1 Determination of Transition Temperature

The DC resistivity of a sample is measured by the voltage drop across a specimen when a current of known magnitude passes. Since the transition temperature of a superconductor depends on both applied field and on current the most accurate T_c can be measured approximately at low fields and low currents. A typical current is 1mA. The terminals used for measuring the voltage pass little current when connected high impedance voltmeter. These terminals are distinct from those used for passing the main part of the current through the specimen, where voltage drops in both leads and contacts are significant. Figure 3.4 shows a schematic diagram of four probes connected to a specimen whose temperature is measured by temperature sensor close to the specimen and similarly well connected on the surface of cold head. The thermal contact between the specimen and the surface of the cold head is important on that purpose we use a thermal conductive grease between the specimen and the surface. The contacts on the specimen actually four point resistance measurements is used to minimize the effects of lead resistance primarily in low resistance measurements. Additionally, the corrections can be made for thermal emf's by reversing the current at each reading and taking the average voltage generated across the specimen for the two direction of current flow. The

measurements were carried on with a computer controlled Cryo system, Figure 3.5. This system provides us to have the temperature dependence of samples between 15 K and room temperature. The system consists of an Oxford Edward Cryostat 1.5, Coolstar cold head model 2/9, Keithley 220 current source, Keithley 2582 nanovoltmeter, Edward mechanical pump, ITC 502 temperature controller GPIB connectors and IEEE 488.2 interface cards for the connection to the computers. The data acquisition software was written in Objectbench. The corrections for thermal emf's by reversing the current at each reading was done by the software.

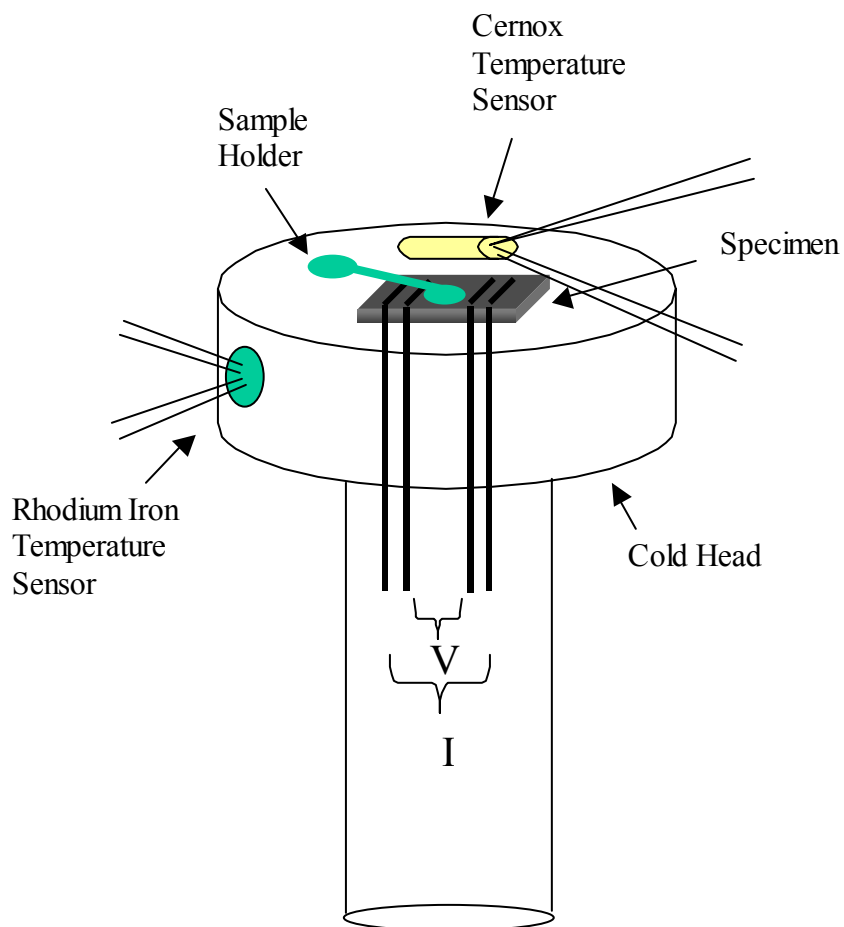


Figure 3.4 Four point probe resistivity measurement.

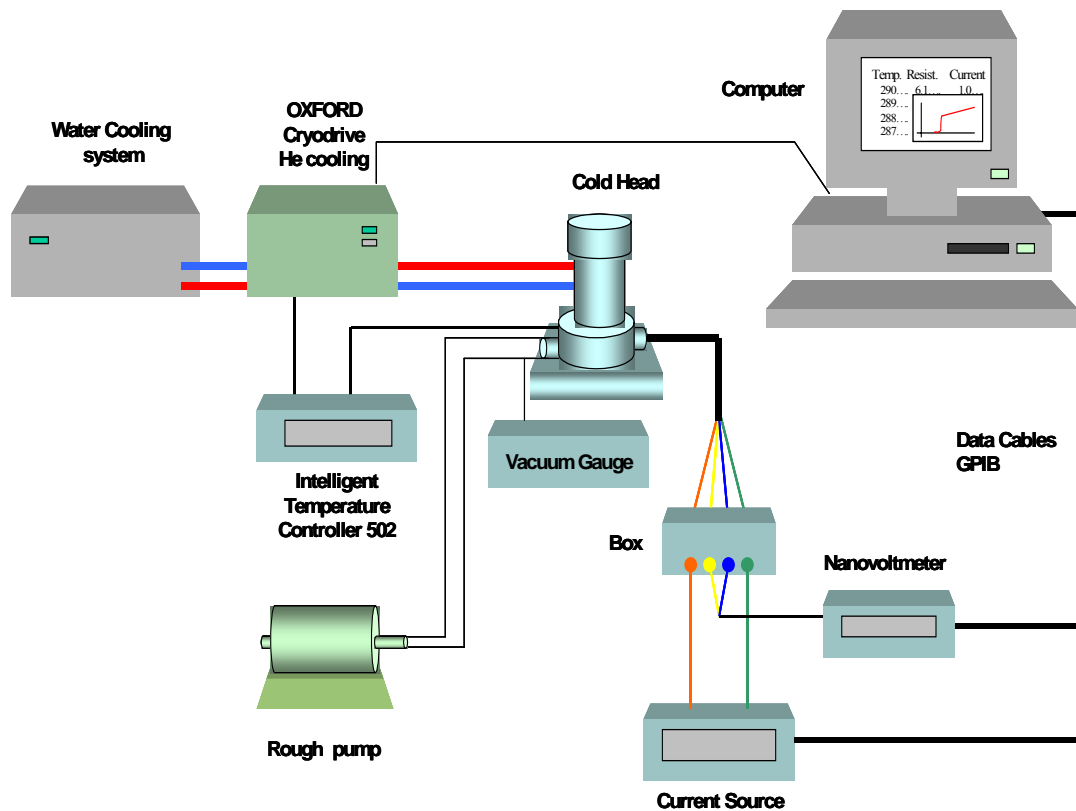


Figure 3.5 The CRYO Pump System.

Standard four probe resistivity measurements give very accurate results about the critical temperature of the superconductors. However, the magnetization measurements have some advantages and differences from resistivity measurements in the following ways:

- i) Specimens do not require electrical contacts, but can be small or even of powder form.
- ii) A magnetic signal is given at temperatures below transition temperature, when resistivity $\rho \rightarrow 0$, so the magnetic signal can be used to characterize the material at this low temperatures
- iii) The superconducting volume fraction can be estimated
- iv) The signal is given even if the superconducting path is not continuous.

- v) Critical current density can be measured independently of contacts and of intergranular weak links.

The magnetization measurements were done at Technical University of Istanbul, therefore I do not mention about the experimental set up of this measurement technique in this thesis.

3.3.2 Mechanical Tests

Since the goal of this thesis is to investigate the applicability of MgB_2/Mg composites for producing wires and targets, the characterization of the mechanical properties of fabricated composites is very important. For that purpose, the compressive mechanical tests were performed using a universal mechanical testing machine. From these tests Stress-Strain curve of the each composite is obtained. A typical stress-strain curve obtained from MgB_2/Mg composites is given in Figure 3.6.

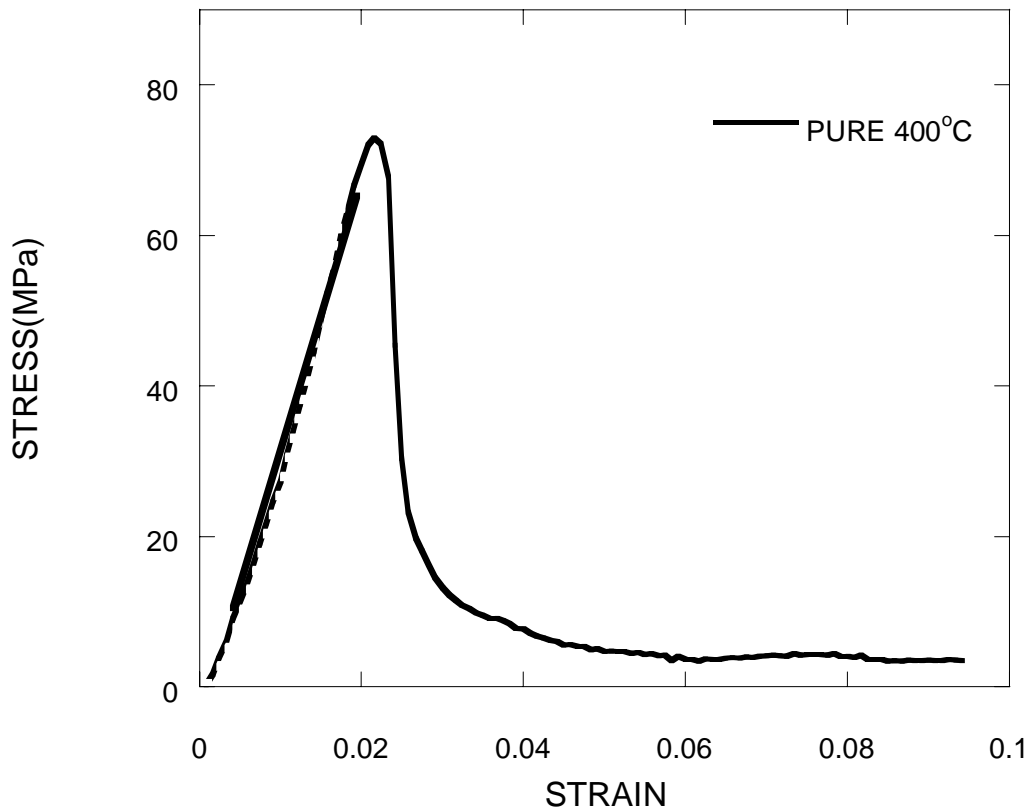


Figure 3.6 A Typical Stress-Strain Curve Obtain From MgB_2/Mg Composites

The stress value in this curve is calculated by dividing applied load (Kgf) to the loading area (m^2). The strain values in this curve are calculated by dividing the stroke (mm) to initial size of the specimen (mm), therefore strain is unitless.

The Fracture Strength (σ_f) values of the specimens were obtained from maximum stress level and Elastic Modulus values are calculated from the slope of the initial part of the stress-strain curve illustrated in Figure 3.7.

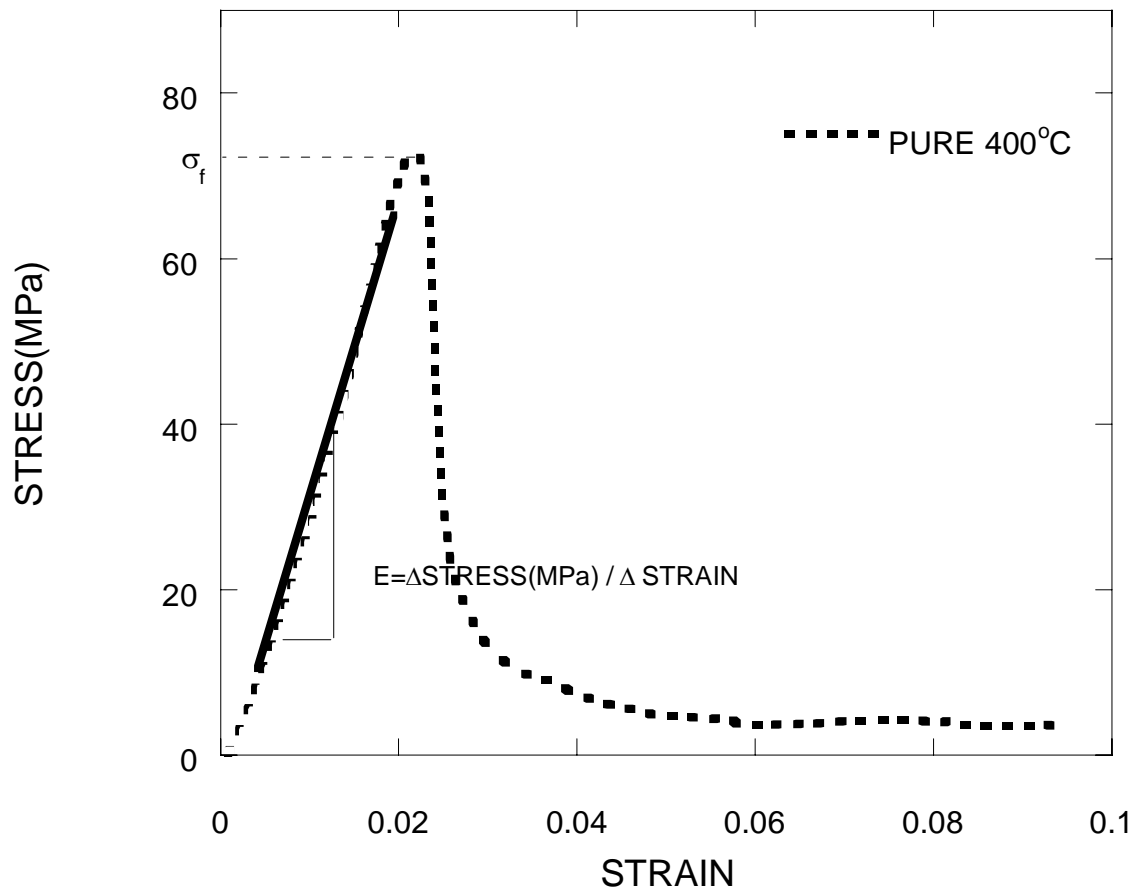


Figure 3.7 Determination of Fracture Strength and Elastic Modulus Values From Stress-Strain Curves.

CHAPTER 4

RESULTS AND DISCUSSIONS

We investigate the potential of MgB₂/Mg composites for various applications such as producing wires. To demonstrate the microstructural properties of MgB₂/Mg, XRD, SEM and EDX measurements were carried on composites. Superconducting properties of the produced composites were characterized by resistivity-temperature and magnetization-temperature measurements. Since this study examines the potential of MgB₂/Mg composites for applications, the mechanical properties of fabricated composites are very important. For this purpose, the compressive mechanical testing was performed to have an idea about the mechanical properties of MgB₂/Mg composites. In this part, I will mainly mention about the results of these measurements.

4.1 Density and XRD Results

MgB₂/Mg composites were produced using hot uniaxial pressing for fabricating dense samples. Producing dense samples is significant in terms of investigating the basic properties of MgB₂ more precisely. Effect of Mg constituent, effect of temperature and pressure on density of the samples were investigated and summarized in Table 4.1 and Table 4.2.

Sample density in these tables was calculated from dividing the pellet mass to pellet volume. Since we are mixing two materials with different density, we can calculate the theoretical density of resulting mixture according to their weight fraction with conventional methods. These theoretical densities for different weight fraction Mg constituent is calculated and given in the fourth column of the Table 4.1 and Table 4.2. The ratio of the sample density of to theoretical density will give us an idea about the porosity ratio in MgB₂/Mg composites.

Table 4.1 Density of the samples prepared at 0.5 GPa.

Press. Temp. C	Mg %	Sample Density (g/cm ³), d1	Theoretical Density (g/cm ³), d2	d1/d2
400	PURE	1.85	2.62	0.7047
400	5	1.84	2.56	0.7201
400	10	1.90	2.49	0.7636
400	15	1.93	2.45	0.7895
400	20	1.96	2.41	0.8132
500	PURE	1.85	2.62	0.7060
500	5	1.85	2.56	0.7239
500	10	1.91	2.49	0.7689
500	15	1.92	2.45	0.7842
500	20	2.01	2.41	0.8341
550	PURE	1.80	2.62	0.6870
550	5	1.83	2.56	0.7148
550	10	1.87	2.49	0.7510
550	15	1.89	2.45	0.7714
550	20	1.99	2.41	0.8257

Table 4.2 Density of the samples prepared at 1GPa.

Press. Temp. C	Mg %	Sample Density (g/cm ³), d1	Theoretical Density (g/cm ³), d2	d1/d2
400	PURE	2.10	2.62	0.8024
400	5	2.10	2.56	0.8209
400	10	2.11	2.49	0.8470
400	15	2.09	2.45	0.8528
400	20	2.12	2.41	0.8777
500	PURE	2.15	2.62	0.8204
500	5	2.17	2.56	0.8475
500	10	2.09	2.49	0.8383
500	15	2.17	2.45	0.8843
500	20	2.12	2.41	0.8810

The ratio of the sample density to theoretical density is given in the last columns of the Table 4.1 and Table 4.2. For instance if this ratio is 0.88 this means this sample is 88% of the theoretical density and it has 12% voids inside. Table 4.1 shows the density of the samples prepared at 0.5 GPa pressure for various temperatures. According to the Table 4.1 for all temperatures it is seen that Mg addition increases the sample density. For all sets of samples the composites have a porosity ratio of approximately 30% in the unsubstituted samples and porosity ratio improves to the value of 19% with addition of 20% Mg. The positive effect of Mg constituents on sample density is also observed in Table 4.2 for the samples prepared at 1 GPa pressure. From table 4.1 and 4.2 it is seen that pressing temperature has no major effect on sample density because the density of the samples prepared at same pressure and same amount of Mg constituent at different temperatures has close density values. The density values given in Table 4.2 are in the range of 2.1 and 2.2 g/cm³ and from the last column. It is seen that the porosity ratio is between 12% and 20%. Thus this shows that pressure has major effect on sample density when Table 4.1 is compared with Table 4.2.

The powder XRD patterns of the MgB₂/Mg composites prepared at 400, 500, 550 °C, 0.5 GPa, and 400, 500 °C, 1 GPa are shown in Figure 4.1 to Figure 4.5. The intensity of each pattern is normalized to their maximum 2θ values. As seen in the figures, the main phase for MgB₂/Mg composites is MgB₂. As the Mg amount increases in composites, Mg peaks become detectable in the spectrum. As seen in the Figure 4.1, as Mg constituent increases intensity of the Mg peaks increases. To show the phases more precisely, the powder XRD patterns of commercial MgB₂ and Mg are added to the plots as reference patterns. It was found that there is no major reaction between MgB₂ and Mg. However, presence of small amount of MgO secondary phase is seen in the pattern. Previous studies on the oxidation behavior of MgB₂ in air reveals that oxidation of MgB₂ to Mg begins about 400 °C but not very extensive up to 700 °C [61]. Since trace amount of MgO is seen in the XRD pattern of commercial MgB₂ powder, presence of MgO may be originated from commercial MgB₂ powder or probably formed during hot pressing process. The advantage of small amount of MgO might enhance the superconducting properties of the composite wires acting as pinning centers and increasing the critical current density J_C. There are a number of studies, which indicate the formation of MgB₄

secondary phase in case of hot pressing [62]. Existence of MgB_4 in superconducting composite is an objectionable situation because it is generally situated around grain boundaries as an insulating layer and degrades the superconducting properties [51]. According to our XRD patterns, no obvious MgB_4 phase is seen in MgB_2/Mg composites. For the samples prepared at 0.5 GPa, there is no significant difference in the XRD patterns of 400 °C samples (Figure 4.1) and 500 °C samples (Figure 4.2). However, from Figure 4.3 it is seen that formation of MgO is more obvious in the samples prepared at 550 °C. Since the melting point of Mg is 654 °C, the oxidation of Mg to MgO is faster above 500 °C. The results obtained from samples prepared under 1 GPa pressure (Figure 4.4 and Figure 4.5) are consistent with results obtained from samples prepared at 0.5 GPa pressure. There is no reaction between the superconducting MgB_2 and Mg addition and trace amount of MgO is observed in the composites.

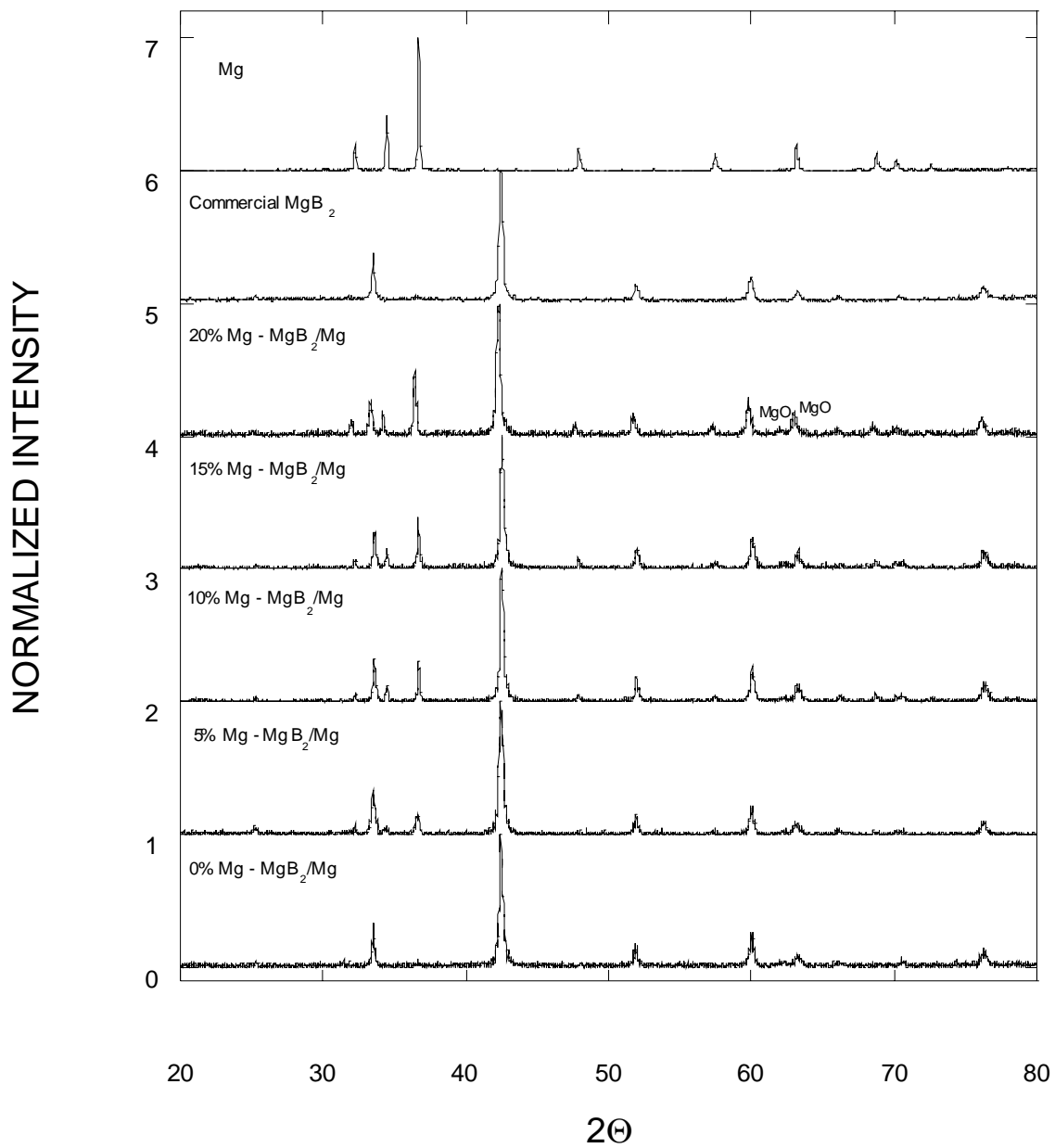


Figure 4.1 The powder XRD pattern of MgB₂/Mg composites prepared at 400°C, 0.5 GPa and commercial MgB₂, Mg.

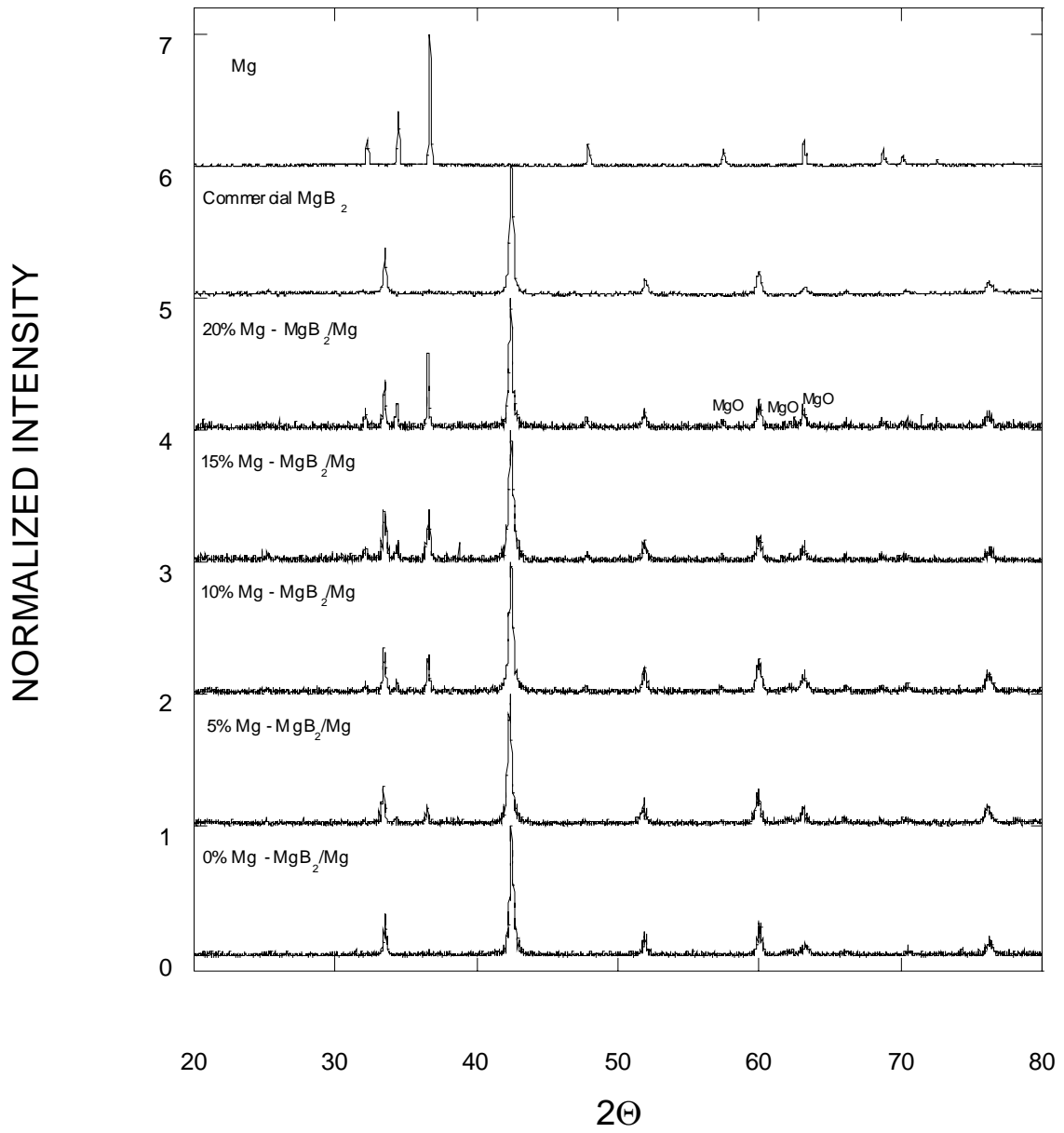


Figure 4.2 The powder XRD pattern of MgB₂/Mg composites prepared at 500°C, 0.5 GPa.

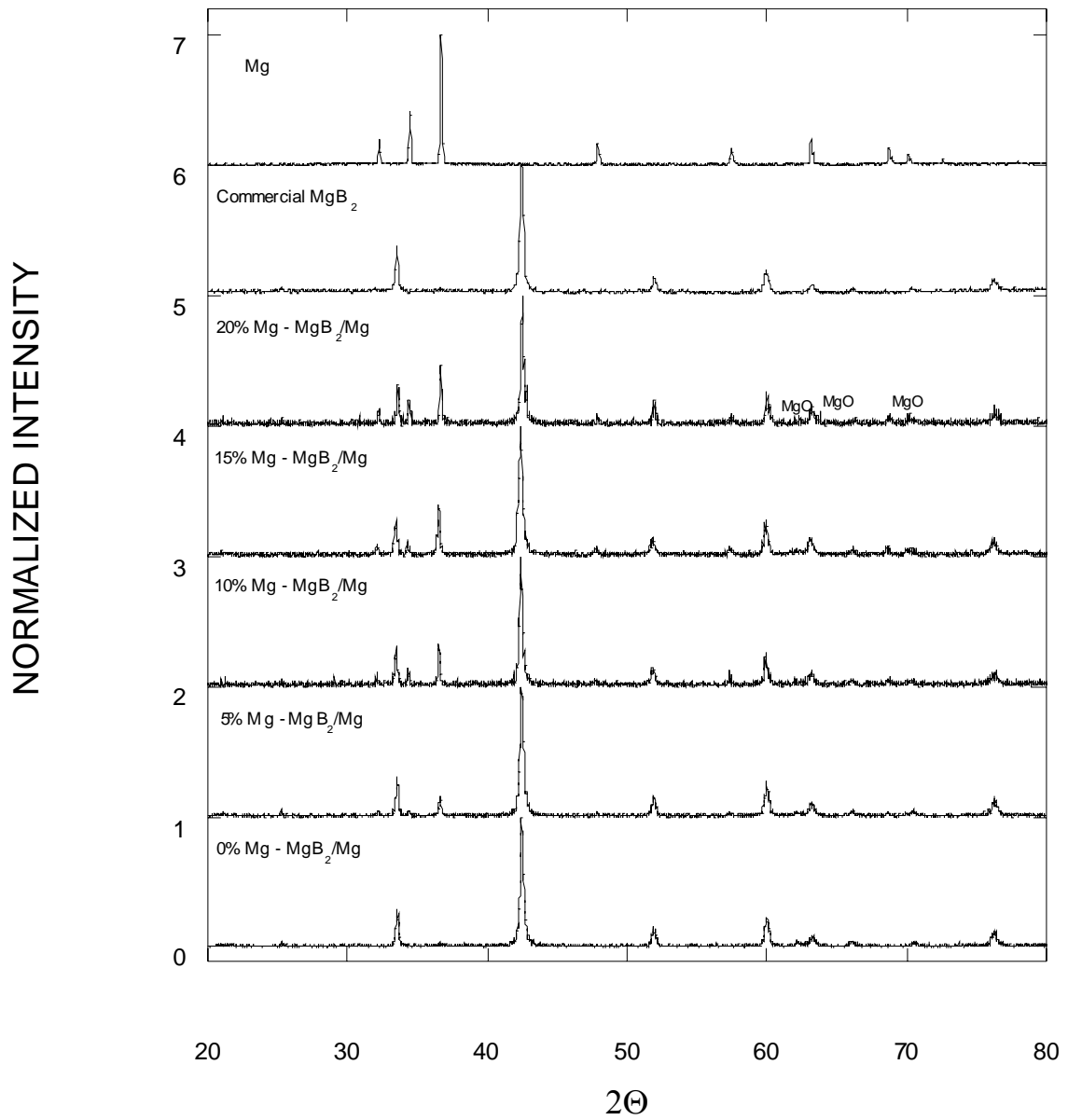


Figure 4.3 The powder XRD pattern of MgB_2/Mg composites prepared at 550°C, 0.5 GPa.

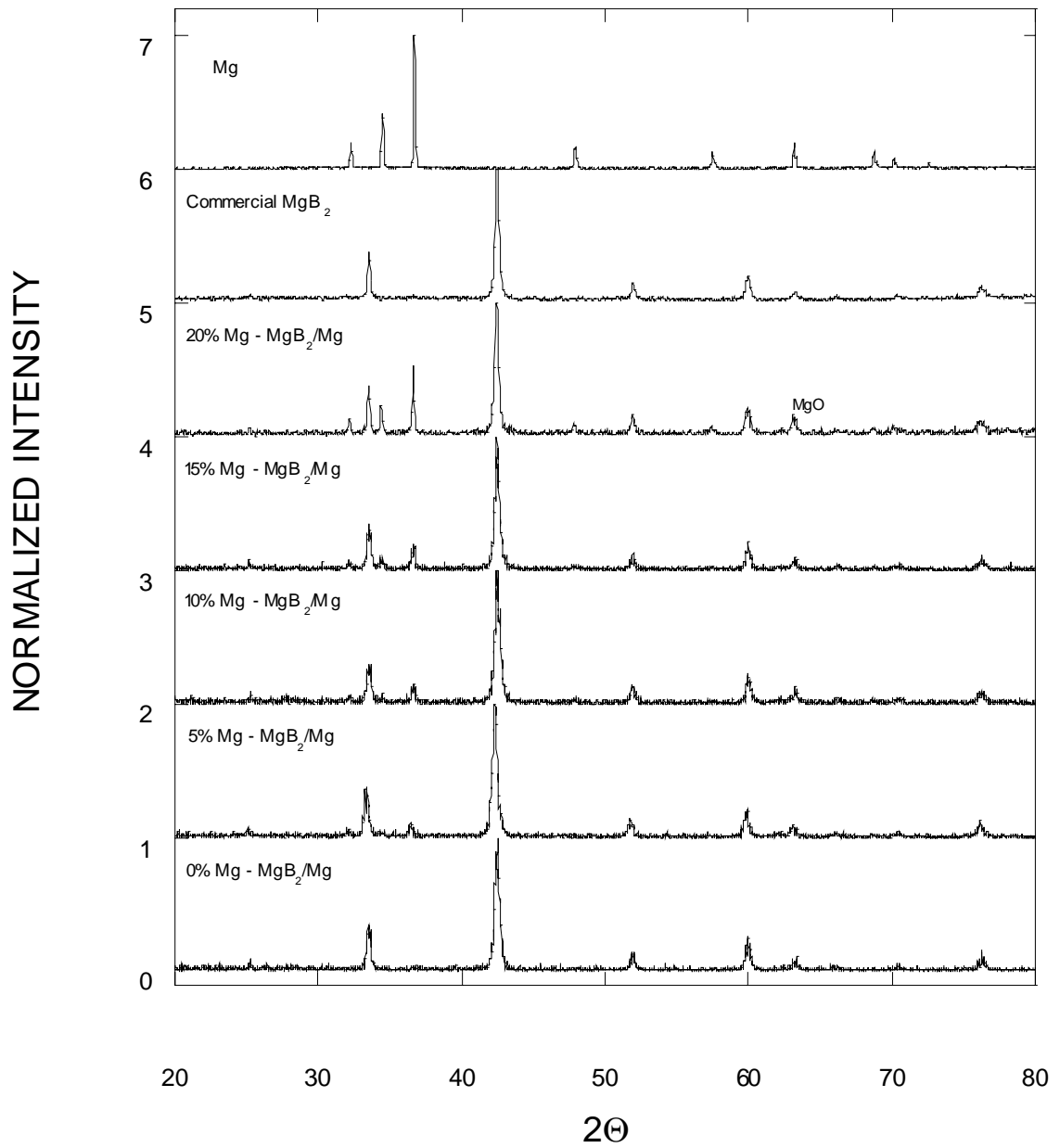


Figure 4.4 The powder XRD pattern of MgB₂/Mg composites prepared at 400°C, 1 GPa.

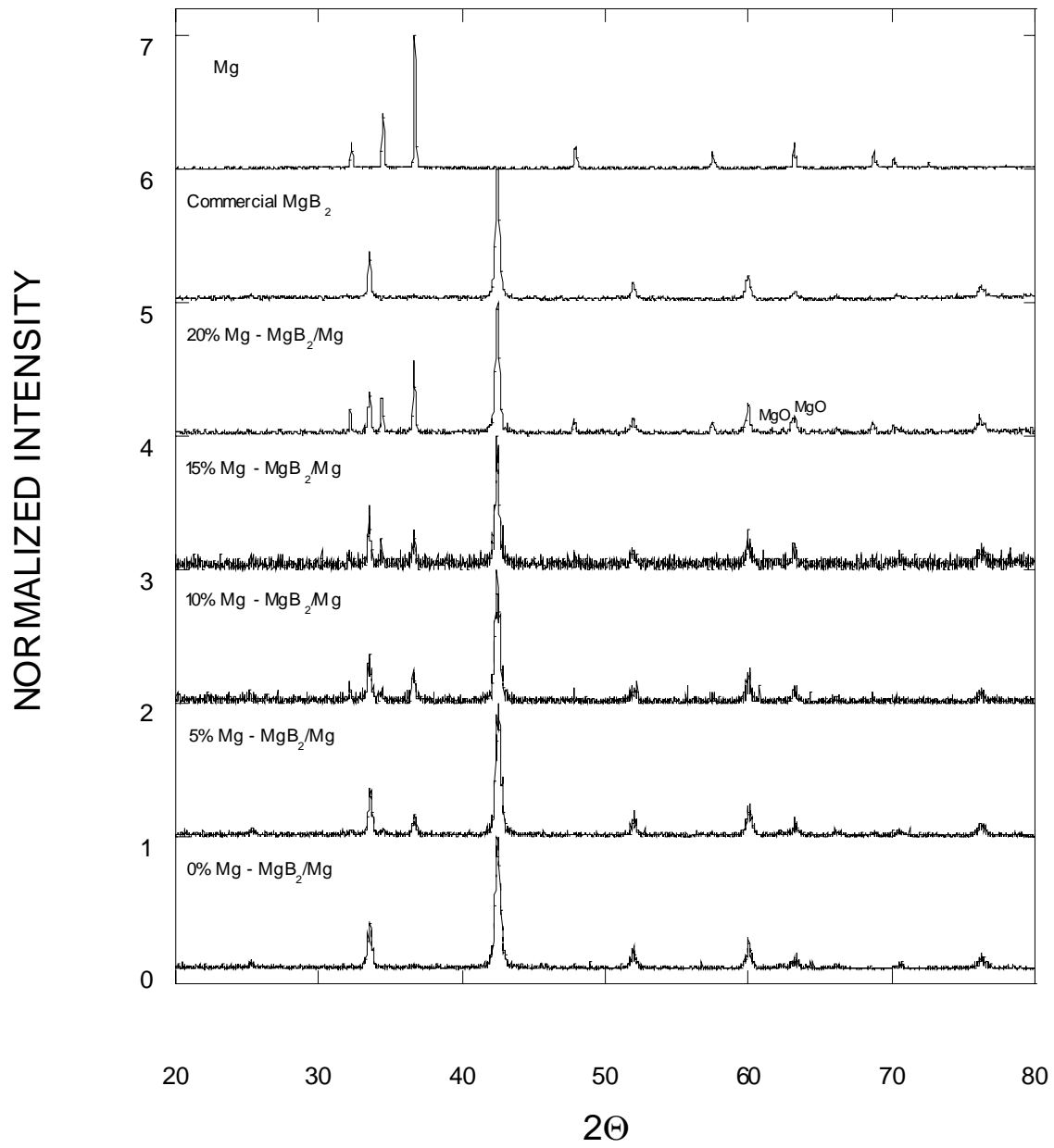


Figure 4.5 The powder XRD pattern of MgB_2/Mg composites prepared at 500°C , 1 GPa.

4.2 SEM and EDX Results

Scanning Electron Microscopy (SEM) analyses were done on MgB_2/Mg composites to characterize the microstructural properties such as average grain size and pore size. For that purpose, the fracture surface images were obtained from SEM analyses. We have been only able to study unpolished surfaces because of surface contaminations in the polishing process and surface fracturing. The main disadvantages of fracture surface analysis are the presence of many layers on each other with different depths. Actually, the samples prepared at 1 GPa were convenient for metallurgical processes like polishing for SEM analyses but to have coherency between the samples prepared at 0.5 GPa, all the SEM images are obtained from fracture surfaces. To investigate the stoichiometry variations formed during heating process and to examine the chemical contents of microstructure of composites Electron Dispersive X-Ray spectroscopy (EDX) analyses were carried on MgB_2/Mg composites. The presence or absence of secondary phases was also examined with EDX.

Figure 4.6 shows the fracture surface images of samples prepared at 400 °C, 0.5 GPa and 550 °C, 0.5 GPa. To make precise interpretation, the same magnification is chosen in these figures. Consistent with density measurements a densification is observed from top to bottom as the Mg constituent increases. In Figure 4.6 on the left hand side the set of samples prepared at 400 °C, 0.5 GPa is seen and on the right hand side the set of samples prepared at 550 °C, 0.5 GPa is seen. Temperature has no considerable effect on the density of the samples according to density measurements. Consistently from Figure 4.6, it is seen that temperature has no considerable effect on porosity ratio. SEM images illustrated that average grain size for 400 °C, 0.5 GPa and 550 °C, 0.5 GPa samples is between 200 nm - 500 nm and between 100 nm - 400 nm respectively. Similarly from the figure it is seen that pore size decreased in the samples prepared at 550 °C compared to samples prepared to 400 °C. Almost in all of the samples there are compacted pieces of Mg surrounded with MgB_2 particles. It seems that these Mg phases planking a relatively large area formed after flow of softened Mg pieces, especially at higher temperatures. Softened Mg begins to flow in the composite. The flow of excess Mg in the composites at 550 °C is more effective than lower temperatures. The densification may be formed as a result of this Mg flow.

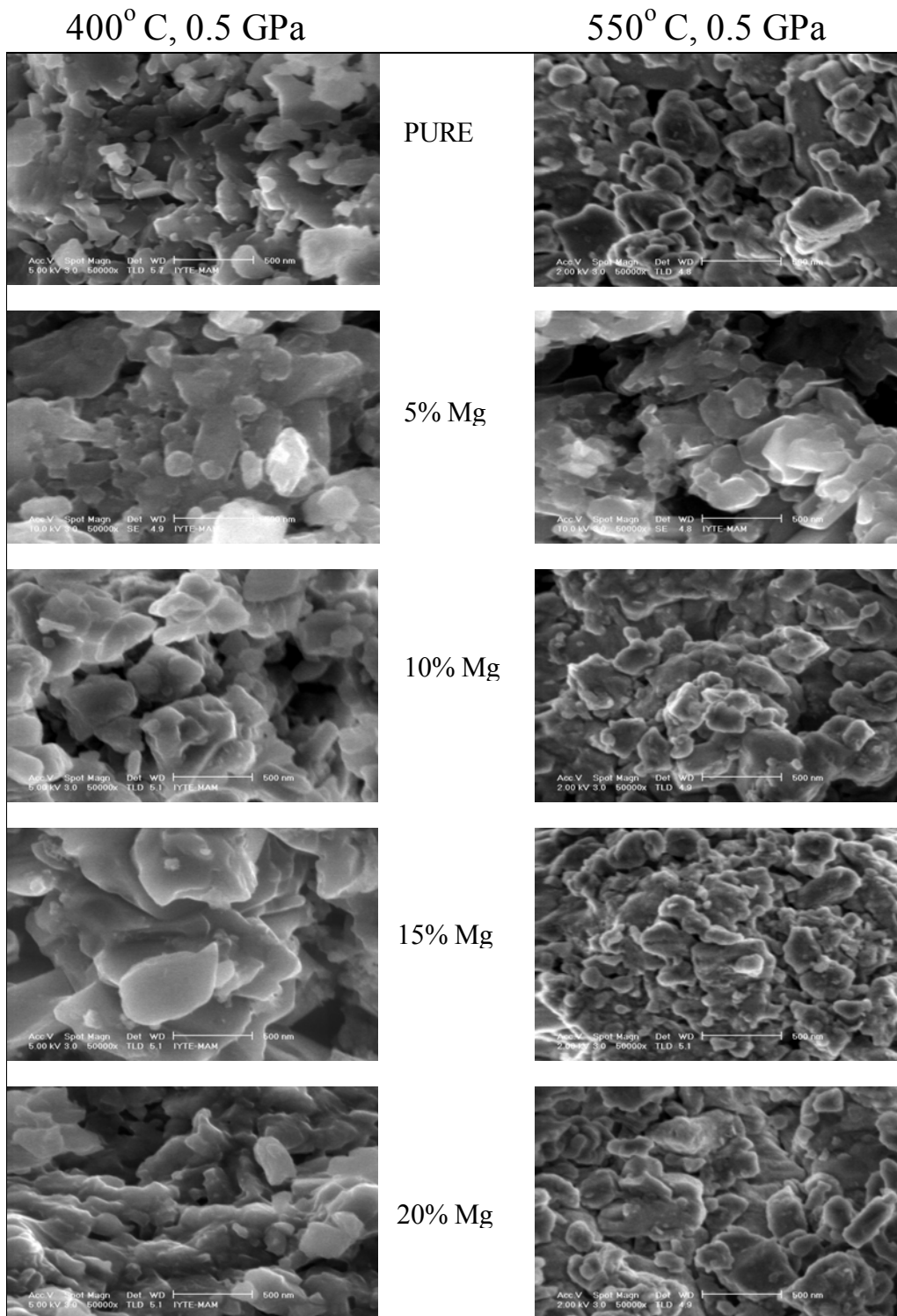


Figure 4.6 SEM fracture surface images of the samples prepared at 400 and 550°C, 0.5 GPa respectively.

Density results show that sample preparation pressure has major effect on the densities of the samples. Figure 4.7 demonstrates the SEM fracture images of the samples with 5% excess Mg prepared at same temperature but different pressures is seen. At the left hand side samples prepared at 0.5 GPa is seen and at the right hand side samples prepared at 1 GPa is seen. The images at the top of the Figure have scale of 1 μm and images at the bottom have a scale of 2 μm . The images reveals that the sample prepared at 1 GPa seems denser than the sample prepared at 0.5 GPa.

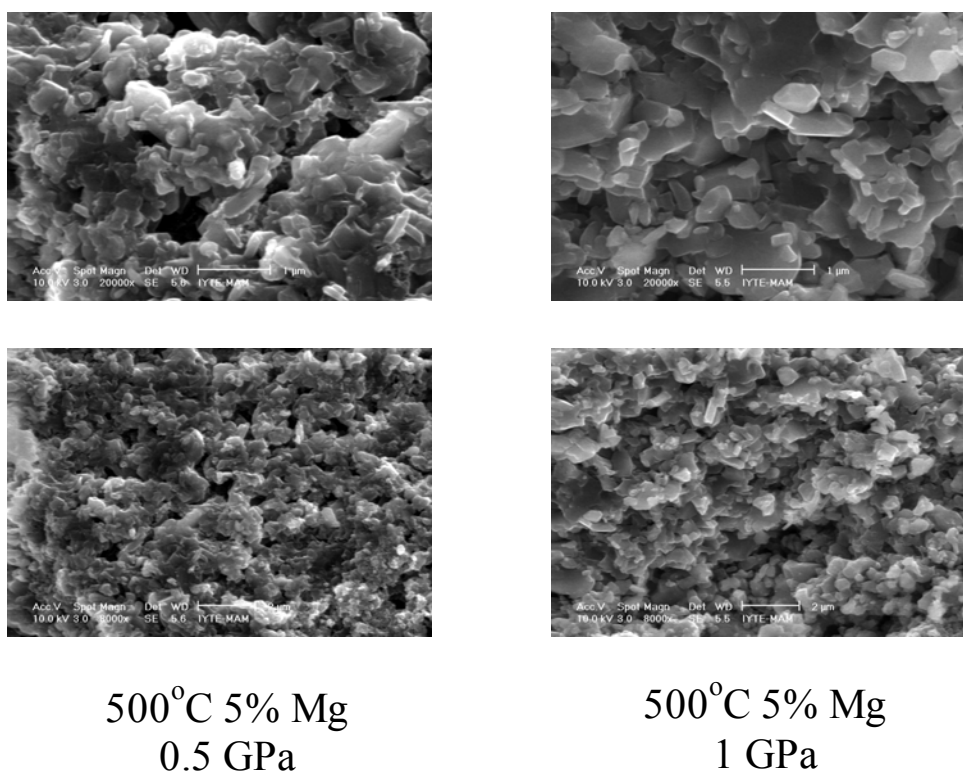


Figure 4.7 SEM fracture surface images of the samples prepared at 0.5 GPa and 1 GPa, 500°C respectively.

XRD diffraction measurements revealed that there exists more oxidation in the samples prepared at 550°C. EDX analyses were carried on samples given in Figure 4.8, to analyze the elemental variations with changing temperature. To obtain more reliable data,

five EDX data are taken from the each sample and average values are given in boxes next to the images.

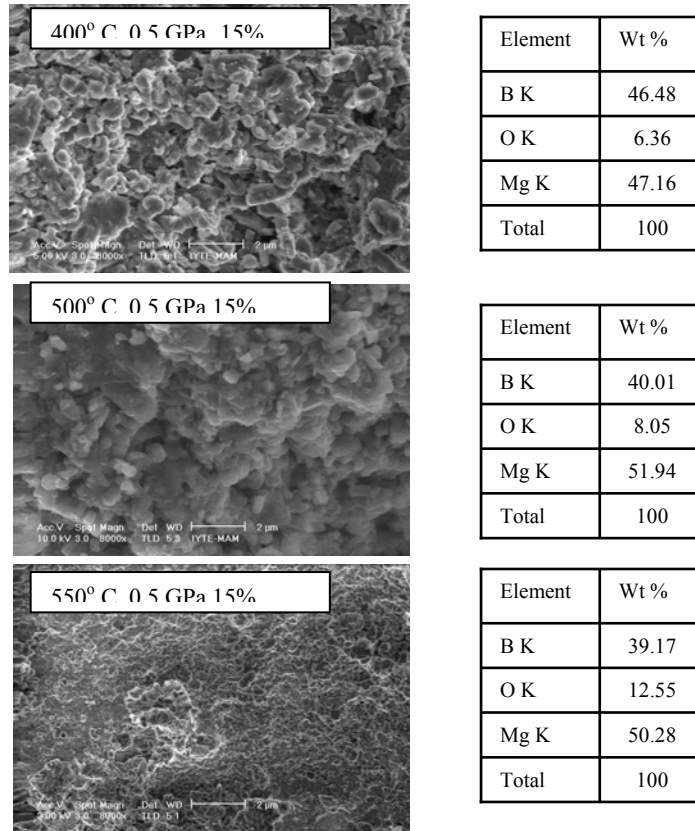


Figure 4.8 SEM and EDX analyses results of the samples prepared at different temperatures.

Figure 4.8 shows that increasing the sample preparation temperature above 500 °C make oxidation processes faster. While increasing the temperature from 400 °C to 500 °C, the oxygen weight ratio goes to 8.05% from 6.36%. However, increasing temperature 550 °C gives an oxygen weight ratio of 12.55%.

4.3 Resistivity and Magnetization Results

Since the simplest explanation of superconductivity is the loss of resistivity below a certain temperature, the transition temperature (T_c), the determination of this temperature is very important. There are mainly two methods for determining transition temperature; the measurements on temperature dependence of sample resistivity and temperature dependence of magnetization. In this study, both temperature dependence of resistivity and magnetization were carried on samples for determining the critical temperatures of produced samples. On the point of physics the temperature, which the transition begins is important, called onset critical temperature. However, on the point of engineering view the temperature that zero resistivity is very important called zero critical temperature. So what will be the critical temperature of the material? There should be standardization for determining the critical temperature. Zero point approach is appropriate for industrial use. In this routine a tangential line to a part of curve in the normal state region is drawn. The value of the temperature at the intersection of the transition curve and line with 90% and 10% heights of the tangential line are denoted by $T_{c10\%}$ and $T_{c90\%}$, respectively and the transition width, ΔT_c is defined as $T_{c90\%} - T_{c10\%}$. Similarly the transition temperature is the 50% height of the tangential line and denoted by T_c [63]. In this study, ΔT_c values for resistivity measurements were calculated using this technique. Figure 4.9 demonstrates the application of this technique for a MgB_2 sample prepared with hot pressing method. Generally the T_c is the value of the temperature at the intersection of the curve at the 50% height of the tangential line. In this study the transition temperatures of the samples were determined using this method. As mentioned above, addition to resistivity measurements magnetization measurements were done on the samples. The transition width, ΔT_c , was determined by taking the first derivative of the magnetization data in Figure 4.10. The width of the 50% height of the peak is supposed to be the transition width of the sample, Figure 4.11.

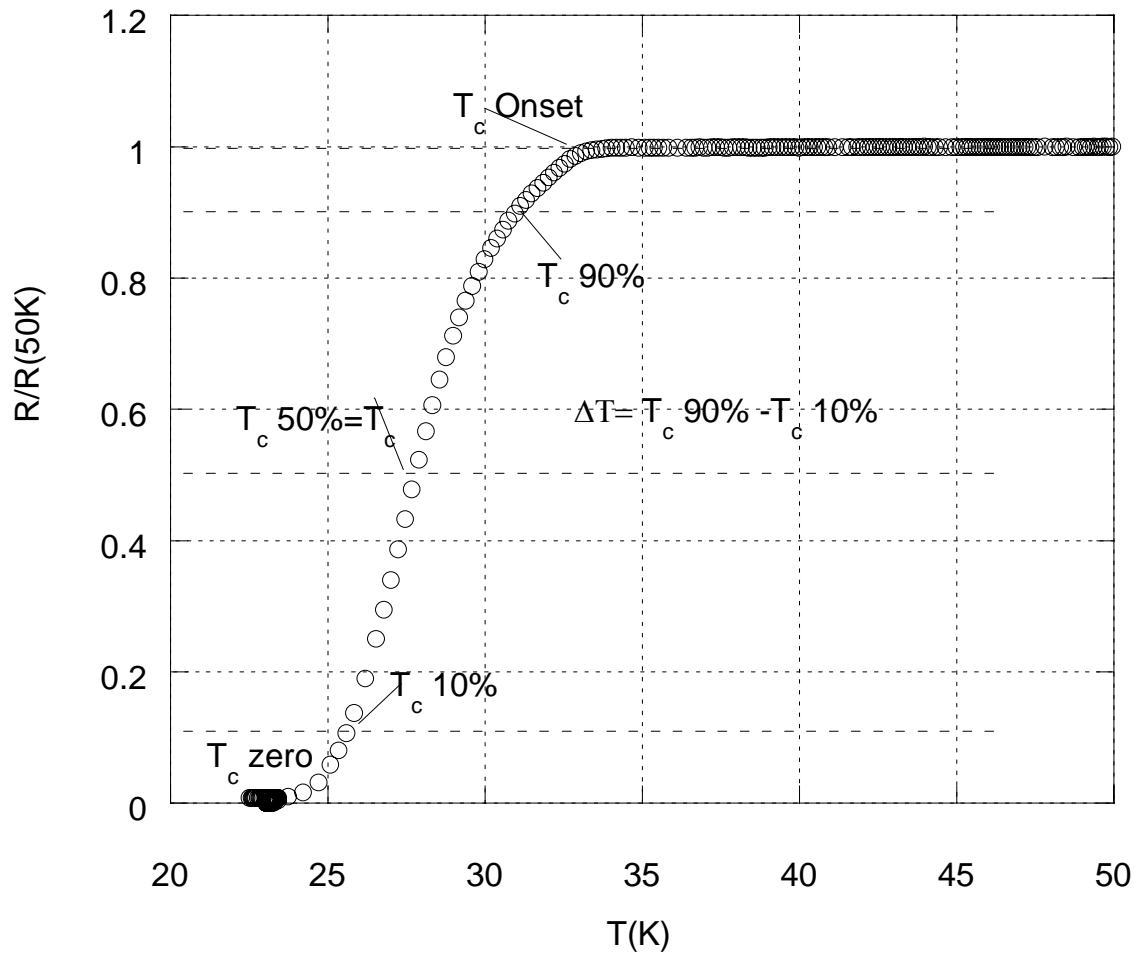


Figure 4.9 Determination T_c from Resistivity versus Temperature curves.

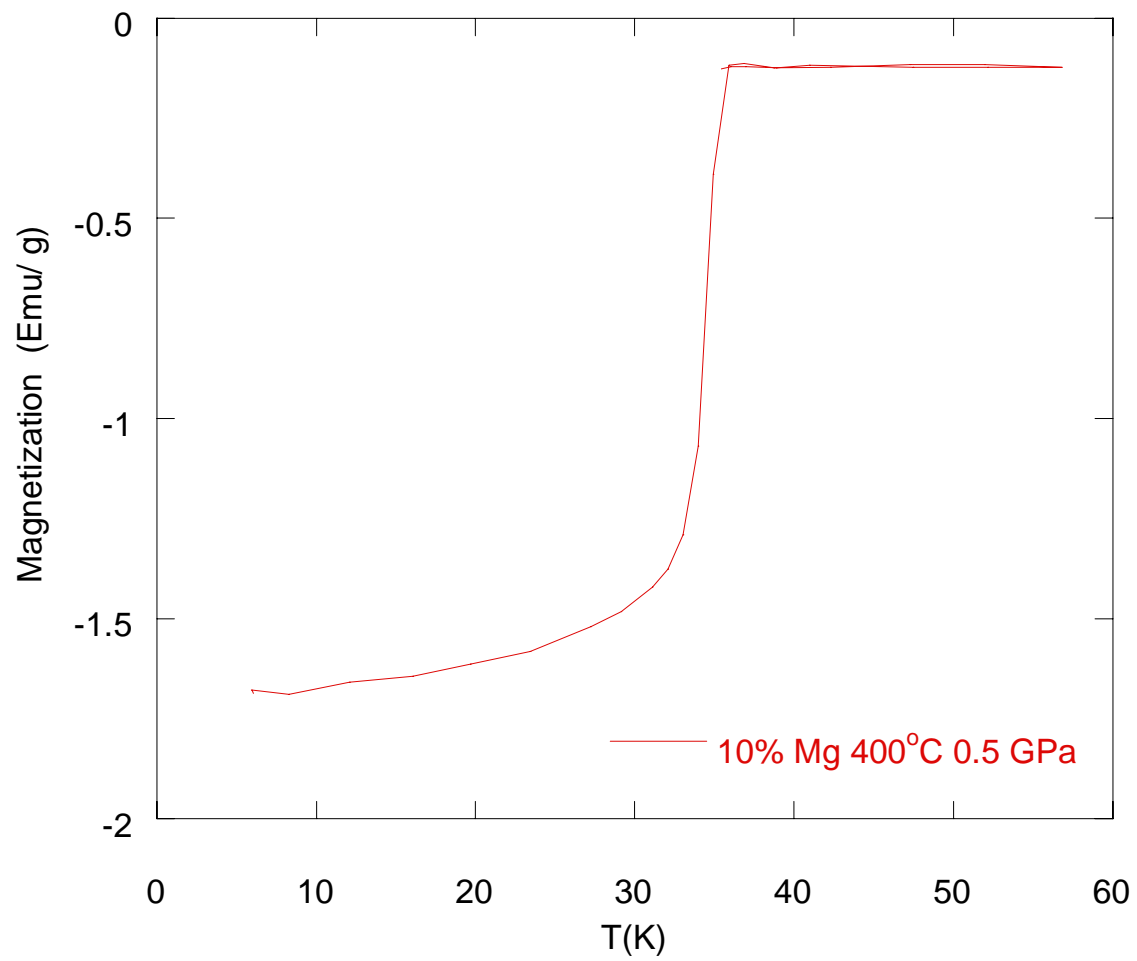


Figure 4.10 A magnetization versus Temperature curve.

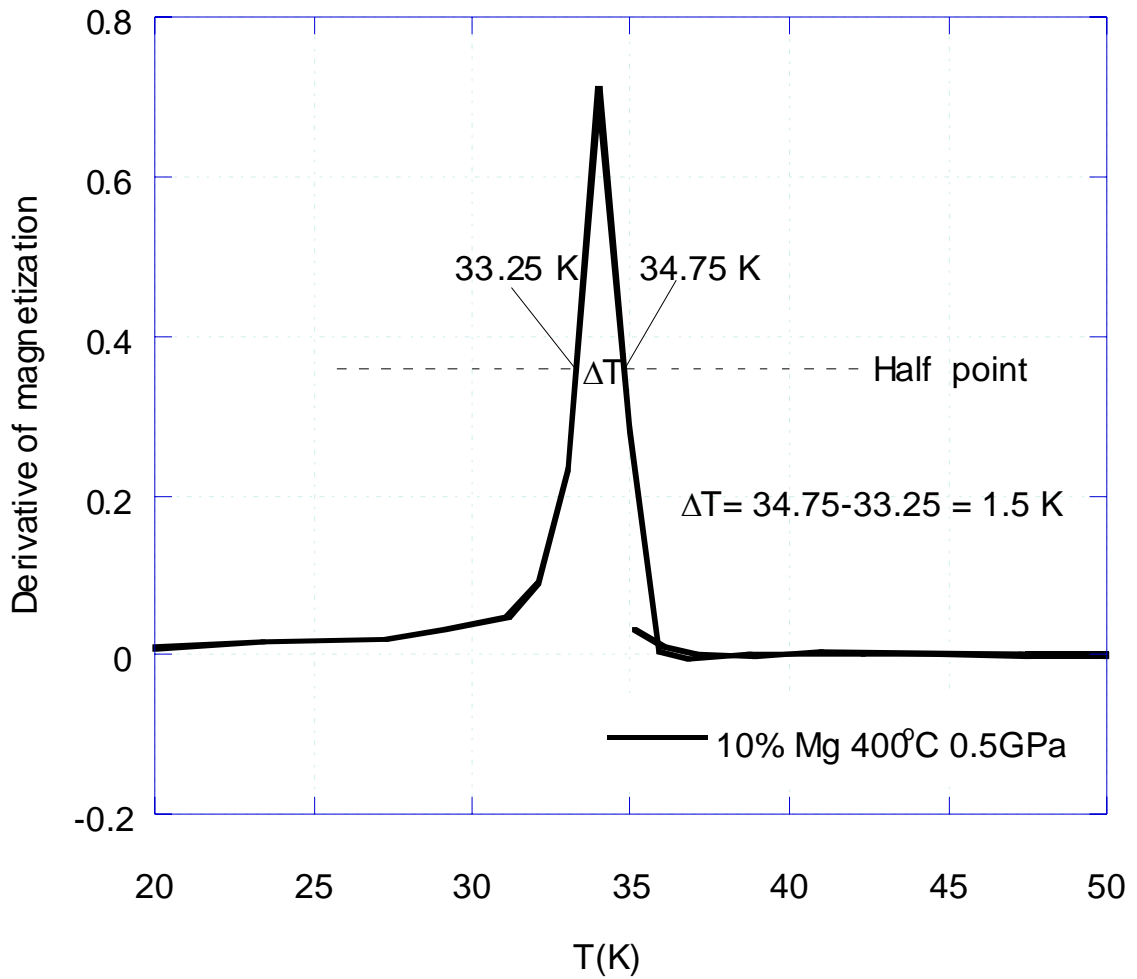


Figure 4.11 Derivative of the data given in figure 4.3.2.

From Figure 4.12 to Figure 4.16 the temperature dependence of the resistivities of the samples prepared at 400, 500, 550 °C (0.5 GPa) and 400, 500 °C (1 GPa) is given. The resistivity in these figures are normalized to their value at 50 K. Additionally from these graphs the T_c , ΔT and T_c^{Onset} values are determined and given in the Table 4.3 to 4.7.

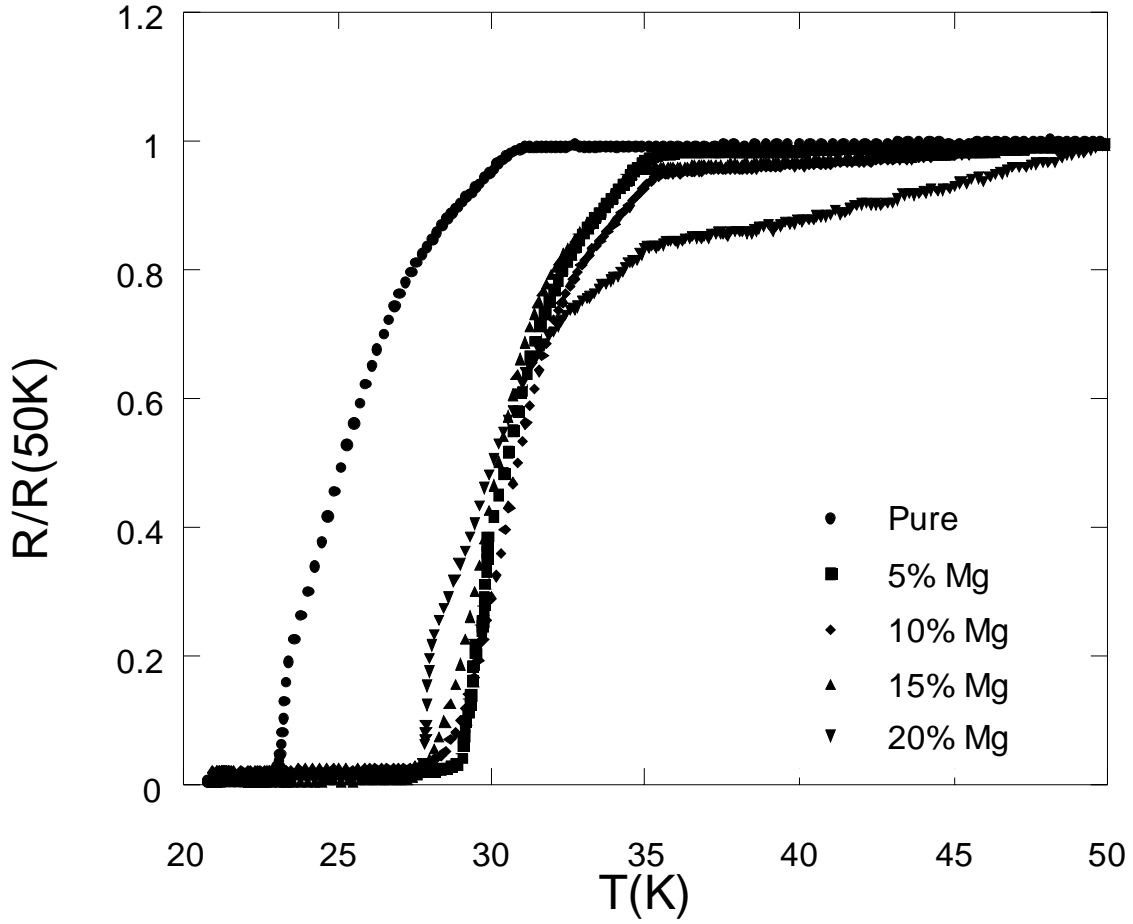


Figure 4.12 Temperature dependence of normalized resistivity of MgB_2/Mg composites prepared at 400°C , 0.5 GPa.

Table 4.3 The T_c , ΔT and T_c^{Onset} values MgB_2/Mg composites prepared at 400°C , 0.5 GPa.

Pres.T emp. C	Mg %	T_c 90%(K)	T_c 10%(K)	T_c ONSET(K)	T_c ZERO(K)	ΔT (K)	T_c Mid(K)
400	PURE	29.43	23.20	30.90	23.50	6.23	25.25
400	5	33.90	29.33	35.40	29.13	4.57	30.40
400	10	33.80	28.70	35.60	28.06	5.10	30.88
400	15	33.12	28.36	34.68	27.87	4.76	30.11
400	20	32.70	27.80	35.16	27.48	4.90	29.62

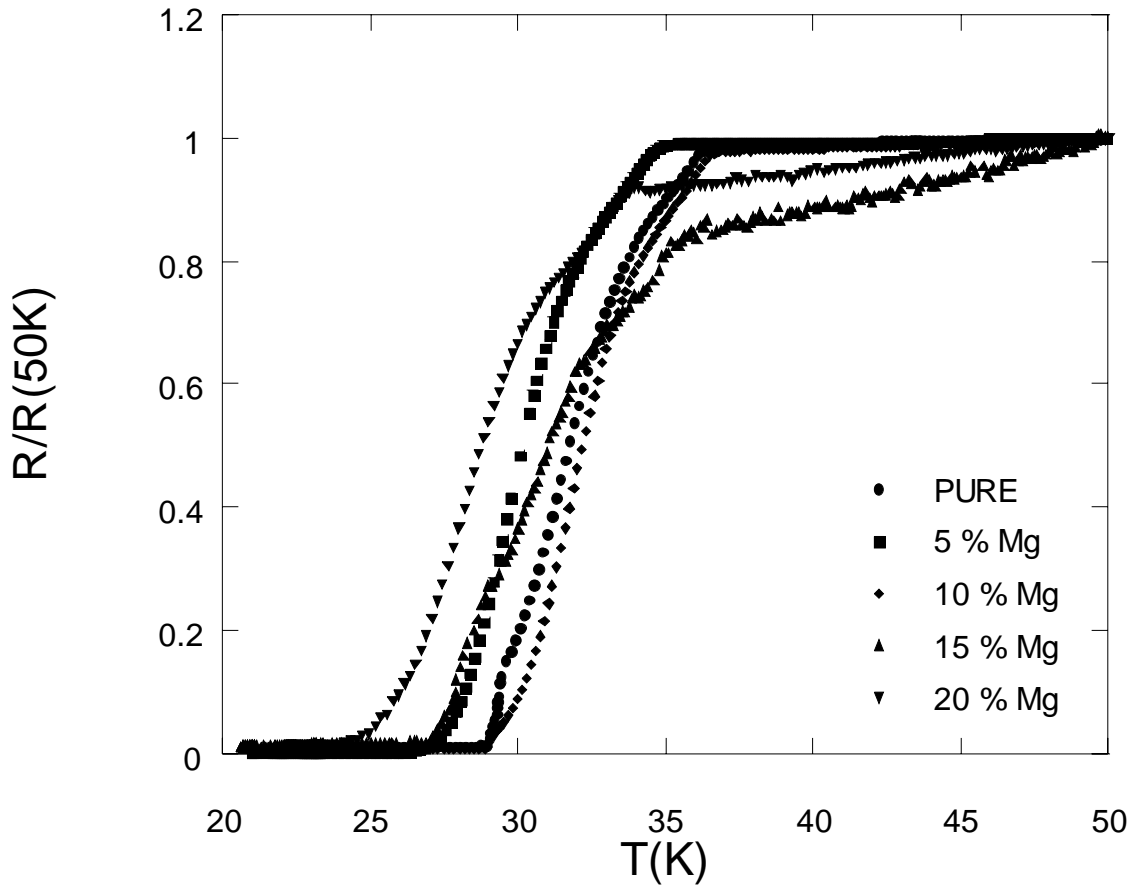


Figure 4.13 Temperature dependence of normalized resistivity of MgB_2/Mg composites prepared at 500°C , 0.5 GPa.

Table 4.4 The T_c , ΔT and T_c^{Onset} values MgB_2/Mg composites prepared at 500°C , 0.5 GPa.

Pres.Temp. C	Mg %	T_c 90%(K)	T_c 10%(K)	T_c ONSET(K)	T_c ZERO(K)	ΔT (K)	T_c Mid(K)
500	PURE	34.97	29.52	36.07	27.48	5.45	31.86
500	5	33.42	28.40	34.90	27.58	5.02	30.25
500	10	35.06	30.11	36.81	29.33	4.95	32.50
500	15	32.05	25.95	34.09	24.86	6.10	28.65
500	20	32.08	26.58	33.90	25.38	5.50	30.69

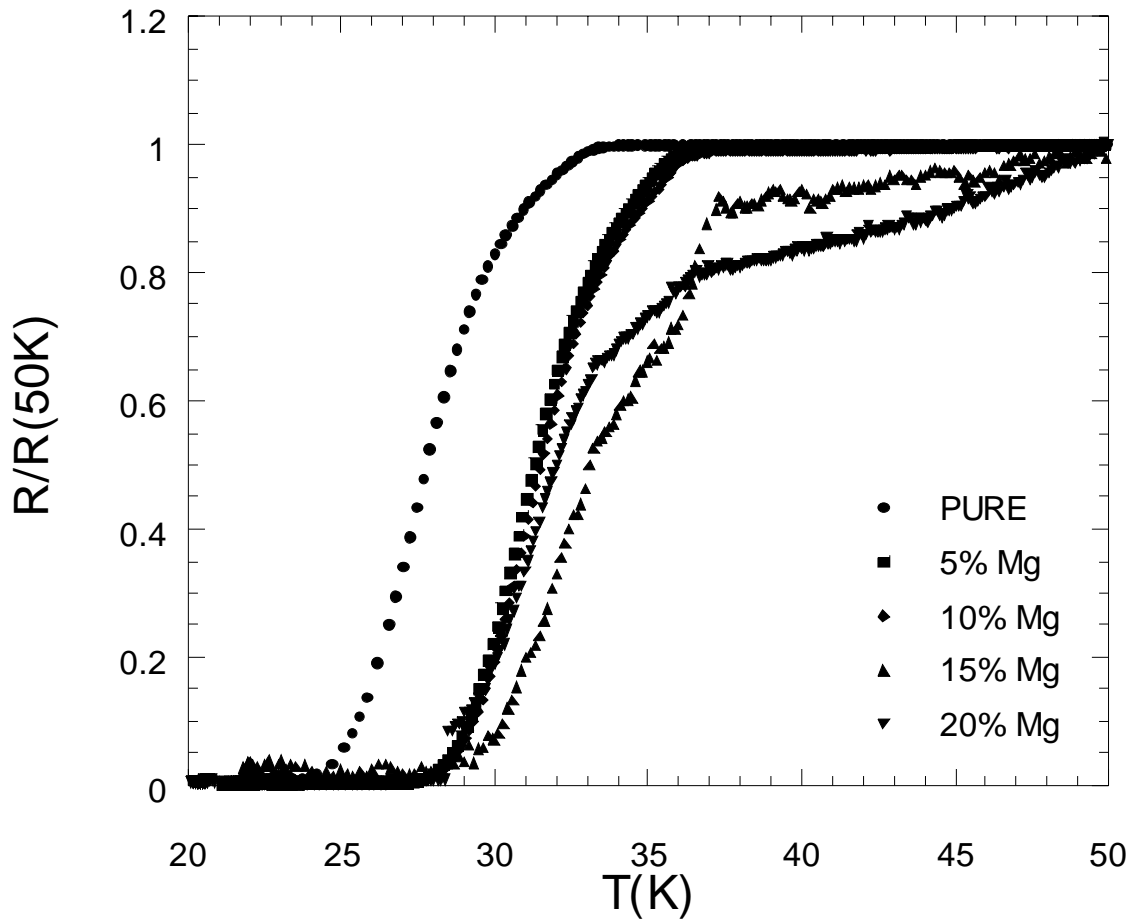


Figure 4.14 Temperature dependence of normalized resistivity of MgB_2/Mg composites prepared at 550°C , 0.5 GPa.

Table 4.5 The T_c , ΔT and T_c^{Onset} values MgB_2/Mg composites prepared at 550°C , 0.5 GPa.

Pres.Temp. C	Mg %	T_c 90%(K)	T_c 10%(K)	T_c ONSET(K)	T_c ZERO(K)	ΔT (K)	T_c Mid(K)
550	PURE	31.08	25.70	33.39	24.86	5.38	27.80
550	5	34.97	29.20	36.32	28.26	5.77	31.47
550	10	34.60	29.43	36.43	28.45	5.17	31.70
550	15	36.45	30.30	37.14	29.23	6.15	33.10
550	20	34.97	28.45	36.11	28.65	6.52	31.60

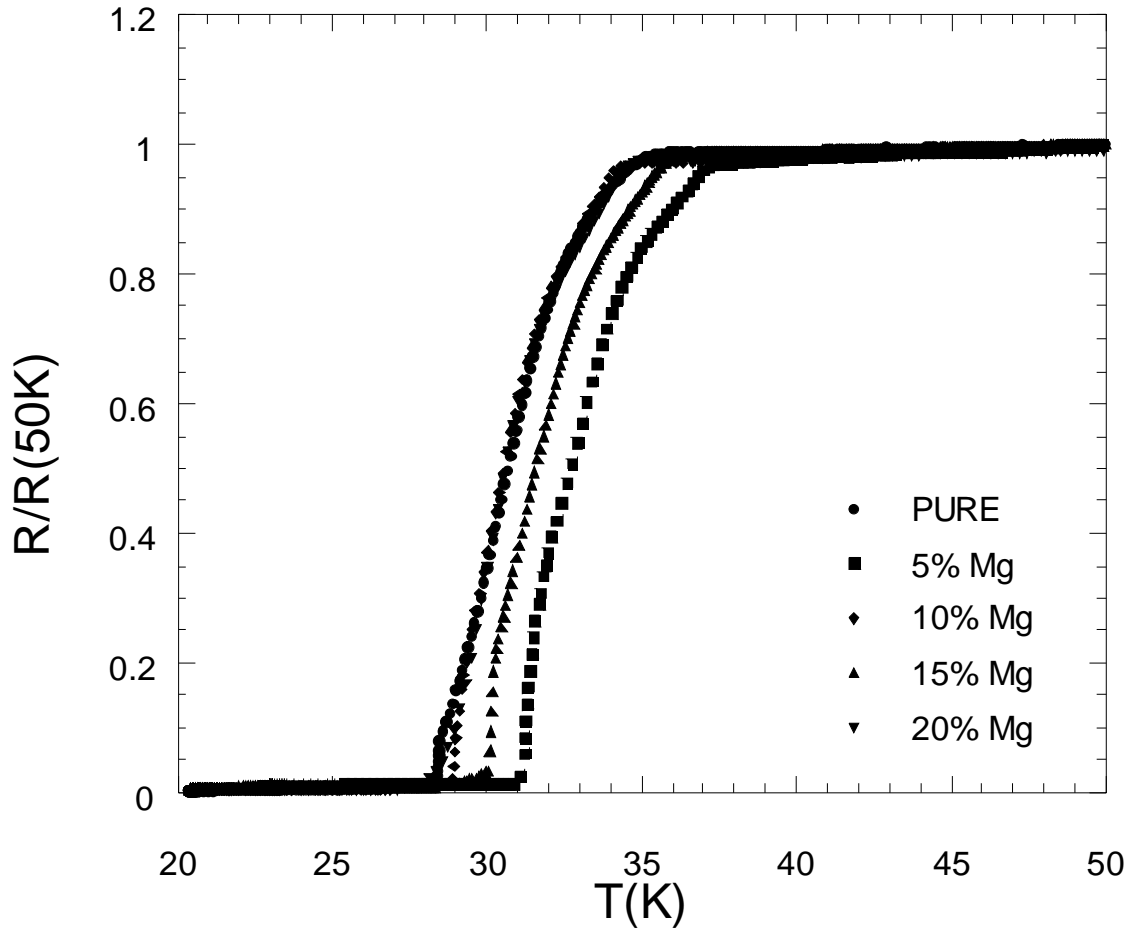


Figure 4.15 Temperature dependence of normalized resistivity of MgB_2/Mg composites prepared at 400°C , 1 GPa

Table 4.6 The T_c , ΔT and T_c^{Onset} values MgB_2/Mg composites prepared at 400°C , 1 GPa.

Pres.Temp. C	Mg %	T_c 90%(K)	T_c 10%(K)	T_c ONSET(K)	T_c ZERO(K)	ΔT (K)	T_c Mid(K)
400	PURE	33.51	28.75	35.26	28.65	4.76	30.88
400	5	35.36	31.18	37.40	31.40	4.18	32.88
400	10	33.22	28.75	34.29	29.13	4.47	30.80
400	15	34.58	30.10	35.84	30.30	4.48	31.70
400	20	33.40	29.22	34.90	28.20	4.18	30.70

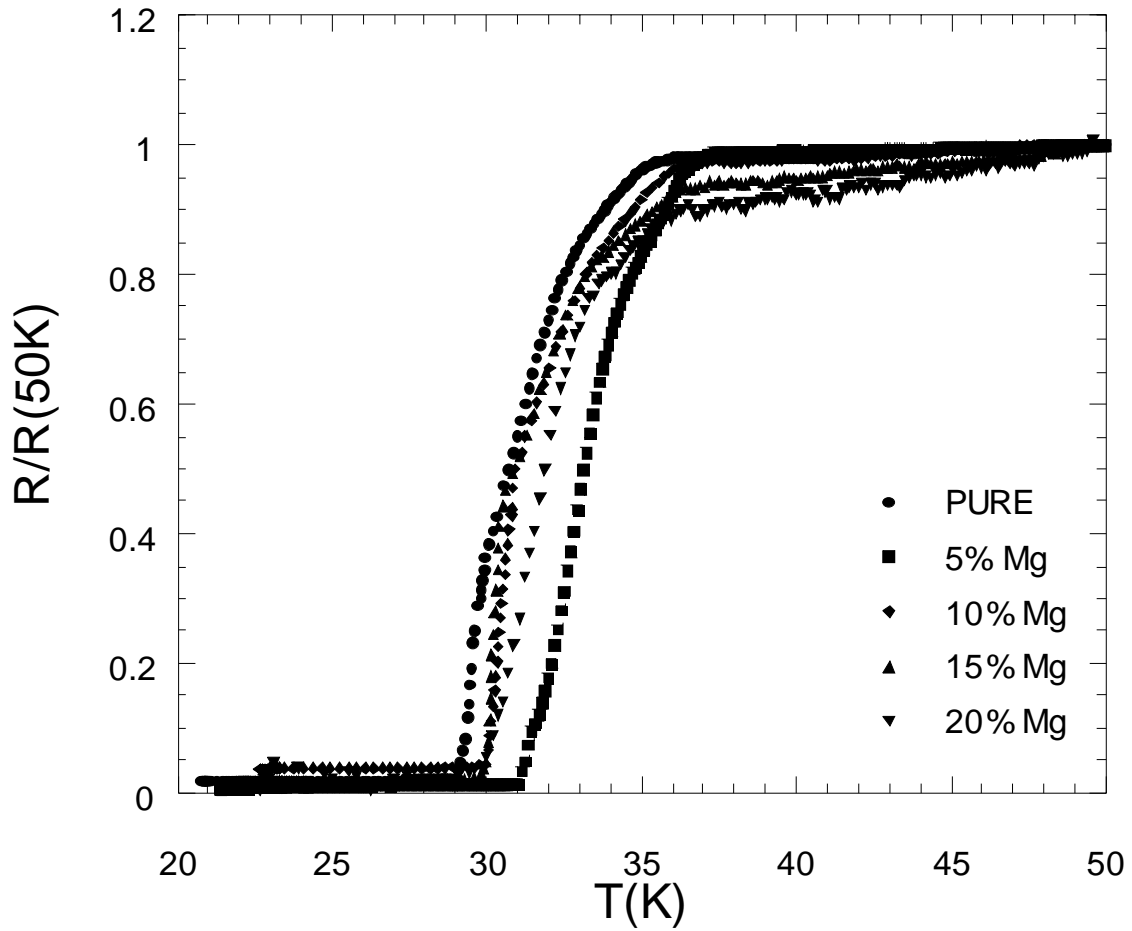


Figure 4.16 Temperature dependence of normalized resistivity of MgB_2/Mg composites prepared at 500°C , 1 GPa

Table 4.7 The T_c , ΔT and T_c^{Onset} values MgB_2/Mg composites prepared at 500°C , 1 GPa.

Pres.Temp. C	Mg %	T_c 90%(K)	T_c 10%(K)	T_c ONSET(K)	T_c ZERO(K)	ΔT (K)	T_c Mid(K)
500	PURE	33.72	29.10	35.15	29.33	4.62	31.08
500	5	36.04	31.70	37.30	31.50	4.34	33.30
500	10	34.60	30.11	36.43	30.30	4.49	31.00
500	15	34.05	30.15	36.88	30.11	3.90	30.50
500	20	34.29	30.20	35.75	29.91	4.09	31.80

From the Table 4.3 it is seen that unsubstituted sample has a T_c^{Onset} value of 30.90 K. It is seen that increasing the Mg percent increases the critical temperatures of the composites. It was observed that all substituted samples have critical temperatures greater than unsubstituted sample, the highest T_c^{Onset} obtained from the sample prepared at 400 °C under pressure of 0.5 GPa is 35.60 K which has 10% excess Mg. Moreover according to table 4.3 these set of composites have large ΔT values varying between 4.57 and 6.23 K. This broaden transition can be caused by high porosity ratio calculated in Table 4.1. From this table it is seen Mg substitution increases the density of the composites therefore decreases the porosity ratio. However, the increasing the amount of substituted Mg increases the nonsuperconducting volume fraction of the composites. Thus the improvement in the T_c values due to decrease in the porosity ratio are expected to continue until a certain amount of substitution, Table 4.3. From the Table 4.4, it is seen that unsubstituted sample has a T_c^{Onset} value of 36.07 K. Similar to the samples prepared at 400°C under pressure of 0.5 GPa the highest T_c^{Onset} value was observed in sample which has 10% excess Mg with 36.81 K for the samples prepared at 500°C under pressure of 0.5 GPa. Different from the samples prepared at 400°C, 0.5 GPa unsubstituted sample has a onset critical temperature (T_c^{Onset}) greater than substituted samples except 10% excess Mg sample in these set of samples. From the Table 4.2 it is seen that an increase of 100 °C for the samples prepared at 0.5 GPa has no major effect on the density of the samples. However, an increase of 5.17 K is observed in T_c^{Onset} value with an increase of 100 °C in the pressing temperature value. For the substituted samples the variation of T_c^{Onset} values are not so large as in unsubstituted samples. This lead us to think that T_c^{Onset} value of 30.90 K 400 °C, 0.5 GPa sample may be caused from thermal contact problems between cold head and sample. Figure 4.14 shows that the highest T_c^{Onset} value for the samples prepared at 550 °C, 0.5 GPa is 37.14 K in 15% excess Mg sample. Compared with the samples prepared at 400 and 500°C a increase in the transition temperature is observed in the 15% and 20% excess Mg samples for 550 °C but the ΔT values remained very high this can be explained by the increase in the amount of oxidation in these samples. Previous studies showed that oxidation of MgB_2 in air begins at 400°C and increasing temperature increases the oxidation [61]. Moreover, Mg is a very reactive metal and its oxidation is very fast above 500 °C. Consistent with our results also

EDX analyses showed this increase in MgO amount especially in the samples prepared at 550 °C. In the Table 4.1 and 4.2, we have mentioned that the density of the samples are slightly has a dependence on pressing temperature but has a significant dependence on pressure. In Figure 4.15, temperature dependence of the resistivity of the samples prepared at 400 °C and 1 GPa is seen. A relatively sharp transition is seen if it is compared with the samples prepared at 0.5 GPa. The ΔT value improved 1.43 K for unsubstituted sample for composite prepared at 1 GPa compared with the composite prepared at 0.5 GPa for 400 °C pressing temperature. Considering the SEM results It can be thought that increasing pressing temperature increases grain connectivity between MgB₂ grains therefore a less broaden transition is observed. For the samples prepared at 400 °C, 1 GPa it is observed that for all samples the T_c^{Onset} temperature is very close to or higher than 35 K. These results are better than the resistivity versus results compared with samples prepared with 0.5 GPa pressure. The T_c^{Onset} was observed in the sample with 5% excess Mg for 400 °C, 1 GPa samples with 37.4 K. Similar to 400 °C, 1 GPa samples best T_c^{Onset} value is observed in the sample with 5% excess Mg for 500 °C, 1 GPa samples with 37.3 K. For all samples in this group table 4.3.5, T_c^{Onset} values are above 35 K T_c values are above 30 K even in 20% Mg sample. This means we are below the percolation threshold of MgB₂/Mg composites. A critical temperature T_c above 30 K is significant for large-scale applications. Mg constituent in composites decreases the slope of the resistivity curve above the transition temperature. Resistance of Mg has a strong dependence of temperature and Mg has relatively lower resistance (1.6 $\mu\Omega\text{cm}$ at 300 K) compared to MgB₂ (4.5 $\mu\Omega\text{cm}$ at 300 K). Therefore increasing amount of Mg decreases the resistivity of MgB₂/Mg composites. In all of the resistivity versus temperature figures the change in the slopes of resistivity versus temperature curves is seen. The change in the resistivity of MgB₂/Mg composites for samples prepared at 500 °C, 0.5 GPa the resistivity values for different amount of Mg addition is summarized in Table 4.8. It can be observed from the table that increasing Mg amount decreases the resistivity of the composites as we expected. The resistivity values for other batch of samples also showed the same character. From the table it is seen that resistivity of unsubstituted sample is 1.88 m Ωcm at room temperature, this resistivity value is quite higher than the resistivity of MgB₂ (4.5 $\mu\Omega\text{cm}$ at 300 K) given above. In 2003 Rowell reviewed the resistivity behaviors of MgB₂

and their temperature dependences for thin films, single crystals and polycrystalline samples [23]. In his study, wide range of resistivity values are reported for bulk samples between a few $\mu\Omega\text{cm}$ and $100\text{m}\Omega\text{cm}$. Rowell showed porosity, structural defects and preparation condition as the reason of very high resistivity values. The resistivity of the unsubstituted samples for all sets of MgB_2/Mg composites is given in Table 4.9. All resistivity values are on the range of $\text{m}\Omega\text{cm}$, high porosity ratio in the samples may be the reason of these high resistivity values.

Table 4.8 The resistivity values of samples prepared at 500°C , 0.5 GPa .

Mg%	$\rho(50\text{ K})\ \Omega.\text{cm}$	$\rho(300\text{K})\ \Omega.\text{cm}$	$\rho(300\text{K})/\rho(50\text{ K})$
0	$1.60\ 10^{-3}$	$1.88\ 10^{-3}$	1.16
5	$9.00\ 10^{-4}$	$1.15\ 10^{-3}$	1.27
10	$6.50\ 10^{-4}$	$9.90\ 10^{-4}$	1.52
15	$2.26\ 10^{-4}$	$4.50\ 10^{-4}$	1.99
20	$4.00\ 10^{-5}$	$1.20\ 10^{-4}$	3.00

Table 4.9 The resistivity values of samples for different preparing conditions.

Press. T ($^\circ\text{C}$)	Press. (GPa)	$\rho(50\text{ K})\ \Omega.\text{cm}$	$\rho(300\text{K})\ \Omega.\text{cm}$
400	0.5	$1.57\ 10^{-3}$	$1.91\ 10^{-3}$
500	0.5	$1.60\ 10^{-3}$	$1.88\ 10^{-3}$
550	0.5	$1.40\ 10^{-3}$	$1.60\ 10^{-3}$
400	1	$1.24\ 10^{-3}$	$1.47\ 10^{-3}$
500	1	$1.03\ 10^{-3}$	$1.25\ 10^{-3}$

Below the T_c^{Onset} the current is carried by superconducting MgB_2 phase and the resistivity character under this temperature is mainly determined by MgB_2 phase and

consequently by their grain connectivity, grain size, porosity and purity. On the point of engineering view, the broadened transition is undesired situation because T_c^{Zero} decreases considerably. Almost in all MgB_2/Mg composites especially for the samples prepared at 0.5 GPa, quite broadened transition is observed. It was also reported in literature that excess Mg causes broadened transition [47]. Besides excess Mg, porosity and insufficient grain connectivity between MgB_2 grains may be the main reasons of the broadened transition in our samples.

As mentioned above magnetization versus temperature measurements were carried on samples with using vibrating sample magnetometry system. From Figure 4.17 to Figure 4.21 the temperature dependence of the magnetization of the samples prepared at 400, 500, 550°C (0.5 GPa) and 400, 500 °C (1 GPa) is given. Additionally, from these graphs the ΔT and T_c^{Onset} values are determined by using first derivative method, these values are summarized in the Table 4.10 to Table 4.14. In these graphs, only the magnetization curves of the pure, 10% excess Mg and 20% excess Mg samples of the each set is given

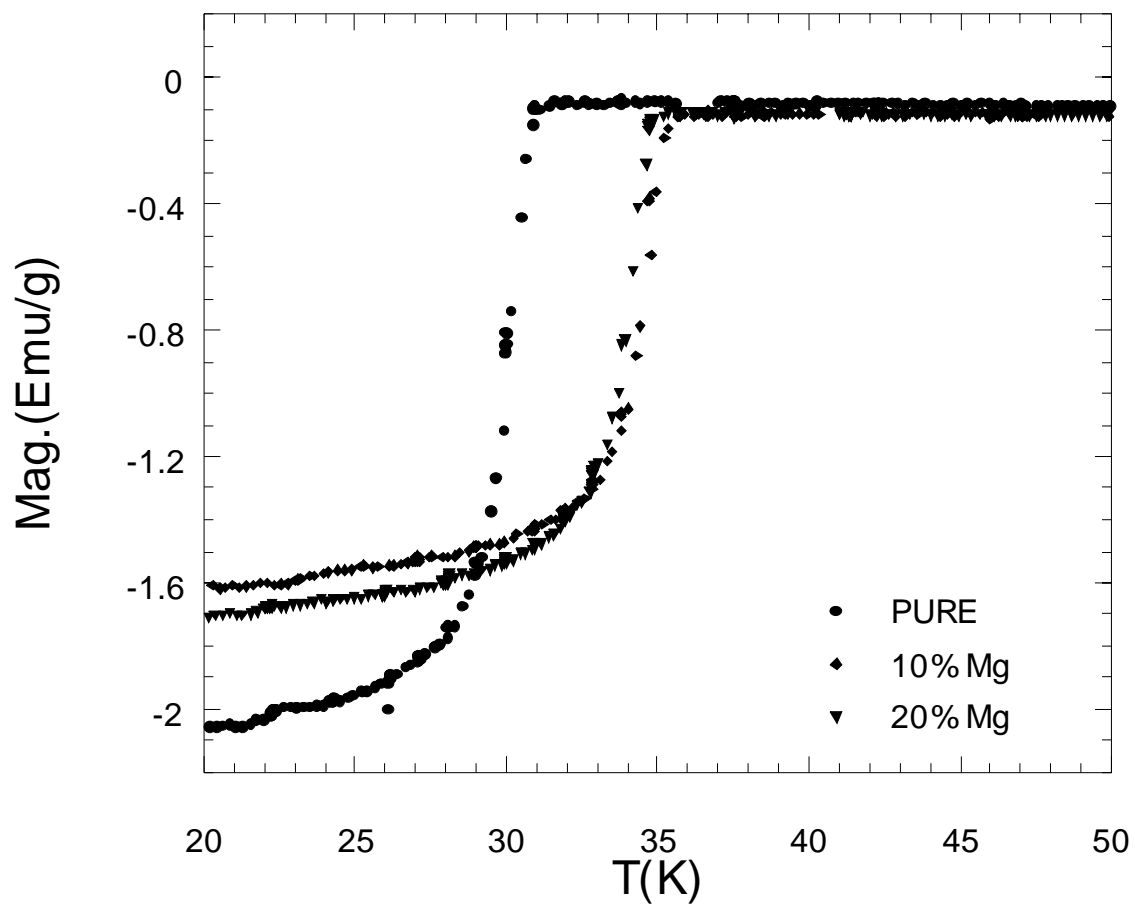


Figure 4.17 Magnetization versus Temperature plot of samples prepared at 400°C, 0.5 GPa.

Table 4.10 ΔT and T_c^{Onset} values of samples prepared at 400°C, 0.5 GPa.

Pres.Temp. C	Mg %	Tc half 1K)	Tc half2(K)	Tc ONSET(K)	ΔT (Mag.)	$\Delta T(R-T)$
400	PURE	30.50	28.35	30.97	2.15	6.23
400	10	35.00	33.33	35.66	1.67	5.10
400	20	36.00	33.83	35.19	2.17	4.90

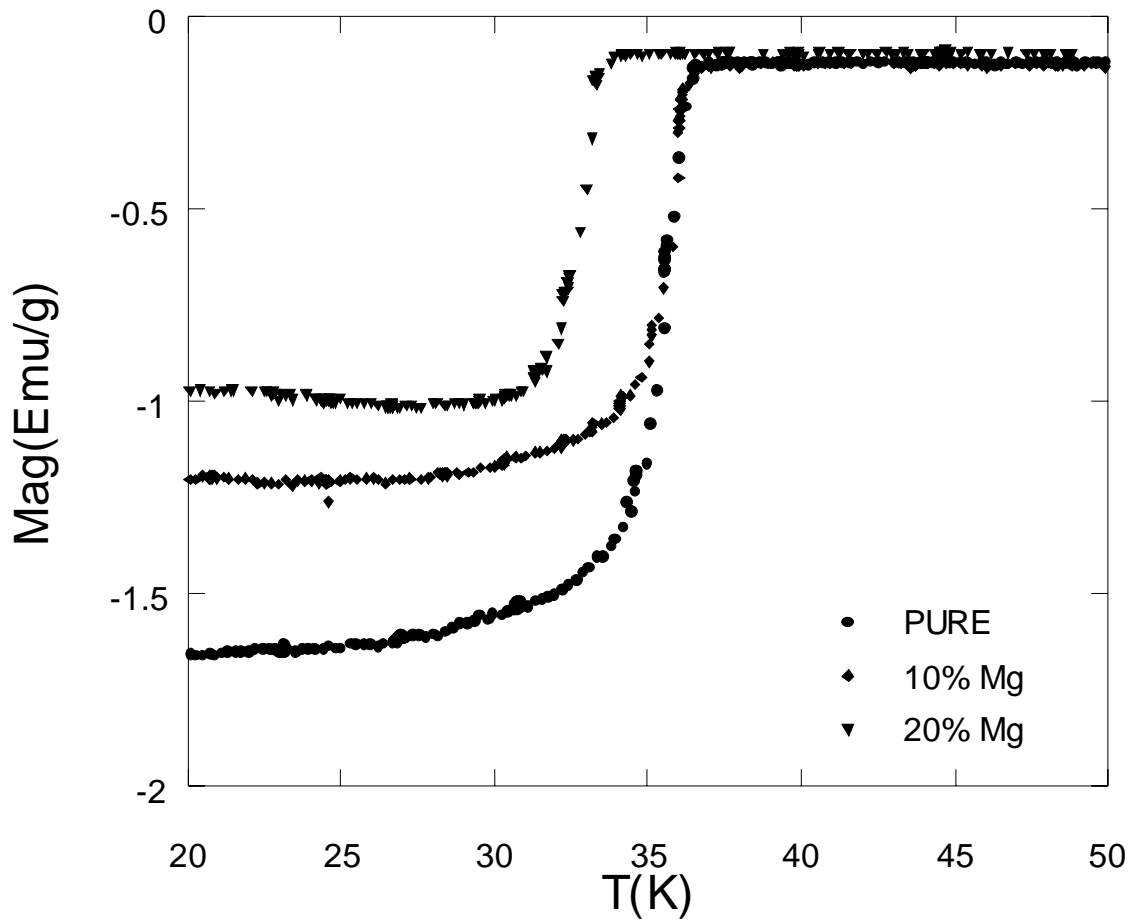


Figure 4.18 Magnetization versus Temperature plot of samples prepared at 500°C, 0.5 GPa.

Table 4.11 ΔT and T_c^{Onset} values of samples prepared at 500°C, 0.5 GPa.

Pres.Temp. C	Mg %	Tc half 1(K)	Tc half2(K)	Tc ONSET(K)	ΔT (Mag.)	$\Delta T(R-T)$
500	PURE	34.47	32.68	36.07	1.79	5.45
500	10	35.83	34.35	36.81	1.48	4.95
500	20	33.60	31.91	33.97	1.69	6.32

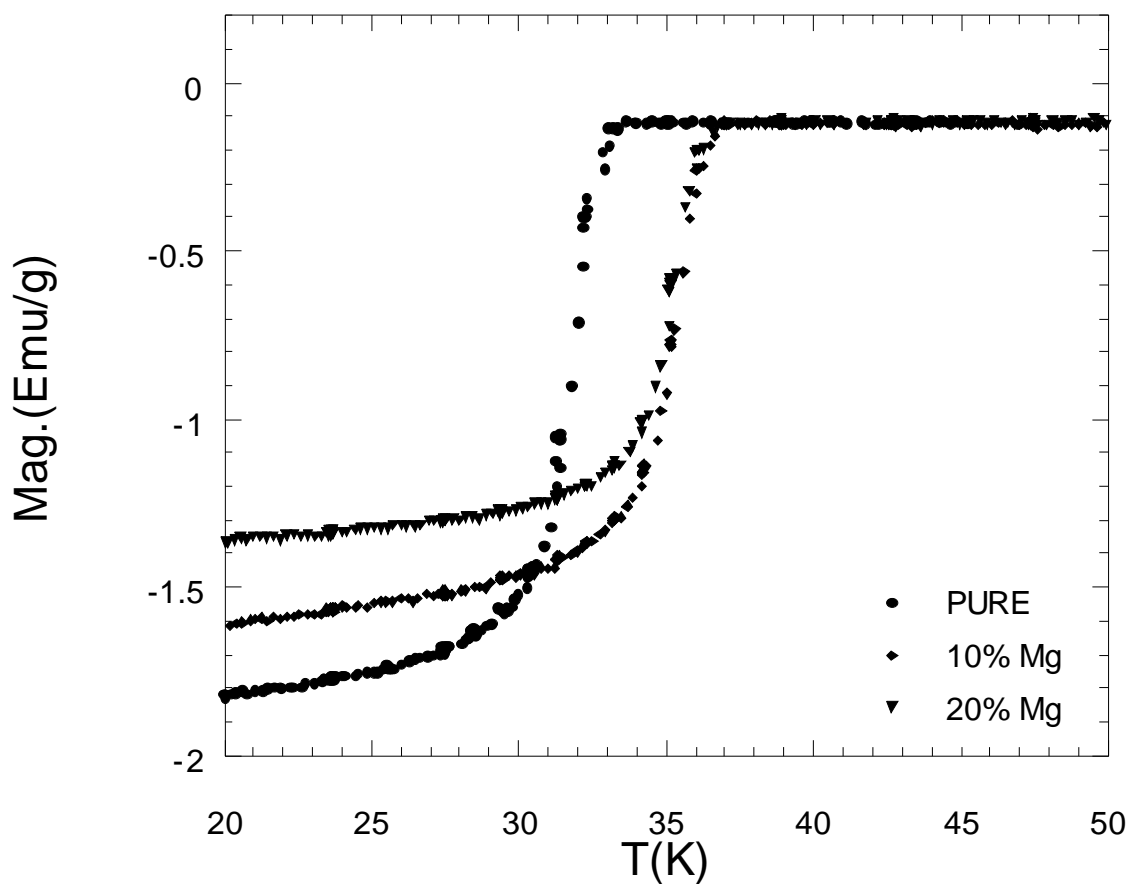


Figure 4.19 Magnetization versus Temperature plot of samples prepared at 550°C, 0.5 GPa.

Table 4.12 ΔT and T_c^{Onset} values of samples prepared at 550°C, 0.5 GPa.

Pres.Temp. C	Mg %	Tc half 1(K)	Tc half2(K)	Tc ONSET(K)	ΔT (Mag.)	$\Delta T(R-T)$
550	PURE	32.38	30.48	33.60	1.90	5.38
550	10	35.66	33.50	36.85	2.16	5.17
550	20	36.00	31.91	36.69	2.50	6.52

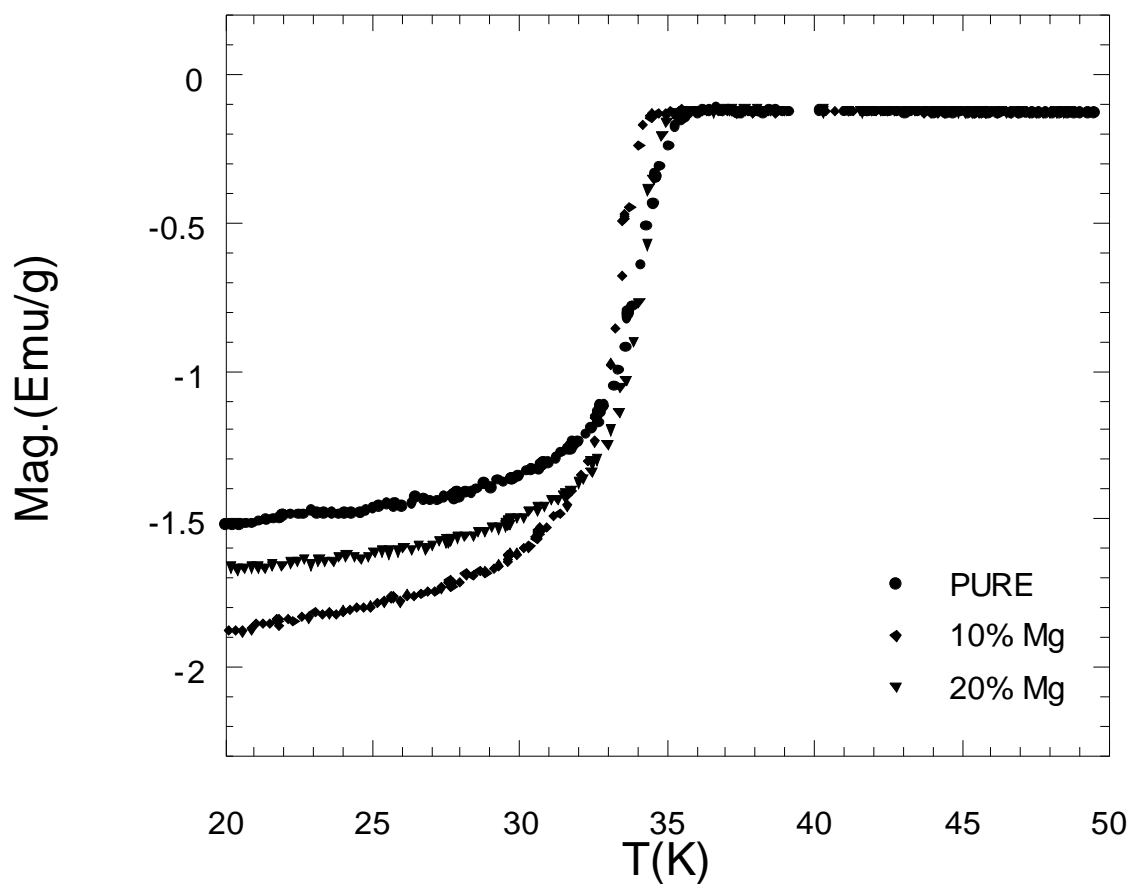


Figure 4.20 Magnetization versus Temperature plot of samples prepared at 400°C, 1 GPa.

Table 4.13 ΔT and T_c^{Onset} values of samples prepared at 400°C, 1 GPa.

Pres.Temp. C	Mg %	Tc half 1(K)	Tc half2(K)	Tc ONSET(K)	ΔT (Mag.)	ΔT (R-T)
400.00	PURE	34.66	32.50	35.31	2.16	4.76
400.00	10.00	33.80	32.16	34.42	1.64	4.48
400.00	20.00	34.50	33.16	34.96	1.34	4.18

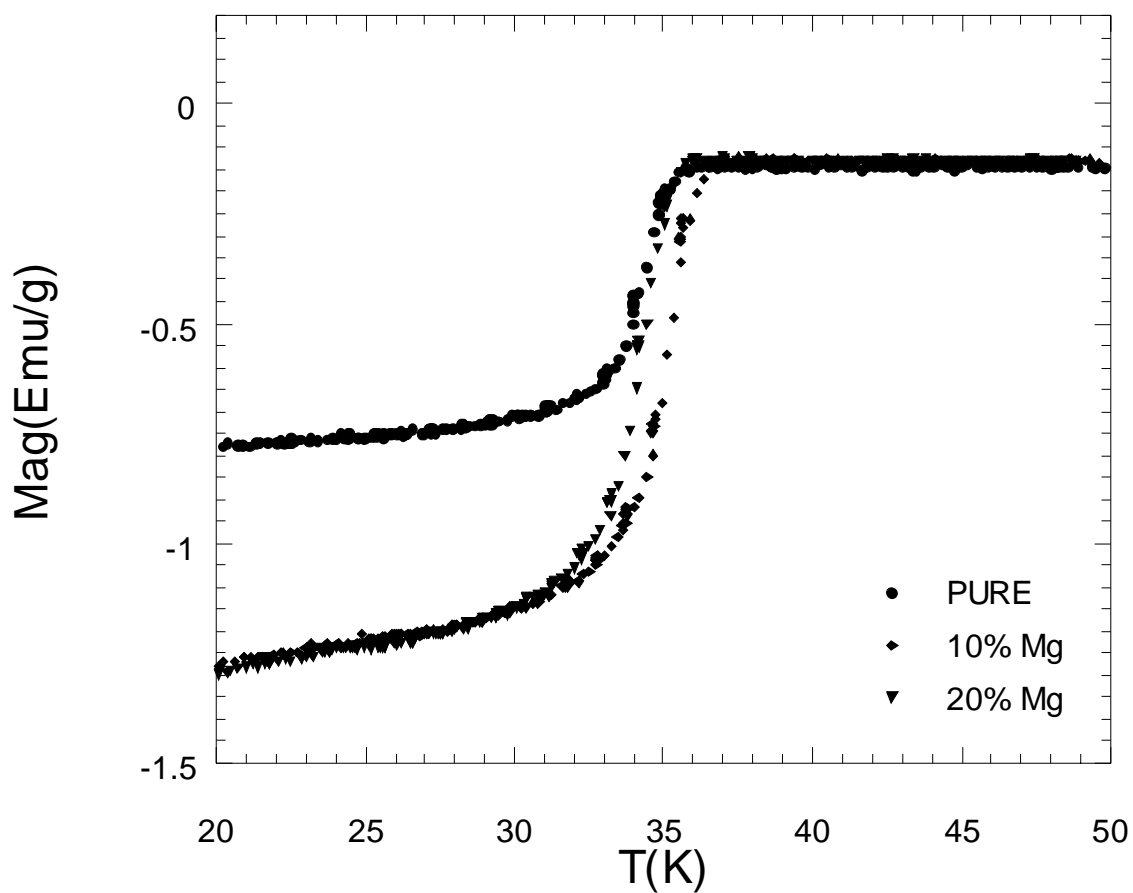


Figure 4.21 Magnetization versus Temperature plot of samples prepared at 500°C, 1 GPa.

Table 4.14 ΔT and T_c^{Onset} values of samples prepared at 500°C, 1 GPa.

Pres.Temp. C	Mg %	Tc half 1(K)	Tc half2(K)	Tc ONSET(K)	ΔT (Mag.)	ΔT (R-T)
500	PURE	34.50	32.50	35.21	2.00	4.62
500	10.00	35.16	33.50	36.50	1.66	4.49
500	20.00	34.83	32.50	35.78	2.33	4.09

The samples prepared for magnetization measurements were approximately same in volume. Therefore it is expected that, the sample which has more superconducting volume fraction will give the strongest diamagnetic transition. For the samples prepared at 500 °C, 0.5 GPa and 550 °C, 0.5 GPa the strongest diamagnetic signal is observed in the unsubstituted sample, Figure 4.18-19. Then in the samples which have 10% excess Mg and the samples which have 20% excess Mg as we expected. In the samples prepared at 400 °C, 0.5 GPa the strongest diamagnetic signal is observed in the unsubstituted sample however the signal of 20% excess Mg sample is seemed to be stronger than 10% Mg sample, Figure 4.17. Localized inhomogeneity in the sample or difference may be the reason of this situation. Both for the sample prepared at 400 °C, 1 GPa and 500 °C, 1 GPa the diamagnetic signal for unsubstituted sample is less strong than the signals from 10% and 20% excess Mg samples. Since the unsubstituted samples are less stiff than the substituted samples, this difference may be caused from the loss of mass during the measuring process. Almost all of the T_c^{Onset} values obtained from the magnetization results are consistent with the results obtained from resistivity measurements. However, there is some difference in the ΔT and critical temperature values. ΔT values obtained from the magnetization results were in the range of 1.5 and 2.5 K, but the ΔT values obtained from resistivity results were in the range of 4 and 6 K. Due to the fact that the methods for calculating the ΔT values for resistivity measurements and magnetization measurements are different we should expect a difference in the values.

4.4 Mechanical Properties

Compressive mechanical testing was performed to obtain stress-strain behavior, elastic modulus (E) and fracture strength (σ_f) values of the MgB_2/Mg composites. Mechanical tests were carried out on at least three specimen for each temperature and weight ratios to obtain standard deviation. Mechanical tests were performed with two sets of composites, 400 °C, 0.5 GPa and 500 °C, 0.5 GPa sets. Figure 4.22 illustrates the stress-strain behavior of pure and with the addition of 20% Mg samples prepared at 400 °C, 0.5 GPa.

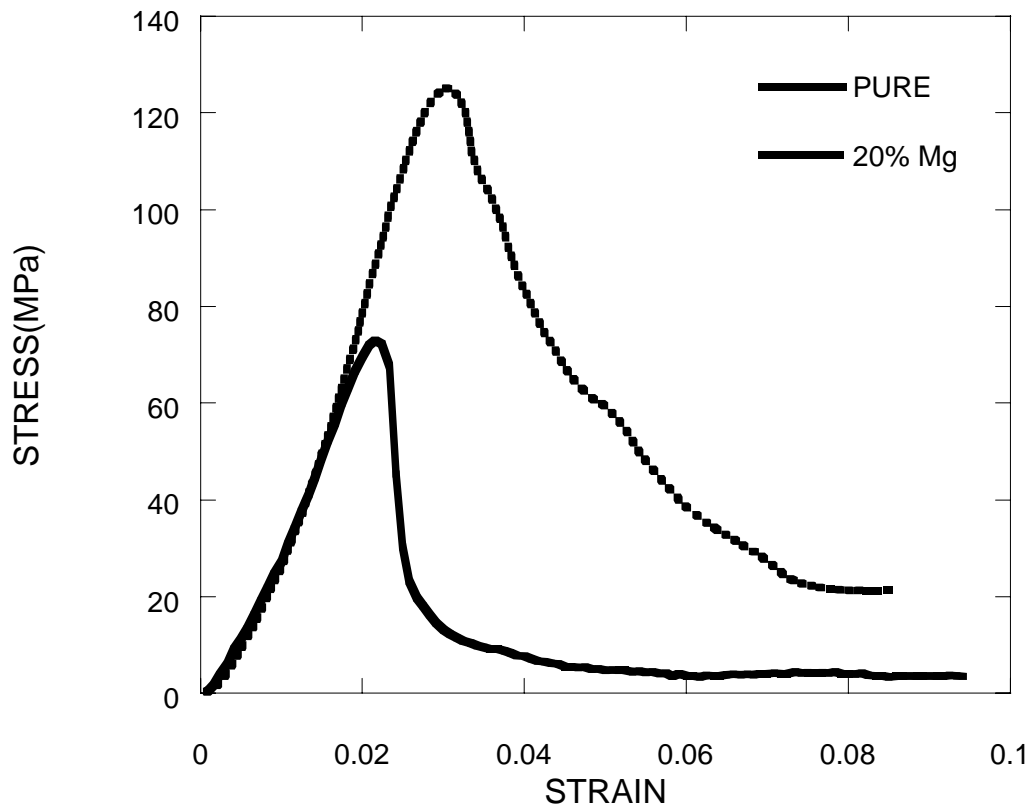


Figure 4.22 Stress strain behavior of pure and 20% Mg samples prepared at 400°C, 0.5 GPa.

Figure 4.22 shows that Mg addition improves the fracture strength of the composites for samples prepared at 400° C. Similarly the Figure 4.23 reveals that Mg addition increases the mechanical properties of the samples prepared at 500° C more than samples prepared at 400° C. Since the area under stress-strain curve determines toughness of the material it is obvious that Mg addition increases toughness of the system. However the results show that addition of Mg has insignificant effect on the modulus of the samples.

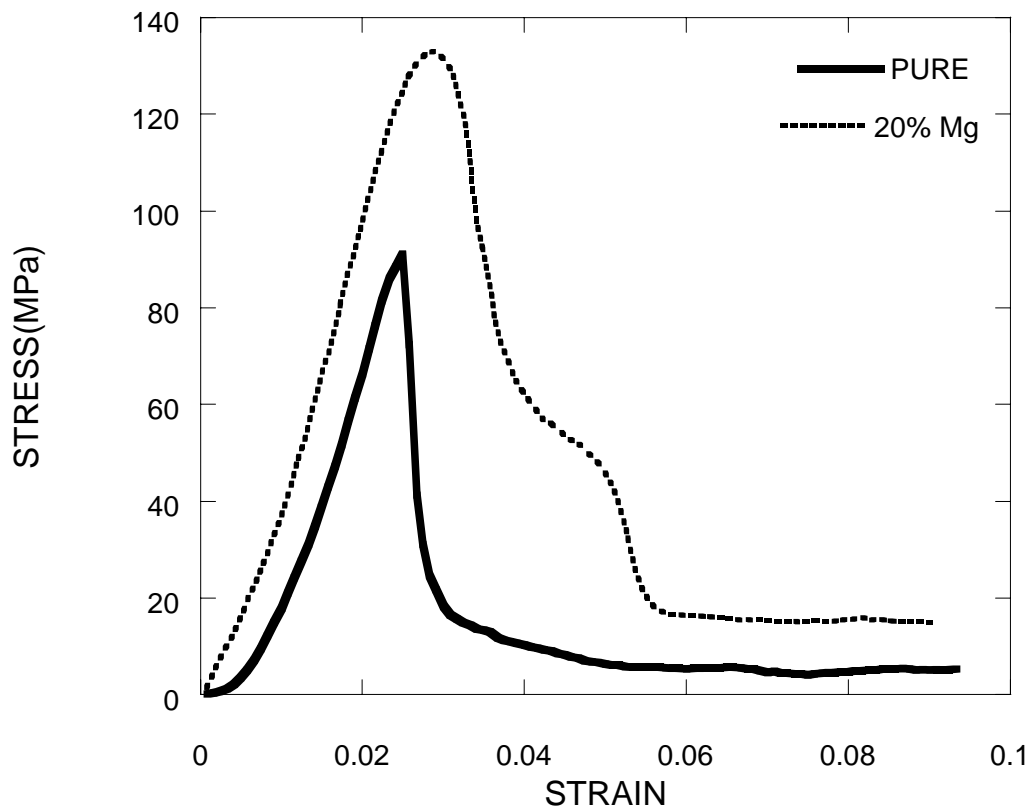


Figure 4.23 Stress strain behavior of pure and 20% Mg samples prepared at 500°C, 0.5 GPa.

The variation of fracture strength with increasing Mg amount is given in Figure 4.24 and 4.25 for samples prepared at 400° C and 500° C respectively. It was found that increasing Mg concentration by 20% the fracture strength value increases by about 56%, for composites prepared at 400 °C. Similarly, temperature has some effect on fracture strength and elastic modulus values.

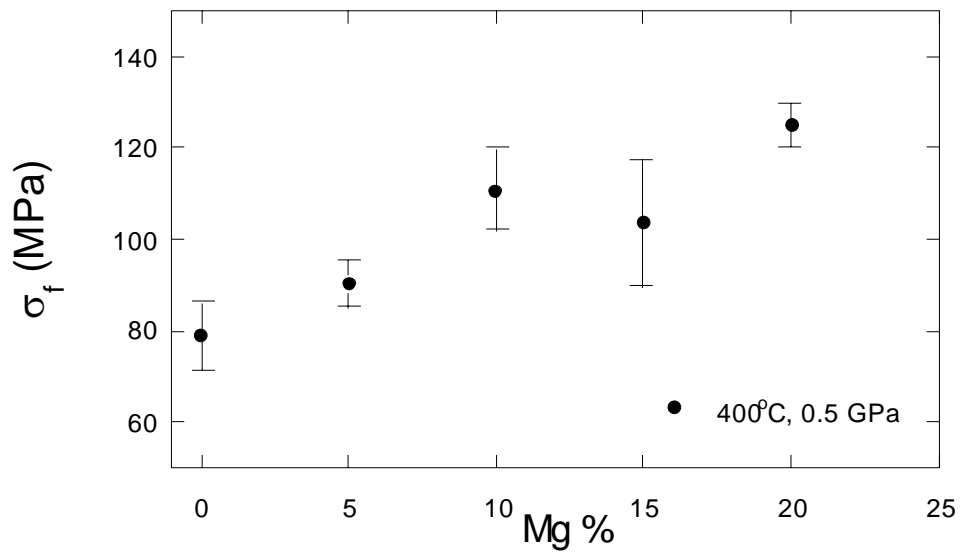


Figure 4.24 Fracture strength values of samples prepared at 400 °C, 0.5 GPa

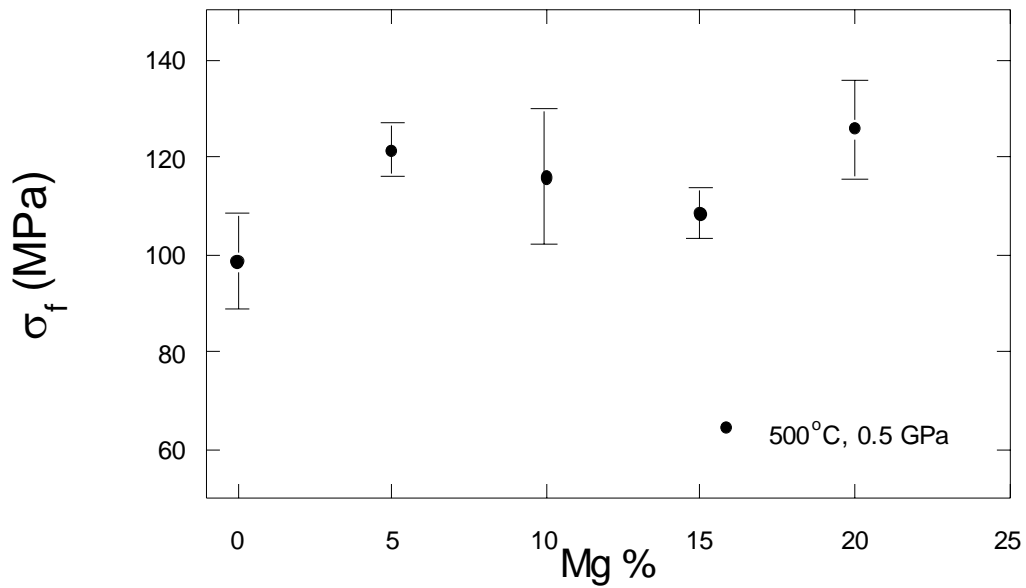


Figure 4.25 Fracture strength values of samples prepared at 500°C, 0.5 GPa.

As seen in Table 4.15, in general as the pressing temperature increases, both strength and modulus values increase with some fluctuations. The highest elastic modulus values obtained from samples heat treated at 400 and 500 °C are 5775 and 6390 MPa, respectively and the highest fracture strength values are 125 and 126 MPa for 20% excess Mg samples.

Table 4.15 Fracture strength and Elastic modulus values for MgB₂/Mg composites.

FRACTURE STRENGTH (MPa)						
Press. Temp. C	Mg %	Pellet 1	Pellet 2	Pellet 3	Average	Std. deviation
400	0	82.40	72.99	82.00	79.13	5.32
400	5	85.48	91.80	94.44	90.44	4.60
400	10	101.36	115.14	115.19	110.56	7.97
400	15	91.55	114.59.23	105.78	103.74	11.62
400	20	122.75	127.72	125.09	125.09	2.49
500	0	104.59	91.05	100.01	98.55	6.88
500	5	122.21	117.42	124.59	121.20	3.37
500	10	134.79	105.38	106.92	115.70	16.55
500	15	111.86	107.20	105.93	108.33	3.11
500	20	132.95	126.43	117.86	125.75	7.57
ELASTIC MODULUS (MPa)						
Press. Temp. C	Mg %	Pellet 1	Pellet 2	Pellet 3	Average	Std. deviation
400	0	4086.10	3721.70	5162.80	4323.53	749.30
400	5	4365.70	4632.70	5292.80	4763.73	477.20
400	10	5285.60	6019.50	5619.50	5641.53	367.44
400	15	5594.00	5272.30	4943.50	5269.93	325.25
400	20	5655.60	5859.50	5810.10	5775.07	106.30
500	0	5519.50	4314.10	5645.70	5159.77	735.08
500	5	6308.30	6198.80	6503.50	6336.87	154.34
500	10	6481.60	5096.40	5374.80	5650.93	732.70
500	15	5344.90	4976.90	5509.50	5277.10	272.60
500	20	6023.70	7422.70	5725.00	6390.47	906.33

A brittle material would fracture almost at the elastic limit. All of the samples prepared fractured in a brittle manner. Increasing Mg amount and temperature increases the elastic modulus and fracture stress of MgB₂/Mg composites however no considerable plasticity was observed in the samples. Further, increase of the Mg amount may make the composites more ductile. However the percolation threshold of MgB₂/Mg composites restrict us to use great amount of Mg. Although resistivity and magnetization results showed that we are below the percolation of MgB₂/Mg composites, increasing the non superconducting volume fraction more than 20% by addition of more amount of Mg seemed to be not advantageous because of probability of degrading superconducting

properties as given in some reports [50, 51]. On the other hand, experiments on measuring critical current density (J_c) in the deformed condition showed that MgB_2/Mg nanocomposites bulk specimen maintains J_c nearly two times better than MgB_2 specimen [64]. Although we did not performed any J_c measurements, a better maintenance of J_c in the deformed condition is expected in MgB_2/Mg composites pellets than MgB_2 pellets. The elastic modulus of MgB_2 strongly depends on sample density. Hot isostatic pressing is used by several groups to prepare dense MgB_2 samples [65]. In these studies a elastic modulus value of 79 GPa is reported for a hot isostatically precised sample which has density of 2.39 g/cm^3 [16] and 207 GPa –273 GPa for the samples which has densities 2.33 g/cm^3 and 2.66 g/cm^3 . Although there are limited studies on the mechanical properties of PIT wires 29 GPa elastic modulus value was obtained for Fe cladded MgB_2 wires [66]. In our samples, a densification is observed by increasing the amount of excess Mg but densities are still low (between $1.80\text{-}1.88 \text{ g/cm}^3$). Therefore relatively low elastic modulus values (between 4-6GPa) are observed. Since a limited amount of excess Mg do not degrades the superconducting properties of MgB_2/Mg composites, it may improves the mechanical properties. MgB_2/Mg /metal composite PIT wires may provide better performance than current MgB_2 /metal PIT wires in normal and superconducting state. Although mechanical tests on samples prepared at 1 GPa, were not performed, the density results of these samples indicate that a better mechanical properties may be expected from these samples.

CHAPTER 5

CONCLUSIONS

The recent discovery of MgB_2 (2001) has aroused a great interest because of its high T_c (39 K). Furthermore, simple crystal structure, large coherence lengths, high critical current densities (J_c) and critical fields (B_{c2}), and transparency of grain boundaries to current promise that MgB_2 will be a good material for both large-scale applications and electronic device applications. Approximately 99% of the superconductor market depends on large-scale applications based on production of wires and tapes. MgB_2 suggests a higher operating temperature (20 K) than the current technology in use (Nb-based superconductors, 4.2 K). Therefore, production of wires from MgB_2 has great significance in terms of science and industry. However, MgB_2 is not a standalone material to produce wires because of its low fracture toughness. The widespread method for producing wires from brittle powders is Powder In Tube Method (PIT). Besides PIT method there is an alternate method for producing tapes, wires and bulk samples from brittle powders called Metal Matrix Composite Method (MMC). In this study, MgB_2/Mg composites were produced by MMC method using hot pressing technique. Mg is chosen as the metal matrix because of its low melting point (653°C) and its inertness to MgB_2 at very high temperatures. To investigate the possibility of producing superconducting wires of MgB_2 , pellets of MgB_2/Mg composites were fabricated at different temperatures and pressures.

XRD results showed that the main phase for all produced composites is MgB_2 . It was found that there is no major reaction between MgB_2 and Mg. However, presence of small amount of MgO secondary phase is seen in the pattern. Previous studies on the oxidation behavior of MgB_2 in air reveals that oxidation of MgB_2 to Mg begins at about 400 °C but not very extensive up to 700 °C. Therefore, the existence of that MgO in the patterns are probably formed during hot pressing process. Typically presence of small amount of MgO enhances the superconducting properties of the composite wires acting as pinning centers and increasing the critical current density, J_c . Also a number of studies indicate the formation of MgB_4 secondary phase in case of hot pressing. Existence of MgB_4 in superconducting composite is an objectionable situation because it is generally

situated around grain boundaries as an insulating layer and degrades the superconducting properties. The XRD results for the samples prepared 400 °C and 500 °C have consistency. However, the MgO peaks in the pattern of samples annealed at 550 °C are more intense than the peaks obtained in other temperatures. As we get close to the melting temperature of Mg (653 °C) the amount of oxide increases. For all temperatures it is observed that Mg constituent increases the density. It can be noted that temperature has some effect on density of the samples; however the major effect on density is the pressure. An obvious increase in the density is observed in the samples prepared at 1 GPa. The porosity ratio is decreased to the 12% in the samples prepared at 1 GPa while it was about 15-20% in the samples prepared at 0.5 GPa. Consistent with density measurements a densification is observed from the SEM pictures of the MgB₂/Mg composites. Although density results did not show a clear densification with increasing pressing temperature, a densification is observed with increasing temperature from the SEM pictures. Another clue for densification with increasing temperature is the decrease in the average pore size in the composites. As we mention above XRD patterns showed an increase in the intensity of the MgO 550 °C. Addition to XRD measurements EDX analyses showed that the oxygen weight fraction in the 550 °C samples are nearly twice in amount of samples prepared at 400 °C. The oxygen amount in the samples prepared at 400 and 500 °C are higher than the oxygen amount in the previous work done by our group about MgB₂/Mg composites [67, 68]. This variation in the oxygen amount is due to the difference in the average grain size of used Mg powders. In this study, we have used -325 mesh (less than 44 micrometer) Mg powders but in the previous study we used -270 mesh (less than 53 micrometer) Mg powders. Smaller particle size of Mg leads to large surface area and therefore more oxidation.

The Mg constituent up to some extent increases the T_c of the samples due to the formation of percolation paths as a result of proximity effect and improvement in the grain connection due to densification. A little improvement was obtained in the density of the samples by increasing the sample preparation temperature to 500 and 550 °C from 400 °C. Consistently, an increase in the temperature brings the T_c^{Onset} and ΔT values to better values. Compared with the samples prepared at 400 and 500 °C an increase in the T_c^{Onset} is observed in substituted samples for 550 °C but the ΔT values remained very high. This

can be explained by the increase in the amount of oxidation in these samples. It was observed that critical temperatures values get better for the samples prepared at 1 GPa. Additionally, a relatively sharp transition is seen in the resistivity versus temperature curves of samples fabricated at 1 GPa, if it is compared with the samples prepared at 0.5 GPa. Density results revealed a densification in the 1 GPa samples therefore a decrease in the porosity fraction. Therefore improvement in the ΔT values can be count on to better grain connection as a result of densification. For all of prepared composites the T_c^{Onset} values do not depressed very evidently hence it may be said that we are below the percolation threshold of MgB_2/Mg composites even if in 20% excess Mg samples. Resistance of Mg has a strong dependence of temperature and Mg has relatively lower resistance ($1.6 \mu\Omega\text{cm}$ at 300 K) compared to MgB_2 ($4.5 \mu\Omega\text{cm}$ at 300 K). Therefore increasing amount of Mg decreases the resistivity of MgB_2/Mg composites. This decrease in the resistivity values of the composites observed in all sets of produced composites. From our results, it is seen that resistivity of our samples are in the range 10^{-3} and $10^{-4} \Omega\text{cm}$ range at room temperature. This resistivity values are quite higher than the resistivity of MgB_2 ($4.5 \mu\Omega\text{cm}$ at 300 K). Rowell showed porosity, structural defects and preparation condition as the reason of very high resistivity values in polycrystalline MgB_2 samples [27]. In our samples, high porosity may be the reason of these high resistivity values. Almost in all MgB_2/Mg composites especially for the samples prepared at 0.5 GPa, quite broaden transition is observed. It was also reported in literature that excess Mg causes broaden transition [47]. Besides excess Mg, porosity and insufficient grain connectivity between MgB_2 grains may be the main reasons of the broaden transition in our samples.

The samples prepared for magnetization measurements were approximately same in volume. Therefore it is expected that, the sample which has more superconducting volume fraction will give the strongest diamagnetic transition. For the samples prepared at 500 °C, 0.5 GPa and 550 °C, 0.5 GPa the strongest diamagnetic signal is observed in the unsubstituted sample. Then in the samples which have 10% excess Mg and the samples which have 20% excess Mg as we expected. In the samples prepared at 400°C, 0.5 GPa the strongest diamagnetic signal is observed in the unsubstituted sample however the signal of 20% excess Mg sample is seemed to be stronger than 10% Mg

sample. Localized inhomogeneity in the sample or difference may be the reason of this situation. Almost all of the T_c^{Onset} values obtained from the magnetization results are consistent with the results obtained from resistivity measurements. However, there is some difference in the ΔT and critical temperature values. ΔT values obtained from the magnetization results were in the range of 1.5 and 2.5 K, but the ΔT values obtained from resistivity results were in the range of 4 and 6 K. Due to the fact that the methods for calculating the ΔT values for resistivity measurements and magnetization measurements are different we should expect a difference in the values.

A brittle material would fracture almost at the elastic limit. All of the samples prepared fractured in a brittle manner. Increasing Mg amount and temperature increases the elastic modulus and fracture stress of MgB_2/Mg composites however no considerable plasticity was observed in the samples. Further, increase of the Mg amount may make the composites more ductile. However the percolation threshold of MgB_2/Mg composites restrict us to use great amount of Mg. Although resistivity and magnetization results showed that we are below the percolation of MgB_2/Mg composites, increasing the non superconducting volume fraction more than 20% by addition of more amount of Mg seemed to be not advantageous because of probability of degrading superconducting properties as given in some reports [50, 51]. On the other hand, experiments on measuring J_c in the deformed condition showed that MgB_2/Mg nanocomposites bulk specimen maintains J_c nearly two times better than MgB_2 specimen [64]. Although we did not performed any J_c measurements, a better maintenance of J_c in the deformed condition is expected in MgB_2/Mg composites pellets than MgB_2 pellets. The elastic modulus of MgB_2 strongly depends on sample density. Hot isostatic pressing is used by several groups to prepare dense MgB_2 samples [65]. In these studies an elastic modulus value of 79 GPa is reported for a hot isostatically sample which has density of 2.39 g/cm^3 16 and 207 GPa –273 GPa for the samples which has densities 2.33 g/cm^3 and 2.66 g/cm^3 . Although there are limited studies on the mechanical properties of PIT wires 29 GPa elastic modulus value is given for Fe cladded MgB_2 wires [66]. In Our samples a densification is observed by increasing the amount of excess Mg but densities are still low (between $1.80\text{-}1.88 \text{ g/cm}^3$). Therefore relatively low elastic modulus values (between 4-6 GPa) are observed. Since a limited amount of excess Mg do not degrades the

superconducting properties of MgB_2/Mg composites additionally improves the mechanical properties. MgB_2/Mg / metal composite PIT wires may provide better performance than current $\text{MgB}_2/\text{metal}$ PIT wires in normal state and superconducting state. We have not performed mechanical tests on samples prepared at 1 GPa, however as the density results of these samples shows better mechanical properties can be expected from these samples.

APPENDIX

Table A- 1 Transition temperatures of some selected superconductors.

Material	Critical Temp. (T_c), Year of Disc.
Nb ₃ Sn	18 K, 1954
Nb ₃ Ge	23 K, 1974
YBa ₂ Cu ₃ O ₇	93 K, 1987
Bi ₂ Sr ₂ Ca ₂ Cu ₃ O ₁₀	110 K, 1987
Bi ₂ Sr ₂ CaCu ₂ O ₈	91 K, 1987
HgBa ₂ Ca ₂ Cu ₃ O ₈	133 K, 1993
MgB ₂	39 K, 2001

Table A- 2 Characteristics of Mg

Theoretical Density	1.738 g/cm ³
Atomic Weight	24.3050
Atomic Number	12
Molar Volume	14 cm ³
Melting Point	650 °C
Boiling Point	1090 °C
Crystal Structure	Hexagonal Close-Packed
Hexagonal Lattice Parameters	a=320.94 pm
	c=521.08 pm
Superconduction Temperature	No data
Electrical Resistivity	440 μΩcm
Atomic Radius	Empirical radius 150 pm
	Calculated radius 145 pm
Young Modulus	45 GPa
Bulk Modulus	45 GPa
Rigidity Modulus	17 GPa
Hardness	2.5 (no unit)

Data in the table obtained from web page

<http://www.webelements.com/webelements/elements/text/Mg>

REFERENCES

- [1] H. Kamerlingh Onnes, Leiden Commun. 120 b, 122 b, 124 c (1911)
- [2] W. Meissner and R. Ochsenfeld, Naturwissenschaft, **21** (1933) 787
- [3] J. G. Bednorz, K. A. Muller, Z Phys. B **64** (1986) 189
- [4] L. R. Testardi, J. H. Wernick, W. A. Royer, Solid St. Commun. **15** (1974) 1
- [5] J. R. Gavaler, M. A. Janocko, C. R. Jones, J. Applied Phys. **45** (1974) 3009
- [6] Nagamatsu. N. Nakagawa, T. Muranaka. Y. Zenitani, J. Akimitsu Nature **410** 63 (2001)
- [7] J. Bardeen, L. N. Cooper, J. R. Schrieffer, Phys. Rev. **106** (1957) 162
- [8] R. J. Cava, H. Takagi, B. Batlogg, H. W. Zandbergen, J. J. Krajewski, W. F. Peck, R. B. Van Dover, R. J. Felder, T. Siegrist, K. Mizuhashi, J. O. Lee, H. Eisaki , S. A. Carter, S. Uchida, Nature **367** 146 (1994)
- [9] C. Buzea and T. Yamashita Supercond. Sci. Technol. **14** (2001) R115
- [10] S. L. Bud'ko, G. Lapertot. C. Petrovic, C. E. Cunningham, N. Anderson and P. C. Canfield, Phys. Rev. Lett. **86** (2001) 1877
- [11] T. Yildirim, O. Gulseren, J. W. Lynn, C. M. Brown, T. J. Oldovic, Q. Huang, N. Rogado, K. A. Regan, M. A. Hayward, J. S. Slusky, T. He, M. K. Haas, P. Khalifah, K. Inummaru, P. C. Cava, Phys. Rev. Lett. **87** (2001) 037001

- [12] D. C. Larbalestier, L. D. Cooley, M. O. Rikel, A. A. Polyanskii, J. Jiang, S. Patnaik, X. Y. Cai, D. M. Feldmann, A. Gurevich, A. A. Squitieri, M. T. Naus, C. B. Eom, E. E. Hellstrom, R. J. Cava, K. A. Regan, N. Rogado, M. A. Hayward, T. He, J. S. Slusky, P. Khalifah, K. Inumaru & M. Haas, *Nature* **410** 186 (2001)
- [13] D.C Larbalestier, A. Gurevich, D. M. Feldmann and A. Polyanskii, *Nature Insight*, **414** 368 (2001)
- [14] D.G. Hinks, H. Claus and J. D. Jorgensen, *Nature* **411** (2001) 457
- [15] B. Lorenz, R. L. Meng, C. W. Chu, *Phys. Rev. B* **64** (2001) 2507
- [16] P. Bordet, M. Mezouar, M. Nunez-Regueiro, M. Monteverde, M. D. Nunez-Regueiro, N. Rogado, K. A. Regan, M. A. Hayward, T. He, S. M. Loureiro and R. T. Cava, *Phys. Rev. B* **64** (2001) 172502
- [17] Y. Eltsev, K. Nakao, S. Lee, T. Masui, N. Chikumoto, S. Tajima, N. Koshizuka, M. Murakami. *Phys. Rev. B* **66** (2001) 180504(R)
- [18] H. Schmidt, J. F. Zasadzinski, K. E. Gray, and D. G. Hinks, *Phys. Rev. B* **63** (2001) 220504(R)
- [19] A. Y. Liu, I. I. Mazin, J. Kortus, *Phys. Rev. Lett.* **87** (2001) 087005
- [20] H. J. Choi, D. Roundy, H. Sun, M. L. Cohen and S. G. Louie *Nature* **418** (2002) 758
- [21] F. Bouquet, R.A. Fisher, N.E. Phillips, D.G. Hinks, and J.D. Jorgensen, *Phys. Rev. Lett.* **87** (2001) 047001

- [22] M. Naito and K. Ueda *Cond-mat* / **0402333**, (2004)
- [23] J. M. Rowell, *Supercond. Sci. Technol* **16** (2003) R17
- [24] J.J. Tu, G.L. Carr, V. Perebeinos, C. C. Homes, M. Strongin, P.B. Allen, W. N. Kang, E-M Choi, H-J Kim, S-I Lee, *Phys. Rev. Lett.* **87** (2001) 277001
- [25] S. L. Bud'ko, C. Petrovic, G. Lapertot, C. E. Cunningham and P. C. Canfield, *Phys. Rev. B*, **63** (2001) 220503
- [26] P. A. Sharma, N. Hur, Y. Haribe, C. H. Chen, B. G. Kim, S. Guha, M. Z. Cieplak and S-W. Cheong, *Phys. Rev. Lett.* **89** (2001) 167003
- [27] T. Masui, S. Tajima, *Physica C* **385** (2003) 91
- [28] Y. U. Eltsev, K. Nakao, S. Lee, T. Masui, N. Chikumoto, S. Tajima, N. Koshizuka, M. Murakami, *Phys. Rev. B*, **66** (2002) 180504 (R)
- [29] W. N. Kang, C.U. Jung, K. H. P. Kim, M. S. Park, S. Y. Lee, H. J. Kim, E. M. Choi, K. H. Kim, M. S. Kim, S. I. Lee, *Appl. Phys. Lett.* **79** (2001) 982
- [30] W. N. Kang, H. J. Kim, E. M. Choi, K. H. P. Kim, H. S. Lee, S. I. Lee, *Phys. Rev. B*, **65** (2002) 134508
- [31] P.C. Canfield, D.K. Finnemore, S.L. Budko, J.E. Ostenson, G. Lapertot, C.E. Cunningham, C. Petrovic, *Phys. Rev. Lett.* **86** (2001) 2423.
- [32] M. Eisterer, B.A. Glowacki, H.W. Weber, L.R. Greenwood, M. Majoros, *Supercond. Sci. Technol.* **15** (2002) 1088.

- [33] A. Serquis, L. Civale, D.L. Hammon, J.Y. Coulter, X.Z. Liao, Y.T. Zhu, D.E. Peterson, F.M. Mueller, *Appl. Phys. Lett.*, in press, cond-mat/0208293
- [34] S.X. Dou, S. Soltanian, J. Horvat, X.L. Wang, S.H. Zhou, M. Ionescu, H.K. Liu, P. Munroe, M. Tomsic, *Appl. Phys. Lett.* **81** (2002) 3419.
- [35] S.D. Bu, D.M. Kim, J.H. Choi, J. Giencke, S. Patnaik, L. Cooley, E.E. Hellstrom, D.C. Larbalestier, C.B. Eom, J. Lettieri, D. G. Schlom, W. Tian, X.Q. Pan, cond-mat/ 0204004
- [36] C.B. Eom, M.K. Lee, J.H. Choi, L. Belenky, X. Song, L.D. Cooley, M.T. Naus, S. Patnaik, J. Jiang, M. Rikel, A. Polyanskii, A. Gurevich, X.Y. Cai, S.D. Bu, S.E. Babcock, E.E. Hellstrom, D.C. Labalestier, N. Rogado, K.A. Regan, M.A. Hayward, T. He, J.S. Slusky, K. Inumaru, M.K. Haas, R.J. Cava, *Nature* **411** (2001) 558.
- [37] K. Komori, K. Kawagishi, Y. Takano, S. Arisawa, H. Kumakura, M. Fukutomi, K. Togano, *Appl. Phys. Lett.* **81** (2002) 1047.
- [38] R. Flukiger, H.L. Suo, N. Musolino, C. Beneduce, P. Toulemonde, P. Lezza, *Physica C* **385** (2003) 286
- [39] J. Wang, Y. Bugoslavsky, A. Berenov, L. Cowey, A.D. Caplin, L.F. Cohen, J.L. MacManus Driscoll, L.D. Cooley, X. Song, D.C. Larbalestier, *Appl. Phys. Lett.* **81** (2002) 2026.
- [40] H.L. Suo, P. Lezza, D. Uglietti, C. Beneduce, V. Abuacherli, R. Flukiger, presented at the ASC, 5–9 August 2002, Houston, USA, *IEEE Trans. Appl. Supercond.*, in press.

- [41] G. Giunchi, S. Ceresara, G. Ripamonti, A. DiZenobio, S. Rossi, S. Chiarelli, M. Spadoni, R. Wesche, P.L. Bruzzone, presented at Boromag 17–19 June 2002, SUST, cond-mat/ 0207488, in press.
- [42] A.K. Pradhan, Z.X. Shi, M. Tokunaga, T. Tamegai, Y. Takano, K. Togano, H. Kito, H. Ihara, *Phys. Rev. B* **64** (2001) 212509.
- [43] S.H. Moon, J.H. Yun, H.N. Lee, J.I. Kye, H.G. Kim, W. Chung, B. Oh, *Appl. Phys. Lett.* **79** (2001) 2429.
- [44] K.H.P. Kim, J.-H. Choi, C.U. Jung, P. Chowdhury, H.-S. Lee, M.-S. Park, H.J. Kim, J.Y. Kim, Z. Du, E.-M. Choi, M.-S. Kim, W.N. Kang, S.-I. Lee, G.Y. Sung, J.Y. Lee, *Phys. Rev. B* **65** (2001) 100510.
- [45] Y. Zhao, Y. Feng, D.X. Huang, T. Machi, C.H. Cheng, K. Nakao, N. Chikumoto, Y. Fudamoto, N. Koshizuka, M. Murakami, *Physica C* **378–381** (2002) 122;
 Y. Zhao, D.X. Huang, Y. Feng, C.H. Cheng, T. Machi, N. Koshizuka, M. Murakami, *Appl. Phys. Lett.* **80** (2002) 1640;
 Y. Feng, Y. Zhao, Y.P. Sun, F.C. Liu, B.Q. Fu, L. Zhou, C.H. Cheng, N. Loshizuka, M. Murakami, *Appl. Phys. Lett.* **79** (2001) 3983.
- [46] R. Flukiger, H.L. Suo, N. Musolino, C. Beneduce, P. Toulemonde, P. Lezza, *Physica C* **385** (2003) 286
- [47] C.U. Jung, H.-J. Kim, M.-S. Park, M.-S. Kim, J.Y. Kim, Z. Du, S.-I. Lee, K.H. Kim, J.B. Betts, M. Jaime, A.H. Lacerda, G.S. Boebinger, *Physica C* **377** (2002) 21
- [48] P. C. Canfield, D. K. Finnemore, S. L. Bud'ko, J. E. Ostenson, G. Capertot, C. E. Cunningham and C. Petrovic, *Phys. Rev. Lett.* **86** (2001) 2423.

- [49] M. Xu, H. Kitazawa, Y. Takano, J. Ye, K. Nishida, H. Abe, A. Matsushita, N. Tsujii, G. Kido, Appl. Phys. Lett. **79** (2001) 2779
- [50] D.G. Hinks, J.D.Jorgensen, H.Zheng, S. Short, Physica C **382** (2002) 166
- [51] R.A. Ribeiro, S.L. Bud'ko, C. Petrovic, P.C. Canfield, Physica C **382** (2002) 194
- [52] A. Serquis, L. Civale, L. Hammon, Appl. Phys. Let. **82** (2003) 17
- [53] H. Xiao, W. H. Song, J. J. Du, Y. P. Sun and J. Fang, Physica C **386** (2003) 593
- [54] B A Glowacki, M Majoros, M Vickers, J E Evetts, Y Shi and I McDougall
Supercond. Scien. Technol. **14** (2001) 193
- [55] W. Goldacker and S. I. Schlachter, Physica C **378** (2002) 889
- [56] H. Kamakura, A. Matsumoto, H. Fujii, K. Togano, Appl. Phys. Lett. **79** (2001)
2435
- [57] S. Soltanian, X. L. Wang, I. Kusevic, E. Babic, A. H. Li, M. J. Qin, J. Horvat, H.
K. Liu, E. W. Collings, E. Lee, Physica C **361** (2001) 84
- [58] Y Feng, G Yan, Y Zhao, X J Wu, A K Pradhan, X Zhang, C F Liu, X H Liu and L
Zhou, Supercond. Scien. Technol. **16** (2003) 682
- [59] David C. Dunand Appl. Phys. Lett. **79** (2001) 4186
- [60] G. Giunchi, S. Ceresera, G. Ripamonti, P. L. Bruzzone, Cond-mat 0207488,
(2002).

- [61] D. Yang, H. Sun, H. Lu, Y. Guo, X. Li and X. Hu, Supercond. Scien. Technol. **16** (2003) 576
- [62] T C Shields, K Kawano, D Holdom and J S Abell, Supercond. Scien. Technol. **15** (2002) 202
- [63] S. Murase, K. Itoh, H.Wada, K.Noto, Y.Kimura, Y. Tanaka and K. Osamura, Physica C **357-360**, (2001), 1197-1200.
- [64] Qiang Li, J. E. Ostenson, D. K. Finnemore, Appl. Phys. Lett. **82** (2003) 2103
- [65] V. F. Nesterenko, Y. Gu, Appl. Phys. Lett. **82** (2003) 4104
- [66] K Yamamoto, K Osamura, S Balamurugan, T Nakamura, T Hoshino and I Muta Supercond. Scien. Technol. **16** (2003) 1052
- [67] A. Gunel, Electrical and structural properties of MgB₂/Mg composites, M.S. thesis, Izmir Institute of Technology, (2003).
- [68] M. Egilmez, A. Gunel, S. Okur, M. Tanoglu, L. Ozyuzer, Key Engineering Materials **270** (2004) 1197